SCALE MODEL SEISMIC EXPERIMENTS.

THESIS

submitted by

SYDNEY H. HALL, M.Sc.

for the

Diploma of the Imperial College

Department of Geophysics,
Imperial College of Science and Technology,
London.

September, 1954.

ABSTRACT.

A model seismic experiment is described using an electric spark as source and Barium Titanate as detector. The measures taken to reduce pick-up from the spark discharge are described and an account is given of the design of the low Q Barium Titante detector. The theory of the Barium Titanate detector is developed, but could not be applied to the detector at low Q.

Experiments were conducted in a tank 1 metre square by 30.5 cms. deep, filled with water, and a sequence of records taken with the detector at various depths beneath the water surface revealed a striking change in waveform. The first and second arrivals were the direct (P) and reflected (PP_1) waves respectively, and it is suggested that interference is the probable cause of the phenomenon. Horizontal traverses were made across the tank with a slate slab model, 48 x 63.5 cms. x 3.8 cms. thick, in various positions in the tank. Reflections, refractions, and direct waves were discerned in the records. For traverses with the detector at the surface there was no evidence of a high-frequency water wave as encountered in seismic work at sea. Evidence of a coda was found on the refracted wave from the slab.

CONTENTS.

INTRODUCTION.

Perhaps, of all the earth sciences, seismology has revealed most information about the structure of the earth. In geophysical prospecting too, it can be claimed that the seismic method has, considering all other methods, been the most successful in the search for oil. With the introduction of the first sensitive seismograph by Milne, seismology became quantitative and from seismic records the information accumulated has led to the identification of the various boundaries within the earth's interior. The same information has also led to the development of Travel-time tables of which the most familiar is the Jeffrey's-Bullen tables. All this information, together with a knowledge of time of occurrence of the initial disturbance, is based upon the interpretation of the seismograph record.

In the simple case of a vertical impulse on the free surface of a semi-infinite medium, the seismograph or geophone detects at positions on the surface a complex disturbance compounded of a number of waves or "arrivals" of differing velocities and different modes of motion. The components, longitudinal (P) and transverse (S), which travel though the medium with a high velocity are the body waves and that propagated along the surface at a lower velocity is called the Rayleigh wave (LR) whose motion, consisting of longitudinal and transverse movements, takes place in the vertical plane parallel to the path of the wave. For a surface layer, resting upon a medium of higher velocity, another surface wave can exist known as the Love wave (LQ) whose motion is transverse to the direction of its path and whose velocity depends upon the wavelength and varies between that of the S wave in the lower medium and that of the surface layer. The geophone or seismograph motion, in this case is further complicated by the additional arrivals generated by reflection and refraction of the body waves at the lower boundary of the surface layer. These "arrivals" all arise from the vertical impulse applied to the free surface, and moreover undergo selective absorption and dispersion in their passage through the medium. Part of this complexity is due to the elastic behaviour of the medium and part due to the nature of the initial disturbance.

The aforementioned travel-time tables assist in the identification of these waves in addition to certain empirical criteria such as the nature of the onset, the period and change of phase. It is obvious that if similar records could be obtained in the laboratory under controlled conditions much knowledge might be gained in identification of the "arrivals" and of the processes involved in their propogation. In addition, it would enable a study of the mode of generation of the waves to be made since the nature of the source is largely known. Other aspects, hitherto neglected, whose study may be well worth while, are the "ground roll" encountered in seismic prospecting, the information that would accrue from the examination of amplitudes in seismic records, the mode of propagation of waves along layers of the dimensions of the wavelength. Again, the Lamb problem[1] where the cause of the dispersion that converts a single impulse into a long train of waves is not fully understood, although the recent work of Margery Newlands[2] is a step forward to the solution of this problem. Another subject that is opening up new fields of investigation is seismic work at sea with the recently discovered "water wave", "rider wave" and "Airy phase" in shallow water work.[3]

Generally, seismology and seismic prospecting has to deal with media of unbounded lateral extent and of thickness of the order of the wavelengths encountered. Reproduction of this situation in the laboratory is feasible if frequencies considerably higher than those found in the field are used. As shown by Kaufman & Roever[4] with the same elastic constants of media as in the field a reduction factor of 10^{-3} for length gives a factor of 10^{3} for frequency. Hence for 5-100 c.p.s. as normally used in seismic work (seismological frequencies are lower than these) the frequencies in the laboratory need to be of the order of 5-100 kc.p.s., the wavelengths for which are sufficiently great to be unaffected by the particle size of the medium and sufficiently small to construct models of the same order of thickness. For the case of a tank containing the medium in which the model to be examined is placed, the dimensions of the medium are restricted so that the observation time is limited to that of the highest velocity component of the initial disturbance travelling by the shortest reflected path. The medium must be homogeneous and of fine grain and preferably possess elastic constants that give the highest velocity contrast between the various phases. The transmission loss of the medium must be low if severe attenuation is to be avoided; media used by workers in this field have been either water, wax or concrete. Water has no serious transmission losses but does not propagate shear waves. Of wax and concrete, wax has the higher transmission loss and both are difficult to cast as a homogeneous block as in setting there is the tendency for the gravitational separation of components, and with wax in particular, cavitation or the rapid solidification of the outer surface while the inside remains molten, makes casting a troublesome problem.

The first account of a model seismic experiment, which initiated this work, was in a paper delivered at the Third World Petroleum Congress at the Hague, 1951,[4] and since then a number of papers have been published on the subject. Kaufman and Roever[4] used an electric spark as source and a miniature displacement geophone as detector with a wax medium. Compressional and Rayleigh waves were detected in a time-distance traverse across the block and shear waves by embedding the detector within the wax so that it was unaffected by the surface waves. The experimental results for the Rayleigh wave showed no evidence of dispersion, agreeing well with the theory of Lamb. In contrast, Northwood and Anderson,[5] using a concrete block and Rochelle salt source and detector, reproduced the oscillatory character of the typical seismic record. Also, using a source giving a shear stress to the medium and acting transverse to the line from the source to the detector, produced a strong S phase. By experimenting with a free surface consisting of a metal hemisphere covered with rubber with an air film between, they showed that minimum path reflections produced a tail or "coda" and maximum paths a "prelude". Howes, Tedaja-Flores and Randolph[6] used an electric spark source and a Barium Titanate accelerometer on limestone immersed in water. Evans and his co-workers[7] working with a Lithium Sulphate source and a similar detector on a medium of plastic plates have identified clearly P, L, PS, SP and multiple reflections. They also described methods of visual observation of elastic waves by photoelasticity and schlieren photography.

A brief report has been published by Levin and Hibbard[8] of an entirely different approach to model study. An analogue computer is presented with a single layer case and records are produced of all the arrivals commonly met in seismic prospecting. Oliver, Press and Ewing[9] describe an elegant method for model seismology in two-dimensions, applying ultrasonic pulses at brief time intervals to thin discs by means of Barium Titanate transducers and presenting the event as a stationary wave on an oscilloscope screen. Since the form of the equation for Rayleigh waves is unaffected if the solid dilatational velocity is replaced by the plate dilatational velocity, model experiments can be performed on thin discs and these can be built up as concentric models to simulate layer problems and model earths. They detected surface and body waves as well as a considerable number of reflected phases. Results on Flexural and Rayleigh wave dispersion agreed well with theory.

The model seismic experiment which is described in this thesis uses an electric spark as source and Barium Titanate as a detector. The medium was water and the source impulse was applied above the surface so that no complications arose from the bubble effect. Later experiments were made on a slate slab immersed in the water.

CHAPTER 1.

APPARATUS.

The General Circuit.

In the block diagram of the method, illustrated in Fig. 1, the 3000 volt D.C. power supply charges an 8μF condenser across the two outer electrodes of the spark. A pulse of 100 volts amplitude, initiated by the control oscillator induces a voltage in the secondary of the induction coil sufficient to cause breakdown in the gap between the inner electrode and the outer earthed electrode of the spark. The ionisation of the air between enables the main gap to break down and the 8μF condenser then discharges across it. The time-base of the oscilloscope, connected to the earthed electrode, is triggered at this instant and the beam which is occulted between shots is at the same time restored to a pre-set intensity by a synchronous pulse from the control oscillator. The event, received by the detector in the tank, is amplified and appears on the oscilloscope trace subsequent to firing. The time is measured by the number of cycles appearing on the second trace, the amplifier of which is connected to the timing oscillator. The stabilised power supply provides high stability H.T. to the wide band amplifier.

The Tank.

This was constructed of wood, the inner surfaces

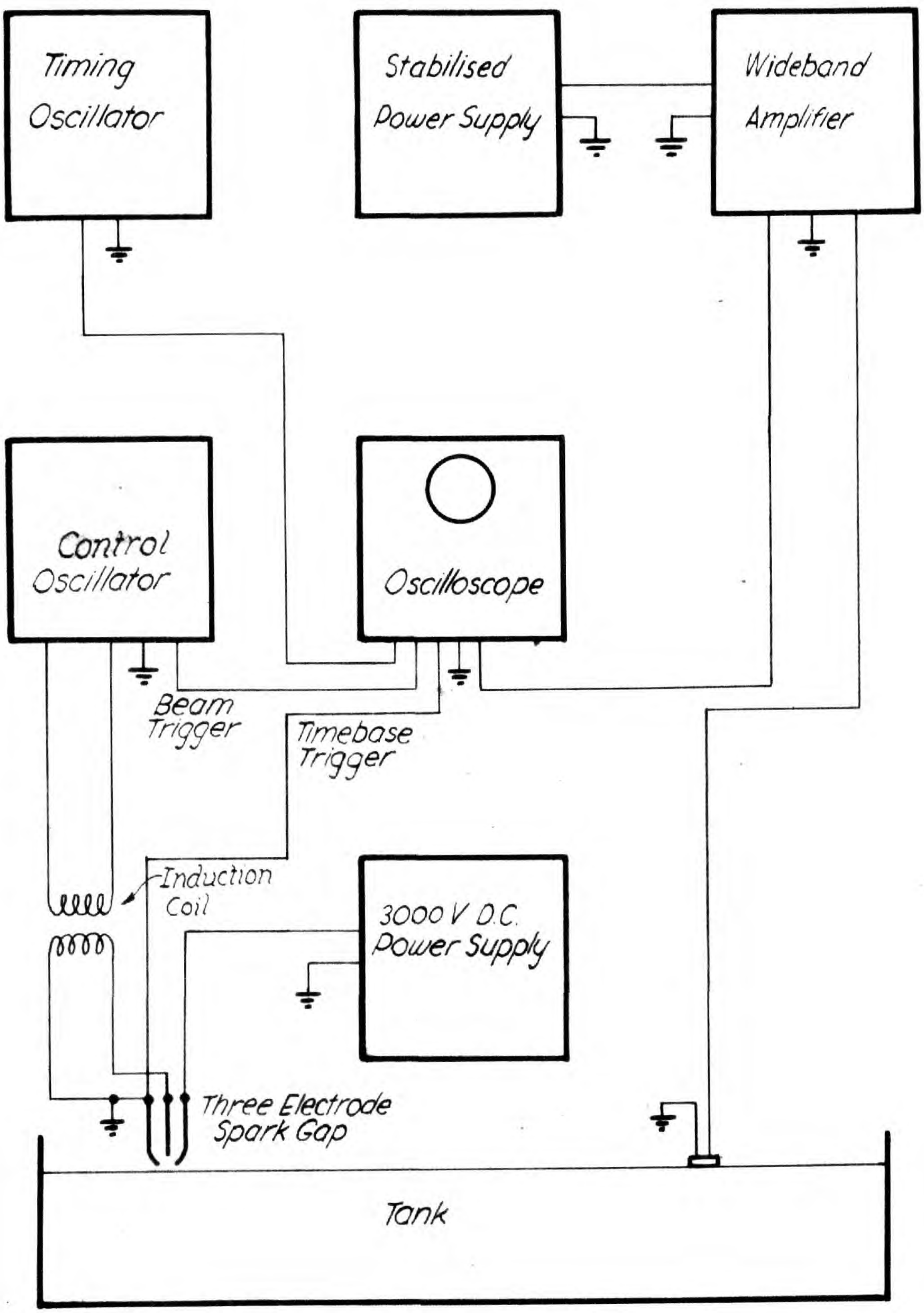

FIG. 1. EXPERIMENTAL ARRANGEMENT

being coated with a tar compound to render it waterproof. Its internal dimensions, 1 metre square x 30.5 cms. reduced the useful distance between the spark and detector, mounted along the centre line (Fig. 2) to $\sqrt{50^2 - d^2}$ where d is the depth of water in the tank. This formula is based on the comparison between reflection from the floor of the tank and from the wall perpendicular to the spark detector axis, assuming the spark and detector to be situated at equal distances from the centre of the tank. For a depth of 15 cms. the maximum separation is 46 cms. which was quite adequate. Reflections from the wall parallel to this axis require $d < 50$ cms. Four 7.6 x 7.6 cms. wooden posts fastened to the corners of the tank supported in cantilever two wooden rails 12.7 cms. apart. By this means the spark suspended from one rail was mechanically isolated from the detector suspended from the other. To make a time-distance traverse across the tank, the spark was permanently bolted to its rail and the detector moved at 2.54 or 1.27 cms. intervals by bolting it through pairs of holes 5.1 cms. apart at intervals of 1.27 cms. Previously, the tank had extensive use in laboratory resistivity work and was thoroughly saturated with salt, precluding the use of the spark below the surface of the water.

<u>Source</u>.

(Fig. 3) Three electrodes of brass were mounted

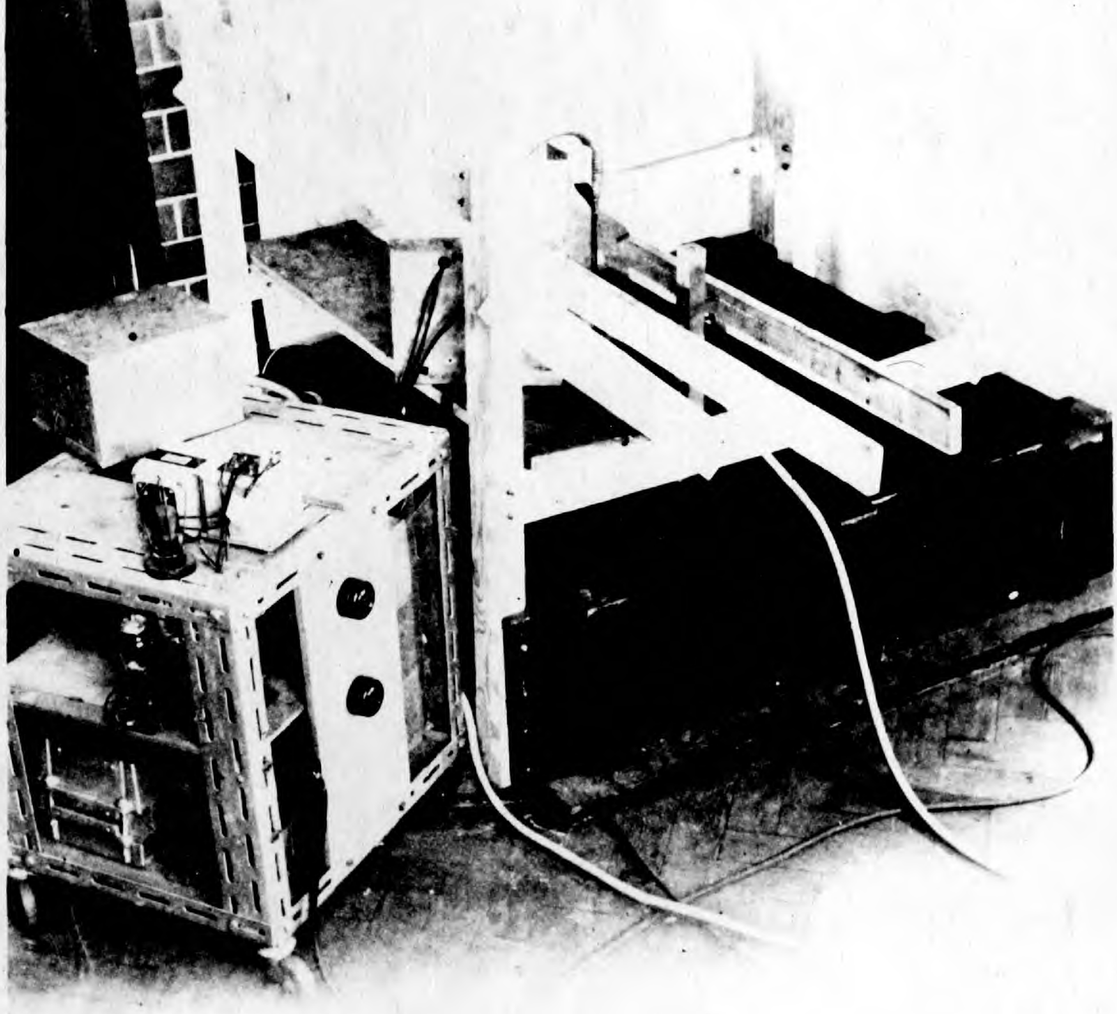

FIG.2. TANK & HIGH VOLTAGE
POWER SUPPLY

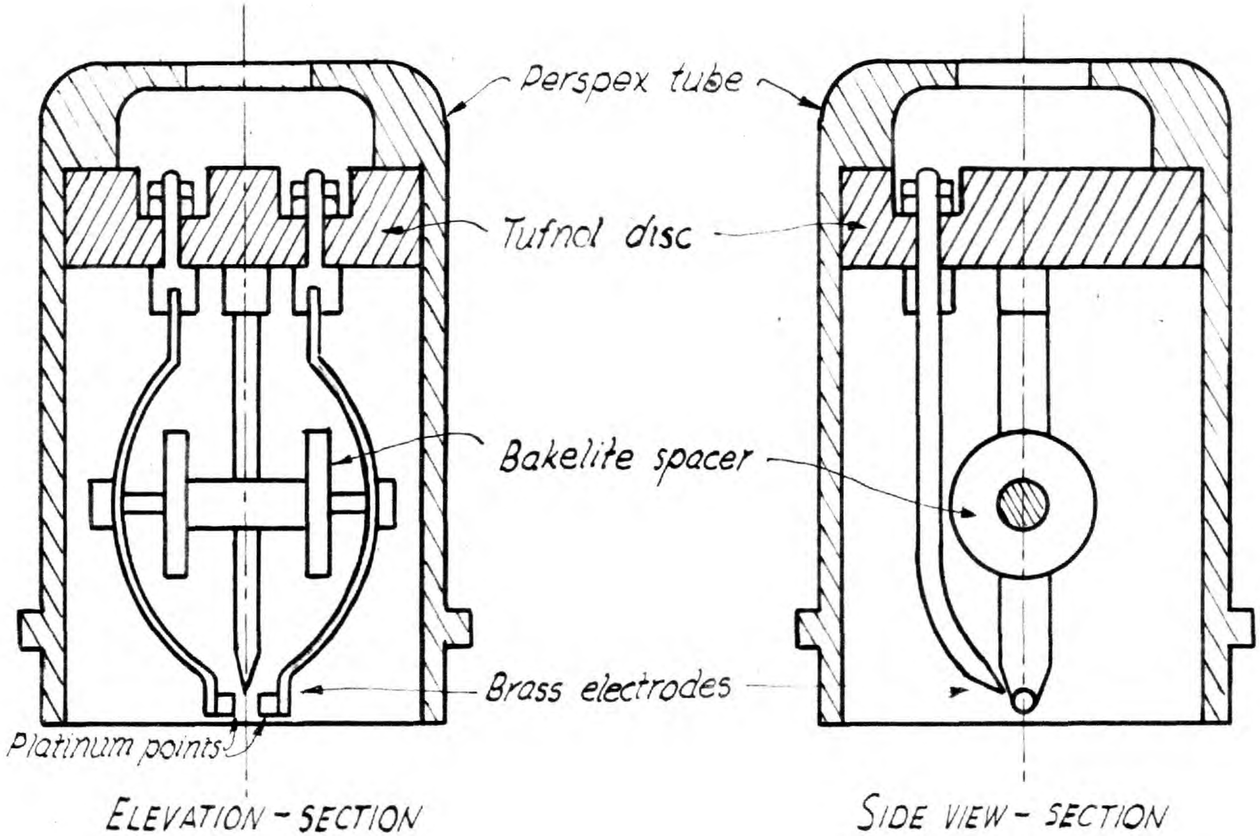

FIG. 3. SOURCE: SPARK CONSTRUCTION

in a 1.27 cms. disc of tufnol with recessed holes on its opposite side for attaching the leads. On the tips of the outer electrodes small platinum points were mounted to reduce burning and the gap was adjusted by a milled bakelite spacer in the ends of which were fixed a left-handed and a right-handed screw which were threaded into small bosses on the electrodes. Polythene tubing was fitted to the ends of the leads and sealed to the tufnol disc with araldite cement and effectively prevented any flash over at this point. A perspex tube was fitted around the electrodes and screwed to the tufnol mount. The rear of the tube was closed but drilled to allow the passage of the leads to the 8 μF condenser. Power for this condenser was provided by a voltage doubler full wave D.C. power supply whose constructional details are illustrated in Fig. 4. Two rectifiers, (Brimar R11's) shown in Fig. 4, operating alternately at each half cycle supplied 50mA to the rectifying circuit and the condenser was charged through the load resistance of 60 KΩ to 3000 volts. Separate 4 volts, 10 amps filament transformers were utilized for each valve.

<u>Control Oscillator</u>.

In preliminary experiments with this oscillator pick-up was encountered on the beam triggering pulse due to the oscillatory discharge in the primary of the induction coil and the present circuit, Fig. 5, was evolved

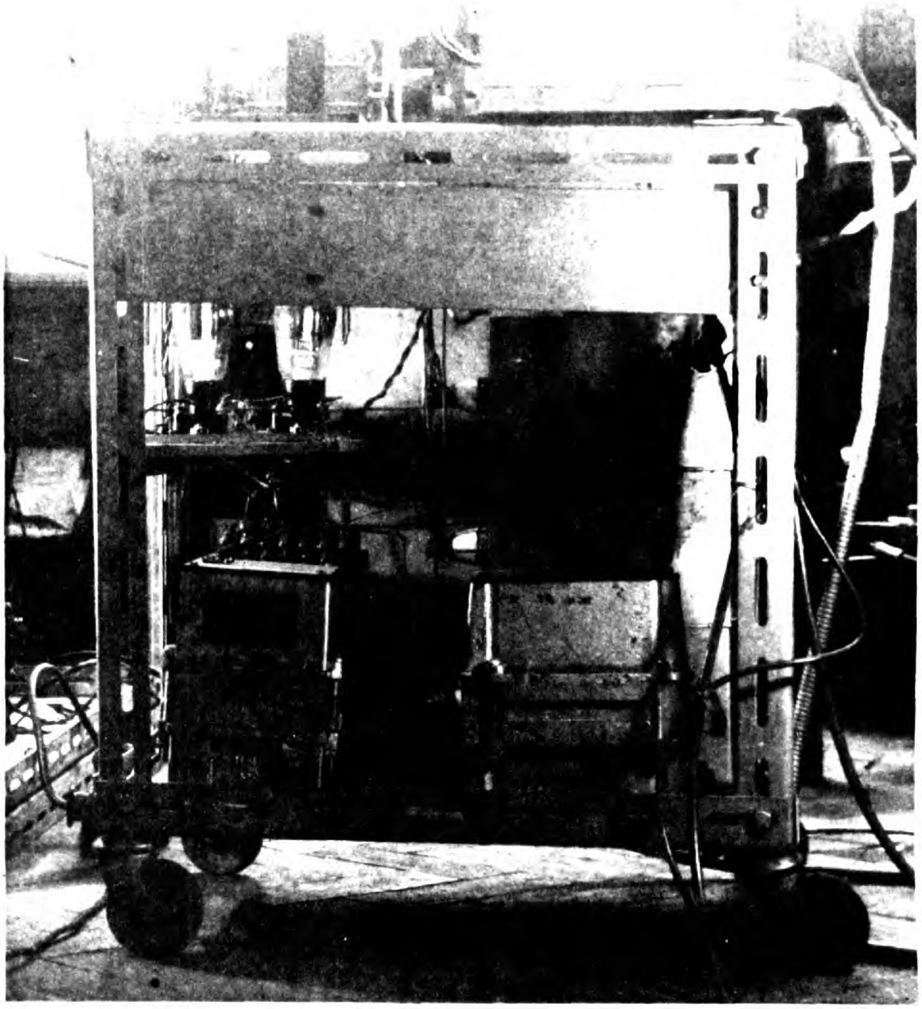

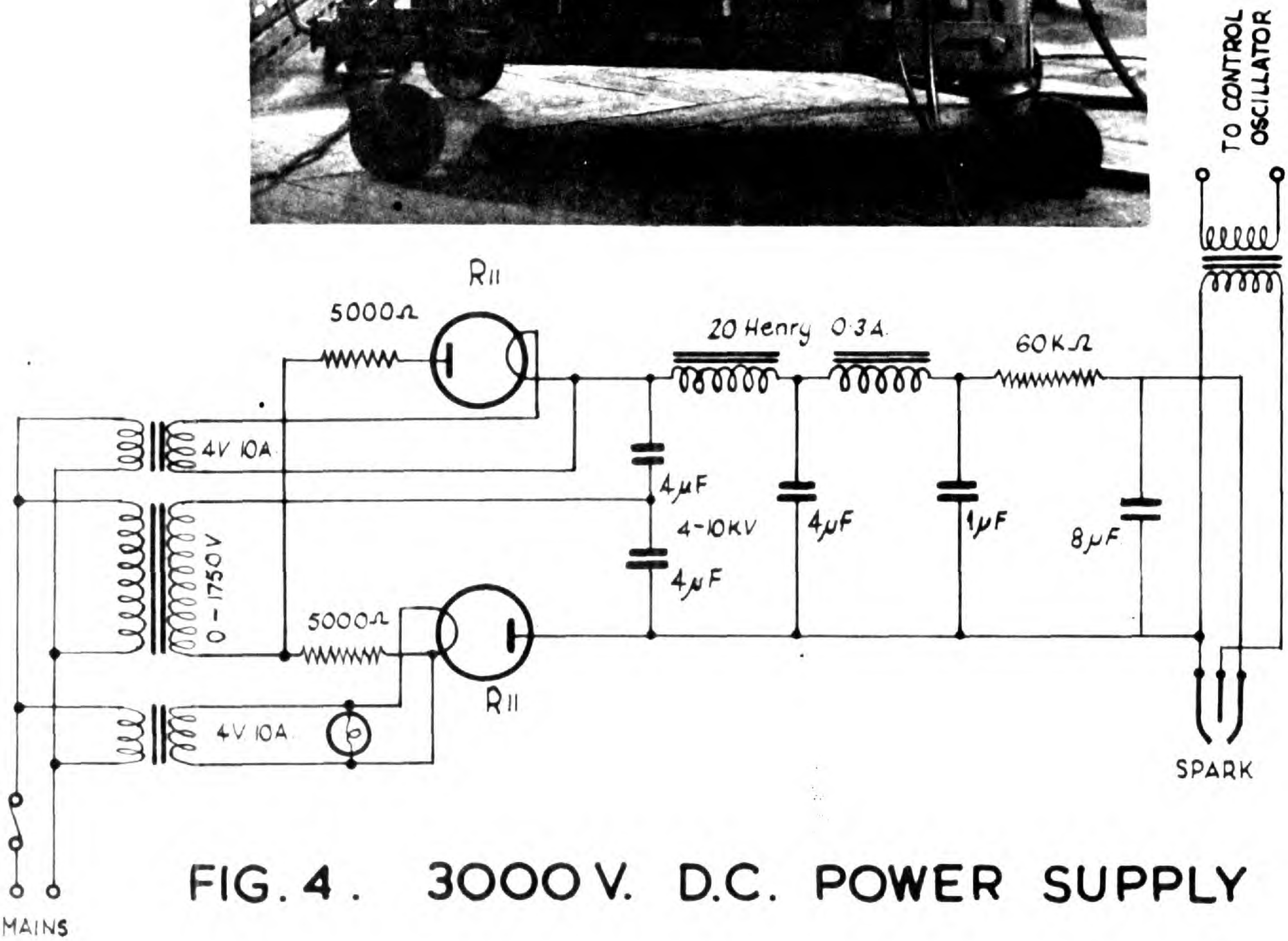

FIG. 4. 3000 V. D.C. POWER SUPPLY

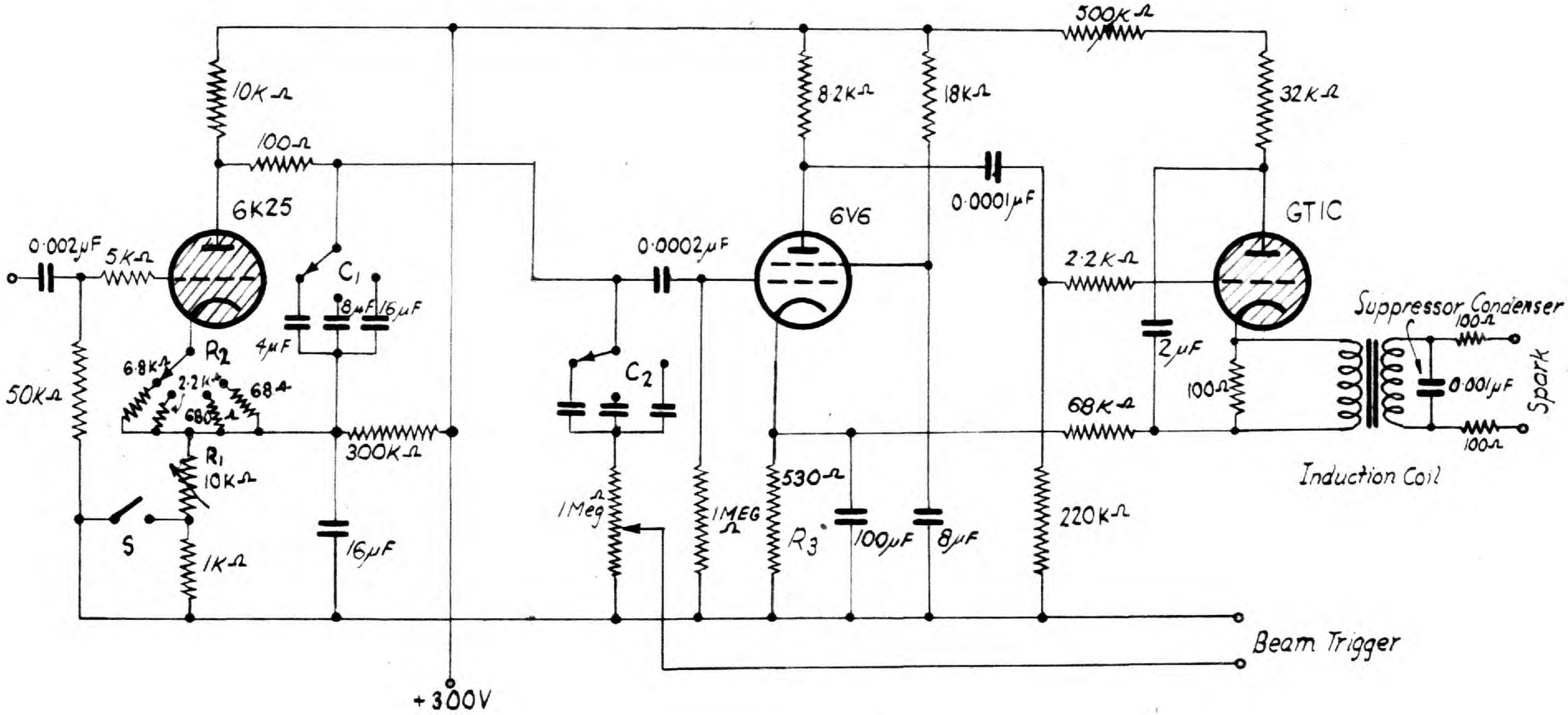

FIG. 5. CONTROL OSCILLATOR

to prevent this. Two thyratron relaxation oscillators are separated by a tetrode, (6V6) which effectively stopped the transfer of damped oscillations from the spark trigger stage to the beam triggering stage while still allowing the thyratron, (6K25) to control the discharge of the thyratron (GTIC). Thyratrons were used as discharge rates of less than 1/second can be obtained. The condenser C_1 in the plate circuit of the 6K25 charges up to the plate supply, 300 volts, and discharge takes place through the thyratron at a grid bias of -15 volts determined by the control ratio or ratio of plate volts to grid volts, which is 20 for the 6K25. By altering the setting of the rheostat R_1 the bias was decreased, increasing the rate of discharge for a given setting of C_1. The pulse width was varied by the variable resistance R_2 in the cathode circuit or by altering the setting of C_2 at the output to the beam trigger. This enabled the duration of the pulse to be co-ordinated with the length of time base used, 150 microseconds (μs), 500μs . For single spark work, as when photographing events, R_1 was adjusted so that the 6K25 thyratron remained quiescent when C_1 was fully charged and the push button S depressed momentarily, decreasing the grid bias, so that a single spark occurred. The event was then automatically recorded by the camera mounted on the oscilloscope with its shutter held open. The thyratron (GTIC) was biassed to quiescence by the fixed voltage drop in the cathode resistor R_3 of the tetrode (6V6), the application of the pulse from its plate to the grid of the thyratron causing discharge.

Amplifier.

For faithful reproduction of the detector output design requirements are best based on time rather than frequency considerations. On receipt of the signal, the response must be rapid, as must be the recovery, and the output wave form must conform with the input. This design, Fig. 6, is similar to the voltage amplifiers used for fast transients in nuclear work[10] and consists of a cathode follower input with two sets of three stage amplifiers, with a feedback loop, each set comprising two high gain stages succeeded by a cathode follower. Rapid response is determined by the bandwidth and a measure of the rapidity is given by the rise time T_r. An approximate relation between rise time and bandwidth is given by [10]

$$T_r f_2 \doteqdot \frac{1}{3}$$

where f_2 is also known as the upper half-power frequency, = 100 kc.p.s. in the present case (see response curve Fig. 7) giving $T_r = 3 \mu s$.

The lower half-power frequency f_1 provides an indication of the recovery time and the faithful amplification of the transient. It can be shown [10] that the amplitude distortion produced by signals closely following each other

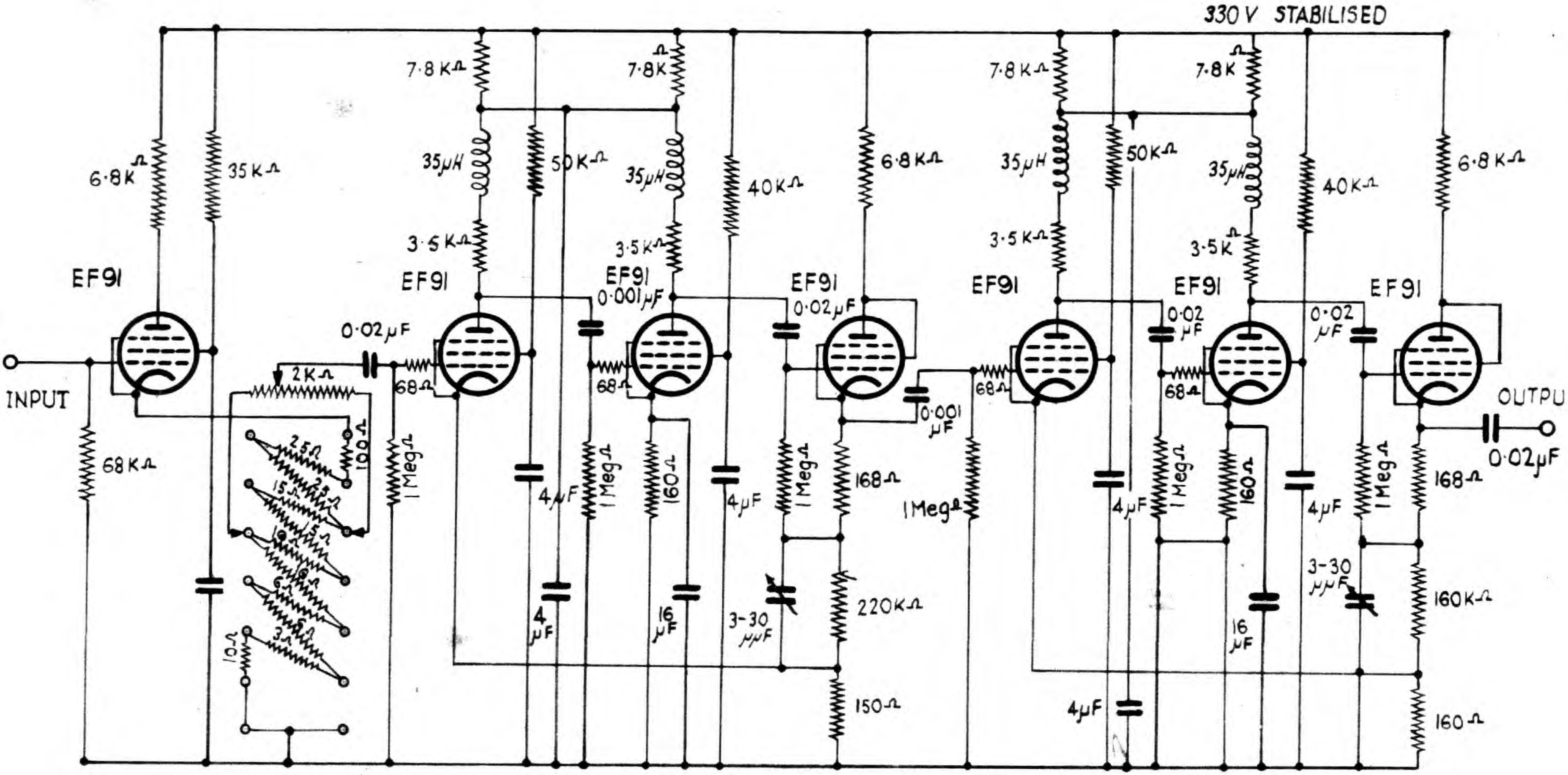

FIG. 6. WIDEBAND AMPLIFIER

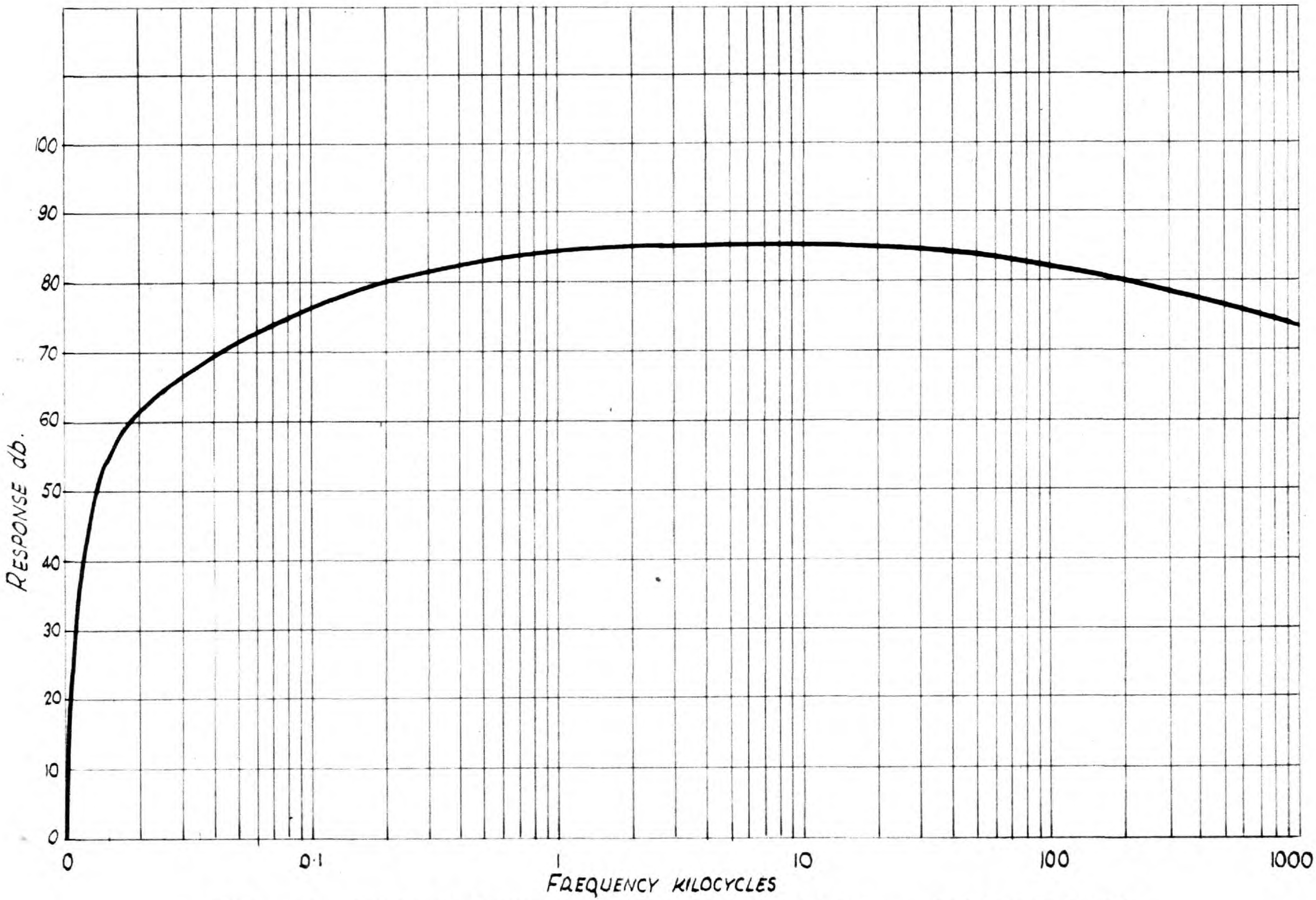

FIG. 7. AMPLIFIER FREQUENCY RESPONSE

is avoided by the insertion of a short time constant in the high gain stages, in this case a 0.001μF coupling condenser with a 1 meg Ω grid leak. This same time constant determines the fidelity, for on the application of a step input, the response for small deviations falls off by the fractional amount[10]

$$\delta = \left(\sum_{1}^{n} \frac{1}{\tau_i} \right) T$$

in time T, where τ_i, $i = 1,2 \cdots n$ are the interstage time constants. In the high gain stages the interstage time constants are 0.02 μ secs. and 0.001μ secs. so that $\delta \doteqdot 2000T$. Hence the response following a step function input drops 1% in 5μs.

The gain of the amplifier (Fig. 7) in the mid band position, 50 kc.p.s. is 15,000 and is 3db down at 400 c.p.s. At 1 megacycle it is 10db down, a reduction of the gain by 1/3. The response at high frequencies was sustained by shunt-compensating the high gain stages inserting 35 micro henry inductances in the plate circuits of the EF91 high frequency pentodes. This inductance was calculated from the formula $L = \alpha R^2 C$ where R is the plate load resistance and C isthe parasitic capacitance, consisting of wiring capacitance and the input and output interelectrode capacitances of the valve, and α determines the amount of compensation. For critical compensation $\alpha = \frac{1}{4}$, for above this value the amplifier overshoots on the application of a step input voltage and oscillates about the signal level. In this case $C = 9\mu\mu F$, $R = 3.5 K\Omega$ giving $\alpha < \frac{1}{2}$.

Each feed-back loop was decoupled by $4\mu F$ condensers and cathode bypassing the second high gain stage in each loop increased the gain considerably. Parasitic oscillations were avoided by the cathode followers between the high gain stages and by the use of feed-back which also improves the gain stability and linearity of response. Small 68Ω grid stoppers were also inserted to destroy these oscillations. The EF91 high frequency pentodes were chosen from the consideration of the gain-bandwidth factor, where if G is the gain and g_m the transconductance of the valve

$$Gf_2 = \frac{g_m}{2\pi C}$$

where C is the parasitic capacitance. The EF91 has a high transconductance of 7.6 mA/V and $C = 9\mu\mu F$. By connecting the pentodes as triode cathode followers the effect of the interelectrode capacitance is reduced and the gain is nearer unity than for a triode. In the input and output the cathode followers provide impedances matching to the detector and oscilloscope respectively for the input impedance is essentially that of the grid leak resistance, $68K\Omega$ which was found to be a satisfactory termination for the coaxial line from the detector. The cathode resistor of the input cathode follower was arranged as an attenuator of 7 positions giving gains of 0,500, 1700, 3000, 5600, 11200, 15000, fine gain control within each attenuator step being provided by the 2KΩ potentiometer. All filaments were A.C. heated except the first which was D.C.

The Stabilized Power Supply.[10]

(Fig. 8) Two triode connected output pentodes (6Y6) in parallel are connected in series with the positive line from a conventional transformer-rectifier-filter supply. A fraction of this output voltage from the cathodes of the 6Y6's is compared with a fixed voltage from the gas-filled voltage stabilizing valve (V.R.105) and the difference is amplifed by the 6SL7 connected as a single triode. The output, applied to the grids of the 6Y6's, affords degenerative compensation for any fluctuation in the rectified supply. The voltage measured at the cathode and grid of the 6SL7 double triode difference amplifier was 100 volts, and the ripple, measured on the oscilloscope was 5×10^{-4} volts.

The Timing Oscillator.

The majority of photographs were taken with 150 μ sec. and 500 μ sec. timebases with timing waves of 100 kc and 50 kc respectively; provided by a Muirhead-Wigan decade oscillator connected to the A_2 amplifier of the oscilloscope. The accuracy is specified as 0.2% so that the period at 100 kc is $10 \pm 0.02\,\mu$ secs. or an error of $\pm 0.3\,\mu$ secs. over the length of the 150 μ sec. time base. For

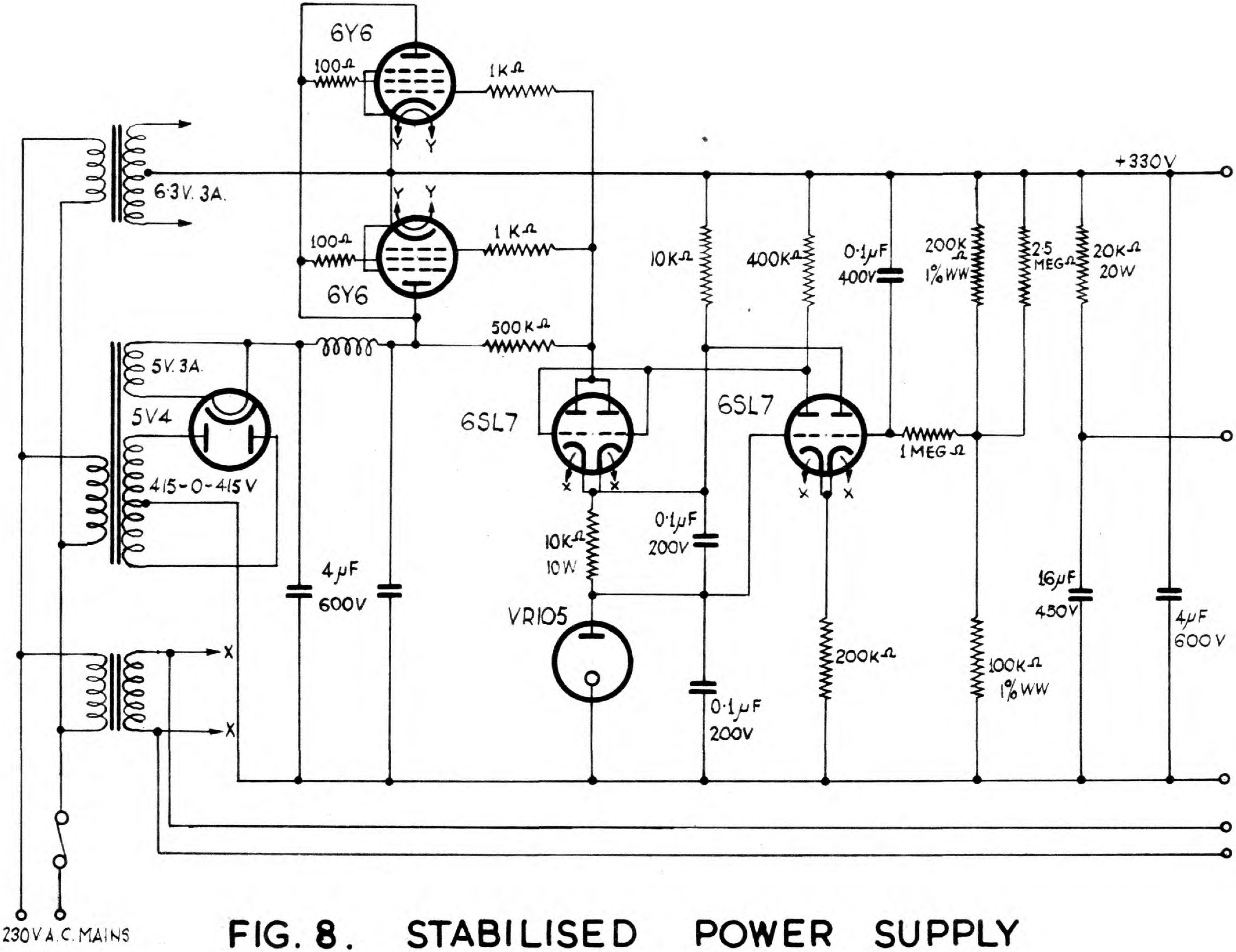

FIG. 8. STABILISED POWER SUPPLY

50 kc at 500 μ secs. the error per period is 20$\pm$ 0.04μ secs. or 1 μ sec. for the entire time base. The hourly stability is 0.05% at all frequencies in kilocycles, representing a change in period of 20$\pm$ 0.01μ secs. at 50 kc.

<u>The Oscilloscope</u>.

A double beam Cossor oscilloscope, model 1049, incorporating beam triggering and time base triggering, the polarity of the latter being selected by the trigger or synch control on the oscilloscope panel and the beam is switched on by the application of a negative signal of amplitude 12V. The output of the preamplifier was connected to the A_1 amplifier whose frequency response was 1-100 kc.p.s with a T_r of 3 μ secs. and whose maximum gain was 900. In most applications the 100 and 300 volt ranges were used representing a gain of 3 and 1 respectively. With the high frequency timing waves on the A_2 beam, inter-modulation occurred between the beams which could only be avoided in recording by taking double exposures with the oscillator switched off and amplifier on for the first, and oscillator on and preamplifier off for the second, and the A_1 beam moved off the face of the oscilloscope tube. To secure adequate exposures in the photography the normal 2kV potential of the tube was altered to 4 kv. The receiving equipment, amplifier, control oscillator, oscilloscope and timing oscillator are shown in Fig. 9.

Photography.

For the short exposures involved it was necessary to use a very fast film. Kodak R60 film was found very suitable but sacrificed resolution for speed. The blue tube of the Cossor model 1049 is a vital factor in this type of photography. The camera, a Cossor model 1428, has an $f/_{3.5}$ fixed focus lens and a reduction ratio of 2.6.:1.

Pick-up.

To complete this chapter, it is worthwhile to devote a separate section to the probem of pick-up. At the outset this proved so severe as to swamp completely the amplifier on the discharge of the spark, with the result that the detector output could not be observed on the oscilloscope. Both the trigger spark and the main spark contributed to this effect as an oscillatory discharge occurred in the secondary of the induction coil which persisted for the entire length of the 500 μ sec. time base. A similar but shorter oscillatory discharge occurred between the main electrodes of the spark. The measures taken to reduce the pick-up to negligible proportions are listed:

(1) coaxial cable between all units

(2) flexible conduit providing additional screening to the coaxial cables for the leads from the 8 μF condenser to the spark and the lead from the detector to the pre-amplifier

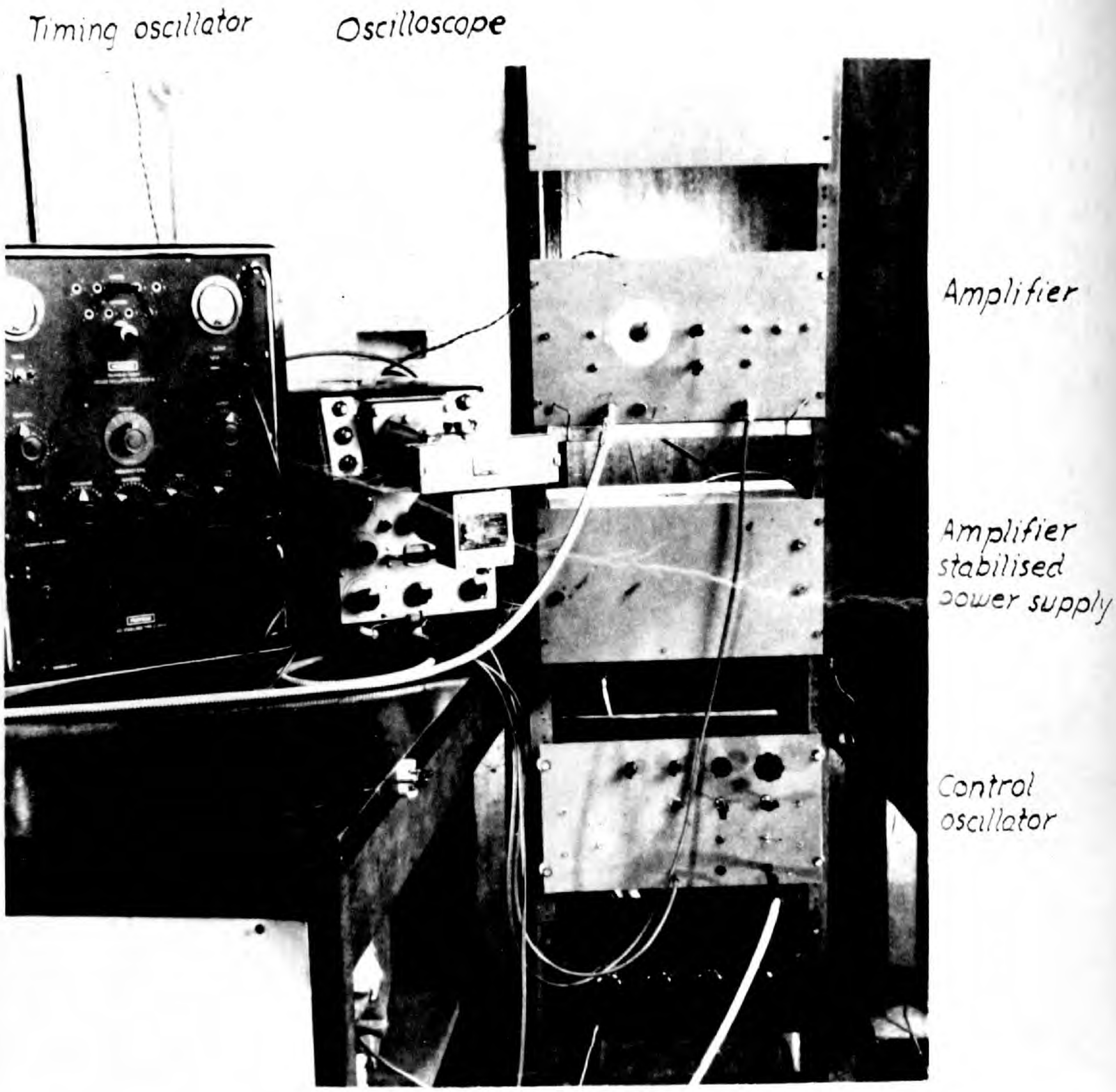

FIG. 9. VIEW OF RECEIVING EQUIPMENT

(3) damping resistors of 100Ω in the secondary leads of the induction coil

(4) a suppressor capacitance of 0.001μF, 4 kV across the secondary of the induction coil

(5) a thyratron across the primary of the induction coil arranged to fire after the first half cycle of oscillation; this was later discarded as it produced no appreciable effect in the secondary

(6) separate earthing; best results were secured by earthing the spark, spark power supply and induction coil secondary to an earth separate from that of the apparatus on the receiving side. Earthing on the source side was provided by a copper hot water pipe, and on the receiving side by a metal stake driven deep into the ground. To avoid loops in the system all earthing was taken to a common point, in the case of the source the earthy side of the 8μF condenser, and for the receiving side a point on the standard chassis frame. (see Fig. 9) 1½" strips of copper foil were then taken from each of these points to earth.

(7) earthing water in tank to the source point, keeping the detector when immersed in the water insulated by a coating of paraffin wax.

(8) greasing the condenser terminals and earth lead. This prevented sparking, an additional source of pick-up.

(9) avoiding metal in the vicinity of the detector; the spark and detector rails were originally of dexion and proved most unsatisfactory. In the same manner, in earlier tests on a block of clay, a large iron case was placed around the spark and detector and had the effect, contrary to expectation, of increasing the pick-up.

(10) all A.C. leads were enclosed in earthed metal conduit. 50 cycle mains filters were found to be of value for the control oscillator.

(11) screening all units in metal boxes. For the spark, $\frac{1}{4}$" aluminium completely enclosed it with an aperture in the front plate of 2" diameter to allow the passage of the acoustic pulse. Tests with the spark and detector in different positions showed that the pick-up was much less when the detector was immediately in front of the spark, with its lead in line with the spark leads, than when it was placed alongside the spark with the leads parallel. The insertion of a 4" x 2" diameter brass tube in the front aperture of the spark reduced the pick-up in the first of the above positions considerably. However, it was found necessary, as will be described later, to remove all screening from the spark, for the presence of the metal surround and tube produced unwanted acoustic reflections when placed near the surface of the water.

(12) screened leads were used for connections in the early stages of the amplifier and the attenuator was enclosed in a cylindrical aluminium cannister. All common leads were soldered to a single linerunning the length of the socket assembly and supported on insulated stand-offs. One end of the line was then taken to a single earth point on thechassis.

(13) Short-circuiting the limiting circuit on the grid of the first valve of the oscilloscope A_1 amplifier.

CHAPTER II.

THE DETECTOR.

Factors Influencing the Design.

Resonant Frequency: To minimize amplitude and phase distortion in the detector response, the working frequencies should be within 40% of the resonant frequency.[11] On reducing the field seismic method to the laboratory scale while maintaining the same ratio of wavelength to structure size, the working frequencies are increased by a factor of 10^3, i.e., field frequencies 50-100 c.p.s. become 50-100 kc.p.s. and with the above criterion a resonance of 160 kc.p.s. is necessary.

Size: A further requirement is the size which must not be comparable with the wavelength if diffraction effects are to be avoided. In water at theabove frequencies the wavelength is of the order of 2.5 cms. However, this effect did not prove as troublesome as expected although the dimensions of the detector head were the same.

Q value: A further need, to secure the resolution of later arrivals, is a low Q, of a value less than 10 to resolve arrivals arising at two surfaces of 2.5 cms. separation in a medium of velocity 4,600 metres p.s.

Types of transducer: A number of types of transducer were examined, and quartz, although feasible, proved costly; for the resonant frequency, bimorth units were impracticably small. A Barium Titanate disc was finally selected for reasons of robustness, high sensitivity and the predominant fact that they were donated to the author.

Barium Titanate.

This ceramic becomes electrostrictive on polarizing in a D.C. field of the order of 30,000 v.p.cm., the mode of vibration being determined by the direction of polarization and the shape. The discs used were biased in the thickness direction and the flat surfaces silvered; the fundamental modes were radial and axial in the region of 160 kc.p.s. and 1 megacycle p.s. respectively. In the theory described in the Appendix, the excitation of the fundamental axial mode is neglected as its resonant frequency lies well beyond the working range.

Other workers: A number of authors have investigated the modes of vibration of cylindrical discs, but no attempt has been made to derive the response of a polarised Barium Titanate disc behaving as an accelerometer. The stress equations and electrical impedance have been developed by W. P. Mason[12] for a disc whose thickness is sufficiently small that the displacement in this direction can be neglected. In the Appendix, the electrical impedance is derived under the same conditions, but by the different process of deriving the generalized equivalent circuit which is valid at all frequencies.

An approximate equivalent circuit has been derived for frequencies in the vicinity of resonance by Schmidt,[13] and a very complete account of the mechanical behaviour is given by R. R. Aggarwal[14] who takes into consideration the effect of axial vibrations and demonstrates the complex displacement of the disc's surface at successive resonances.

Response: The standard reciprocity method requires an accurately calibrated transducer to excite the sound field of the unknown, but the method is restricted to frequencies of a few thousand cycles. Harrison, Sykes and Marcotti[15] have extended the range to 10 kc.p.s. and have shown that a calibration can be obtained with three unknown transducers. Three experiments suffice to determine the response, one of which requires a known acoustic impedance between the two transducers and the size of the medium utilized as an impedance determines a limit to the maximum frequency for which the method is satisfactory. Most erratic results were obtained when two Barium Titanate discs were used as driver and receiver on a 15 cm. cube of paraffin wax, and the method was discarded in favour of a theoretical approach.

The electrical impedance was measured experimentally and compared with the computed value of the theoretical expression, which in turn was based upon the physical dimensions, capacity and resonant frequency of the disc. Agreement between the two was improved by the inclusion in the theory of a mechanical loss term which obviously controls the Q value of the disc. To increase the damping and thereby decrease the Q, the disc was backed with metal and the electrical impedance of the composite of disc and backing, again determined experimentally both in air and in water, on the assumption that the Q value determined would thus include the inherent mechanical loss of the disc, the effect of the backing andthe loading effect of the medium. In the theory this necessitated the more accurate calculation of the electrical impedance incorporating loss. Satisfactory agreement between theory and experiment in this case was not secured as described in the section on detector measurements, but the theory did give a good indication of the Q value obtained.

Detector Construction.

It was most desirable in the design to achieve as low a value of Q as possible. Earlier attempts in mounting the Barium Titanate discs under stress met with little success, for the two reasons that the output waveform was not often repeatable and the Q value of the design was insufficiently low. During these tests the polythene core of the coaxial holder on which the unit was mounted produced undesirable effects due to the high elasticity of the polythene, and subsequently Amphenol holders with a hard ceramic core were used.

Eventually the construction was modified to the form illustrated in Fig. 10. The backing, 7.6 cms. long x 2.5 cms. diameter is attached to the rear surface of the Barium Titanate, and at its other extremity is drilled and tapped 4 B.A. A 4 B.A. threaded 1⅛" length of brass is soldered into the pin of the coaxial holder and screwed into the rear of the backing providing mechanical support for the unit. To the front face of the Barium Titanate disc is fitted a circular aluminium sleeve of sufficient diameter to clear the sides of the disc. A circular flange at one end of the sleeve rests against the outer edge of the disc's front face, effectively damping any high frequency vibrations excited by the impact of the acoustic pulse. The whole was surrounded by a brass or copper jacket with 4 B.A. screws soldered at its end and which secured the jacket to the Amphenol socket. Brass and aluminium have a characteristic acoustic impedance akin to that of Barium Titanate.

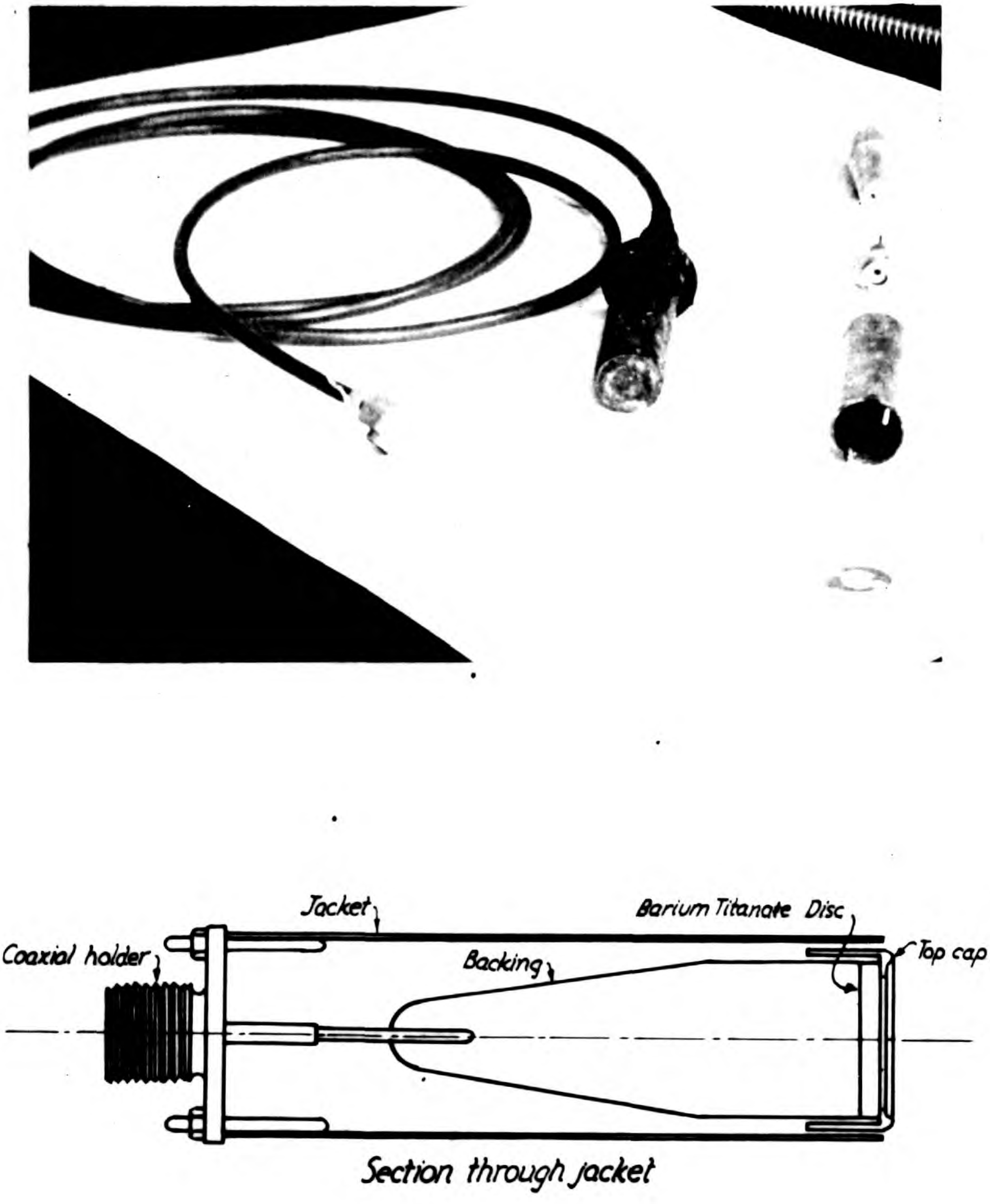

FIG. 10. DETECTOR - ASSEMBLY

Brass $= 2.90 \times 10^6$

Aluminium $= 1.39 \times 10^6$

$BaTiO_3$ $= 2.37 \times 10^6$

and the choice of these materials for backing prevents reflections occurring at the interface between the backing and the disc. Disc No. 21 was backed with brass and disc No. 35 was backed with aluminium. By tapering the backing toward the remote end, the possibility of reflection from this end was further reduced. Of great importance in lowering the Q is the fit of the disc to the backing and immense improvement was obtained by removing the silver plate from the disc and grinding it on the face of the backing with fine grade carborundum powder (Aloxite No.125) until both could be wrung together. To make a permanent bond, various kinds of cement were tried ranging from a mixture of beeswax and resin to dental plastics and cement, but all, being highly non-conducting, required the insertion of a strip of foil between disc and backing, spoiling the effect of the fit obtained by grinding. This was avoided by smearing disc and backing with Aquadag, then heating the join gently until the Aquadag was dry. To make the backing most effective, best results were obtained by making the sealing film as thin as possible. A strip of silver foil was connected between the front face of the disc and the jacket to provide an earth return.

The purpose of the aluminium cap is demonstrated in Fig. 11 showing the output of the detector when mounted directly in front of the spark in air, during stages of construction. Figs. 11a and 11b show the output of the disc and backing alone, (discs 35 and 21 respectively), and superimposed on the damped pulse is a considerable high frequency component which is reduced by the addition of the cap, Figs. 11c and 11d. To avoid "chatter" on the Barium Titanate disc, the inside surface of the cap was plugged with Apiezon Q wax or plasticene and then squeezed onto the disc. Figs. 11e and 11f show the output of the detectors when completely assembled. The complete detectors were coated with Bostik rubber cement and then dipped in paraffin wax to make them waterproof.

The Character of the Source Pulse.

The character of the source pulse is shown in Fig. 12. These records were made with the spark completely shielded as described in the pick-up section (Chapter I). Records (12a) and (12b) are for detector No. 35 in air, immediately in front of the spark, and show a considerable rarefaction following the initial compression. Figures 12c and 12d at 500 and 150 microsecond timebases respectively, were recorded with the detector mounted in front of the spark as before, but with the detector submerged in water

No. 35

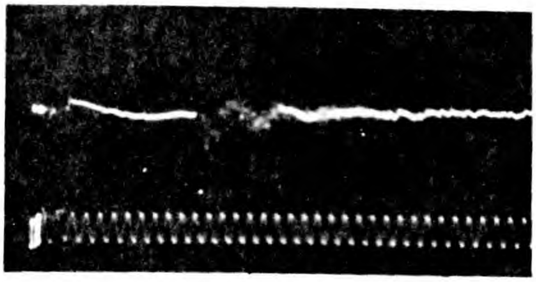

(a) 1500 μ SECS 25 KC GAIN 3000

No. 21

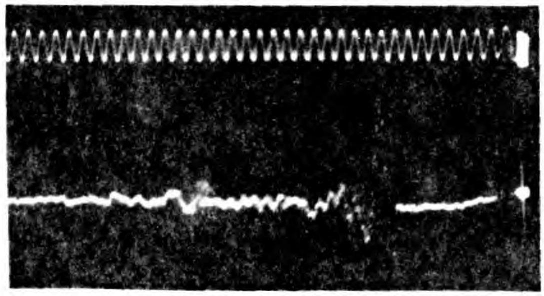

(b) 1500 μ SECS 25 KC GAIN 3000

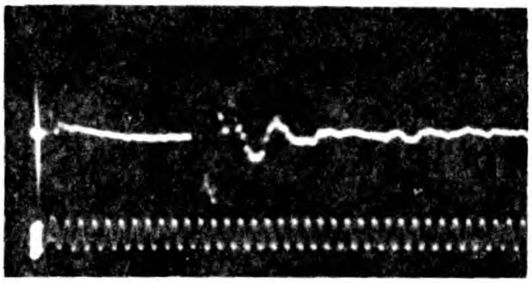

(c) 1500 μ SECS 25 KC GAIN 3000

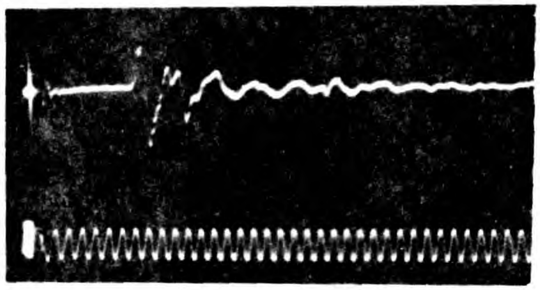

(d) 1500 μ SECS 25 KC GAIN 1700

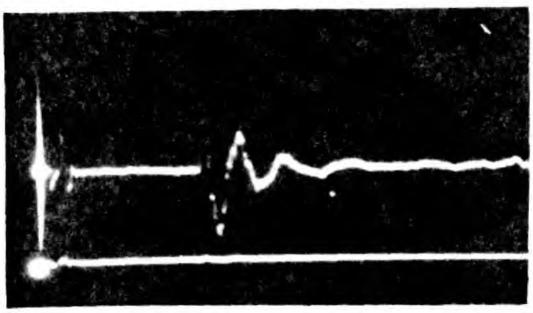

(e) 1500 μ SECS GAIN 3000

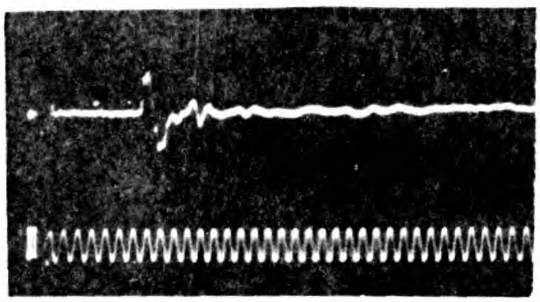

(f) 1500 μ SECS 25 KC GAIN 1700

FIG. 11. DETECTOR OUTPUT DURING ASSEMBLY

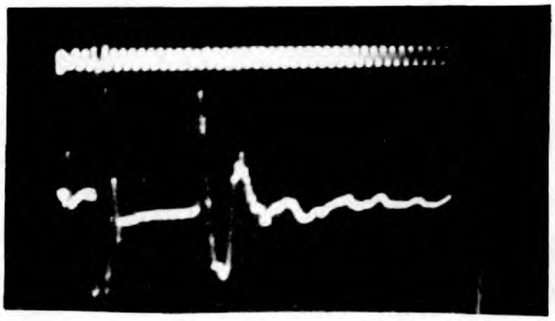

a 500 μ SECS : 50 KC : GAIN 5000
DISTANCE FROM SOURCE 7·94 CMS.

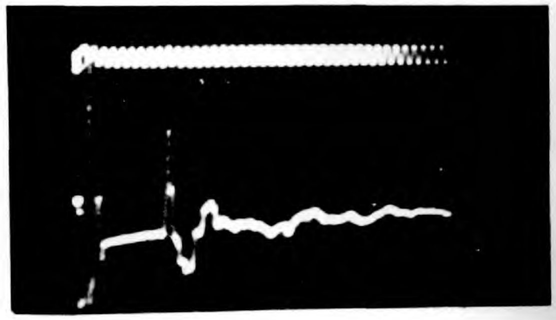

b 500 μ SECS : 50 KC : GAIN 5000
DISTANCE FROM SOURCE 7·62 CMS.

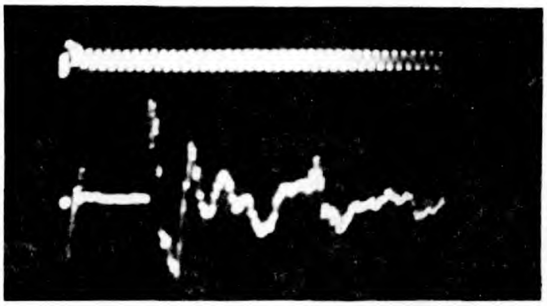

c 500 μ SECS : 50 KC : GAIN 5000
DISTANCE FROM SOURCE 7·62 CMS.
DEPTH IN WATER 1·27 CMS.

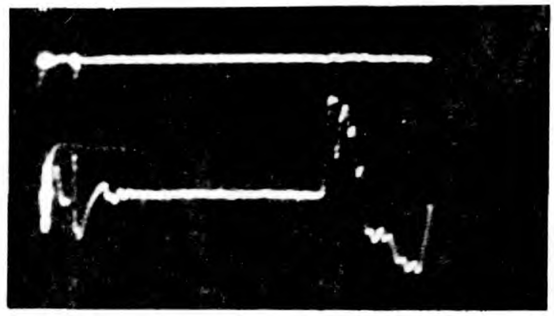

d 150 μ SECS GAIN 5000
DISTANCE FROM SOURCE 7·62 CMS.
DEPTH IN WATER 1·27 CMS.

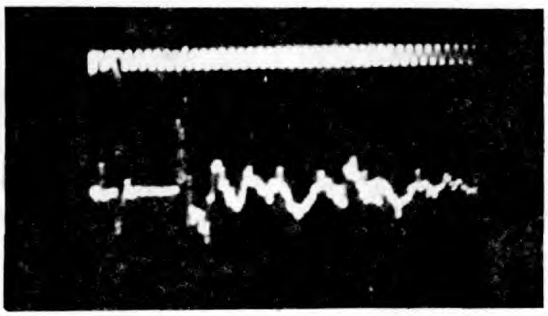

e 500 μ SECS : 50 KC : GAIN 5000
DISTANCE FROM SOURCE 7·62 CMS.
DEPTH IN WATER 3·97 CMS.

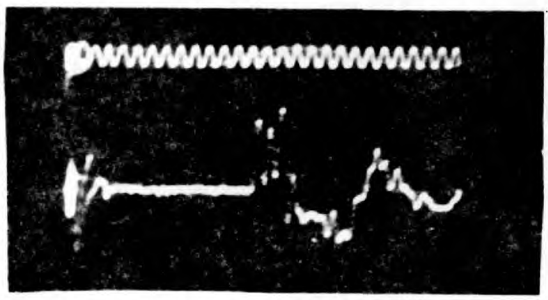

f 150 μ SECS : 100 KC : GAIN 5000
DISTANCE FROM SOURCE 7·62 CMS.
DEPTH IN WATER 3·97 CMS.

FIG.12. CHARACTER OF SOURCE PULSE

to a depth of 1.27 cms. Figures 12e and 12 f represent the same situation but with 4 cms. of water above the face of the detector. A number of small rarefactions and compressions superimposed upon the main compression are evident in 12d and 12f. These effects are apparently due to reflections from the screening surrounding the spark. Records 12c and 12e in addition indicate in that part of the trace following the initial compression, a considerable amount of interaction between the water surface and the front plate of the spark.

Fig. 13 shows the effect of removing the screening surrounding the spark. Initially, only the aluminium plate on the front was removed, retaining the screening at the sides and the space surrounding the electrodes packed with sponge rubber. The effect, Figs. 13a and 13b, for both air and water, showed no reflections and a considerably shorter pulse. The sponge rubber behind the electrodes is also effective in reducing the rarefaction following the initial impulse as 13c, 13d and 13e show with the packing removed.

Figs. 13f, 13g and 13h, in air and water, show the source pulse with all screening removed, but with sponge rubber packed behind the electrodes. The pulse length is 10 secs., representing a frequency of 50 kc.p.s., and is the same in air and water, although in the latter, Fig. 13h,

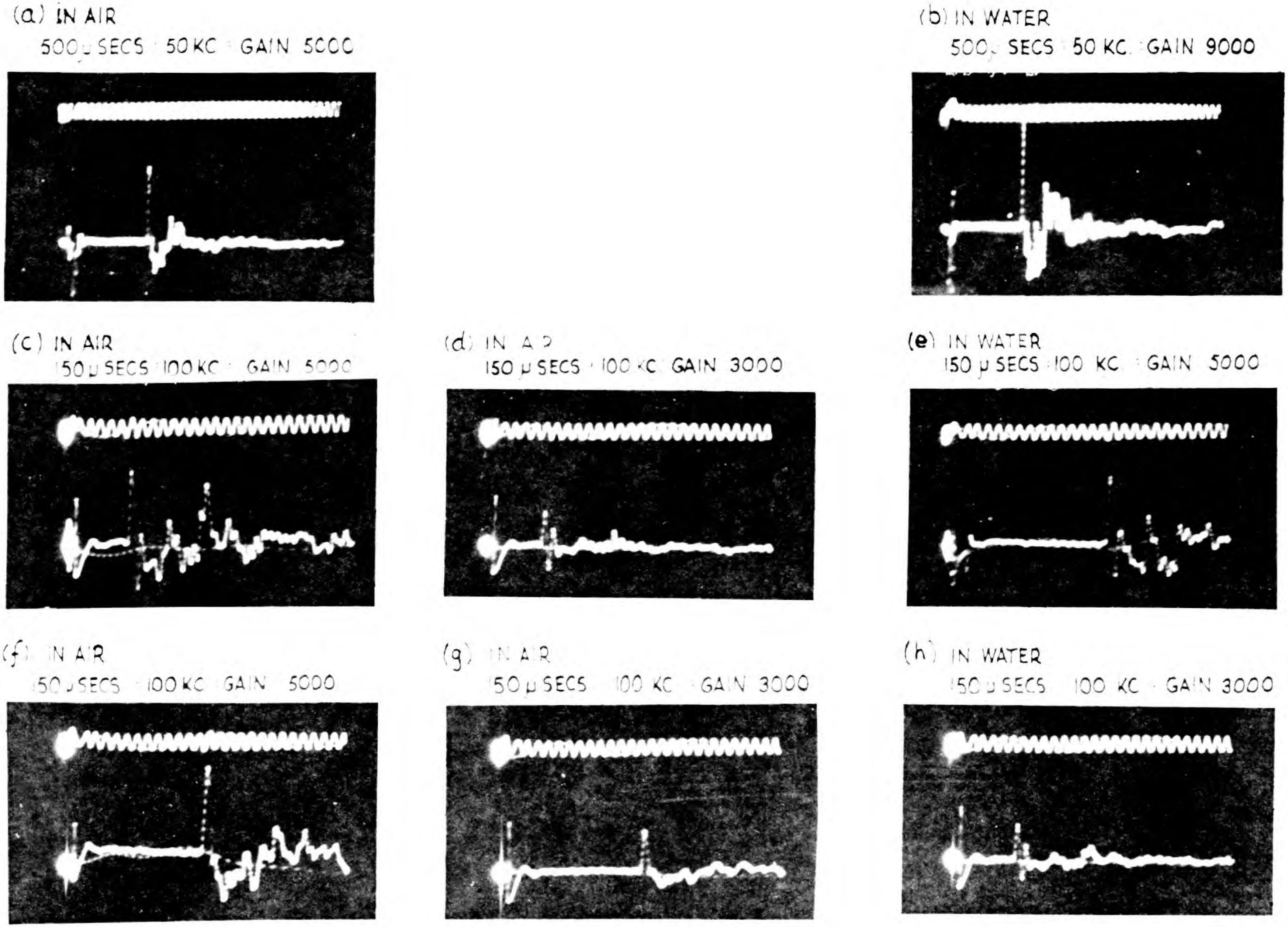

FIG.13. CHARACTER OF THE SOURCE PULSE

the rarefaction is larger.

Detector Measurements.

In all, six Barium Titanate discs were measured for their impedance, and of these, three were fractured in attempting to lower the Q value. Of the remainder, two were used in the final time-distance measurements in the tank. Only the data relevant to one detector are tabulated and calculated.

The thickness and diameter are given in Table 1 for disc 35; the thickness does not include that of the silver plating for this was finally removed as it was roughly applied and continually flaked off.

The low frequency constants were evaluated by measuring the capacity C on a Muirhead bridge with an internal generator of frequency 1000 c.p.s. Figure 14 illustrates the method of measurement of the impedance, resonant and antiresonant frequencies.

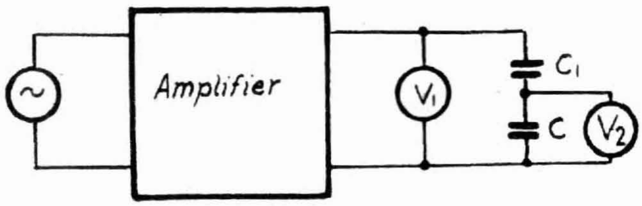

FIG.14.

The amplified output of an AVO signal generator was applied to a capacity C_1, in series with the disc C.

Readings of the voltage V_1 across the combination were made with a Furzehill diode voltmeter and the drop V_2 across the disc by a Marconi valve millivoltmeter; both instruments read R.M.S. values. The noise level was kept at a minimum by the use of coaxial cable throughout. By choosing C_1 to be of the order $\frac{C_0}{50}\mu\mu F$, the impedance load on the amplifier remained essentially capacitive at all frequencies and the voltage V_1 was kept at a constant figure by varying the output from the signal generator. To ensure that there was a minimum mechanical load on the discs, 36 S.W.G. copper leads were secured to the silvered faces by small strips of cellotape, and the disc suspended in air by the leads. The curve of V_2 against frequency, Fig. 15, illustrates the large number of resonances found. The maximum at 150 kc.p.s. is the fundamental radial mode followed by successively smaller peaks due to overtones. At 1 megacycle appears the fundamental thickness mode and its higher order modes, but it is uncertain as to the nature of the resonances preceding the fundamental. In all discs examined, a small resonance appeared between 70-80 kc.p.s. with a maximum of $\frac{1}{30}$ of the fundamental radial maximum; this was independent of the value of C_1 used, and could not be accounted for. Fig. 16 shows the radial mode in the vicinity of resonance with V_2 plotted logarithmically. From the curve, resonance occurs

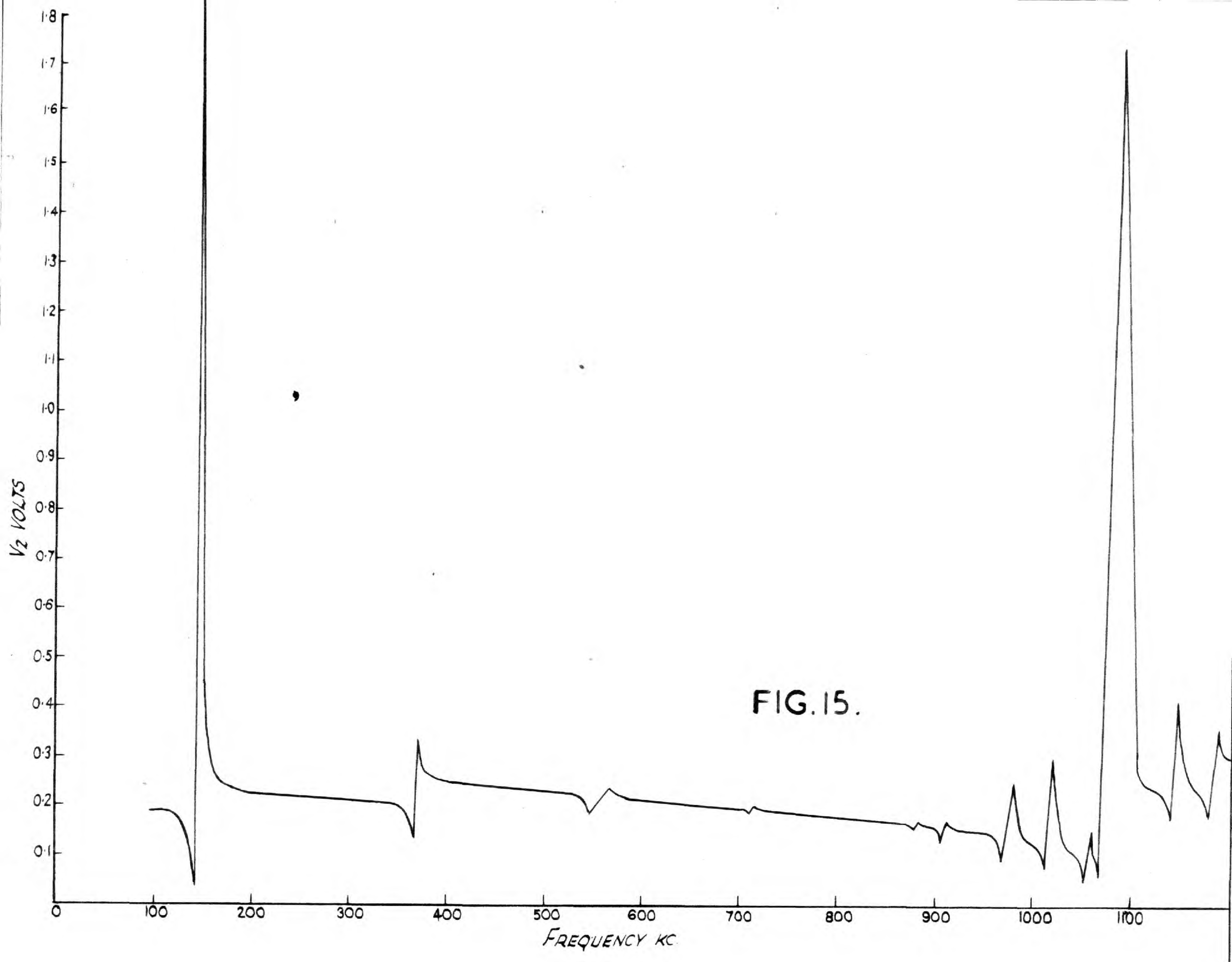

1·8
1·7
1·6
1·5
1·4
1·3
1·2
1·1
1·0
0·9
0·8
0·7
0·6
0·5
0·4
0·3
0·2
0·1
V_2 VOLTS
0
100
200
300
400
500
600
700
800
900
1000
1100
FREQUENCY KC

FIG. 15.

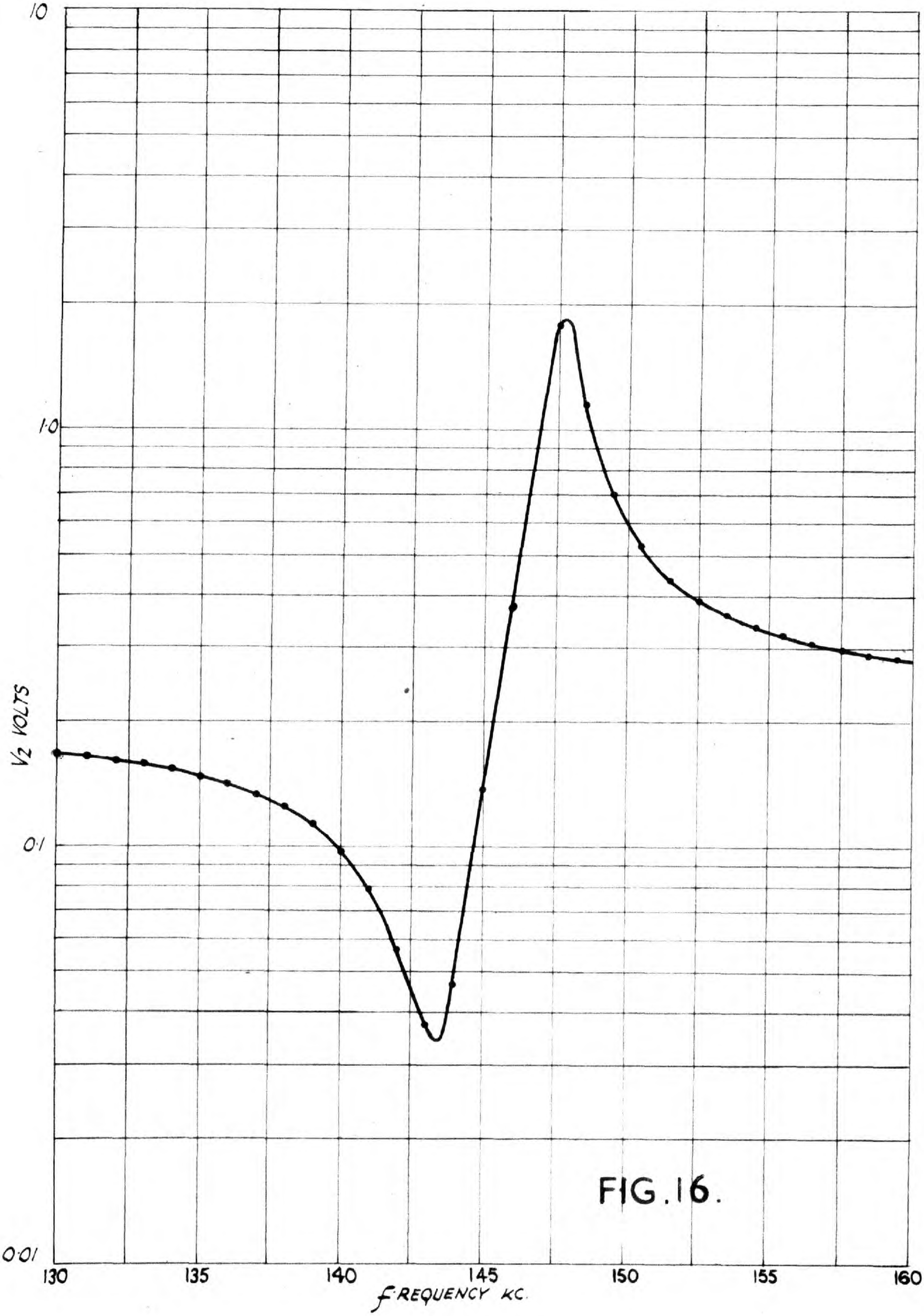

FIG. 16.

at 143.5 kc.p.s. and antiresonance at 147 kc.p.s. The maximum and minimum values were read by carefully adjusting the continuously variable frequency control of the signal generator until the voltmeter was at the top or bottom of its swing. The curves of impedance given by

$$Z_e = \frac{V_2}{\omega C_1 (V_1 - V_2)}$$

are plotted from 0-200 kc.p.s. in Fig. 17. Between 130 and 160 kc.p.s., readings were made in 1 or 2 kc.p.s. steps, all other readings in 10 kc.p.s. steps. Z_e is plotted on the logarithmic scale and follows the curve of impedance of a capacitive reactance until resonance. In the same diagram is drawn a curve of theoretical impedance with no mechanical hysteresis, which is in good agreement with the measured impedance below resonance, but becomes increasingly dissimilar at resonance. Beyond the zero impedance of resonance it falls to a minimum of $-1.73 \times 10^5 \Omega$ at 148 kc.p.s., but at the antiresonance it approaches the measured value, reaching a maximum of 4.75×10^3 ohms at 149 kc.p.s.

The constants of disc No. 35 for high Q and the detector at low Q required for the calculation of the theoretical impedance are listed in Table I. The low frequency constants $\varphi^2 C_m$ & C_0 are given by

$$C = C_0 + \varphi^2 C_m \qquad \text{equation (19), Appendix,}$$

and

$$C = \frac{C_0}{1-k^2} \qquad \text{equation (18), Appendix,}$$

k^2, the electromechanical coupling factor, is given by

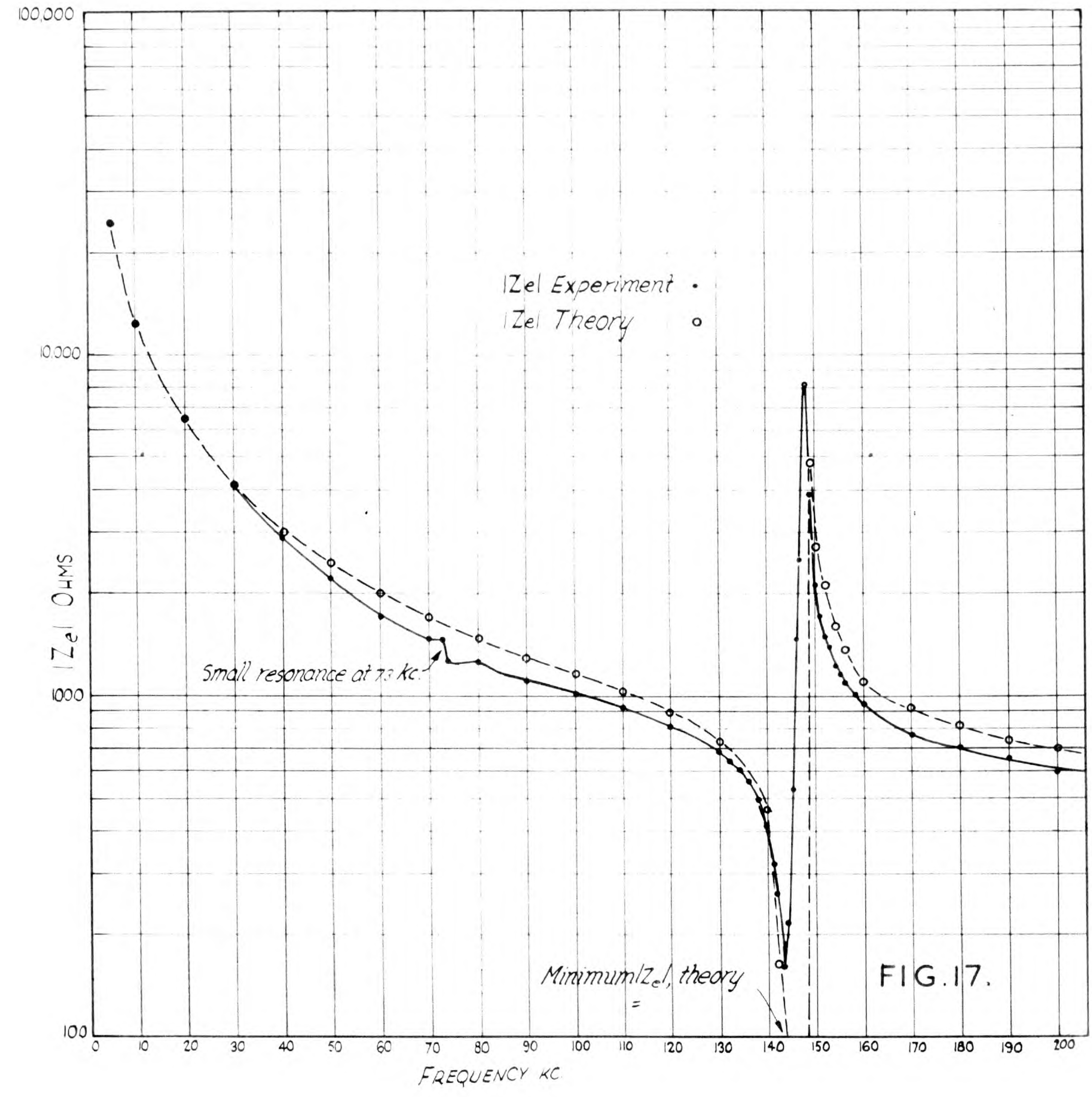
100,000
10,000
1000
100
|Ze| Experiment •
|Ze| Theory o
|Ze| OHMS
Small resonance at 73 kc.
Minimum|Ze|, theory
0
10
20
30
40
50
60
70
80
90
100
110
120
130
140
150
160
170
180
190
200
FREQUENCY KC.

FIG. 17.

$$\frac{k^2}{1-k^2} = \frac{\Delta f}{f_R} \frac{R_1^2 - (1-\sigma^2)}{1+\sigma}$$

where Δf is the separation between the antiresonant and resonant frequencies, $\sigma = 0.27$ is Poisson's ratio for Barium Titanate ($BaTiO_3$), and R_1 is the first root of the resonant condition

$$\left(\frac{\omega a}{V}\right) J_0\left(\frac{\omega a}{V}\right) - (1-\sigma) J_1\left(\frac{\omega a}{V}\right) = 0 \qquad \text{equation (14), Appendix}$$

which can be plotted for arbitrary values of $\frac{\omega a}{V}$. The value given by W. P. Mason[12] is $R_1 = 2.03$, yielding a velocity of 4.3×10^5 cm.p.s., agreeing with the value used by Schmidt[13]. A plot of $\frac{\omega a}{V} J_0\left(\frac{\omega a}{V}\right)$ and $(1-\sigma) J_1\left(\frac{\omega a}{V}\right)$ against frequency in Fig. 22 for this value gives a resonance of 143.5 kc.p.s. in agreement with the experimental value. The equation for the electrical impedance including the effect of mechanical loss (equation 22, Appendix)

$$Z_e = \frac{1}{j\omega C_0} \Big/ \left[1 + \frac{k^2}{1-k^2} \frac{(1+\sigma)\left\{J_1\left(\frac{\omega a}{V}\right) + \frac{j}{2Q}\left(\frac{\omega a}{V}\right) J_2\left(\frac{\omega a}{V}\right)\right\}}{\frac{\omega a}{V} J_0\left(\frac{\omega a}{V}\right) + \left(\frac{\omega a}{V}\right)^2 \frac{j}{2Q} J_1\left(\frac{\omega a}{V}\right) - (1-\sigma) J_1\left(\frac{\omega a}{V}\right) - (1-\sigma)\frac{j}{2Q}\left(\frac{\omega a}{V}\right) J_2\left(\frac{\omega a}{V}\right)} \right]$$

yields the Q value of the disc when the resonant condition is substituted, (equation 23, Appendix).

$$Q^2 = \frac{R_1^2}{4(A_1 - R_1)^2} \left[\left(\frac{1}{\omega_{R_1} C_0 |Z_{e_{R_1}}|} \right)^2 - \left\{ 1 + (1+\sigma) \frac{A_1 - R_1}{R_1} \right\}^2 \right]$$

and using the same constants as before, $|Z_e|$ can be calculated. This curve is shown in Fig. 18 together with the experimental $|Z_e|$, andthere is much closer agreement between the two.

When the complete detector was assembled with back-

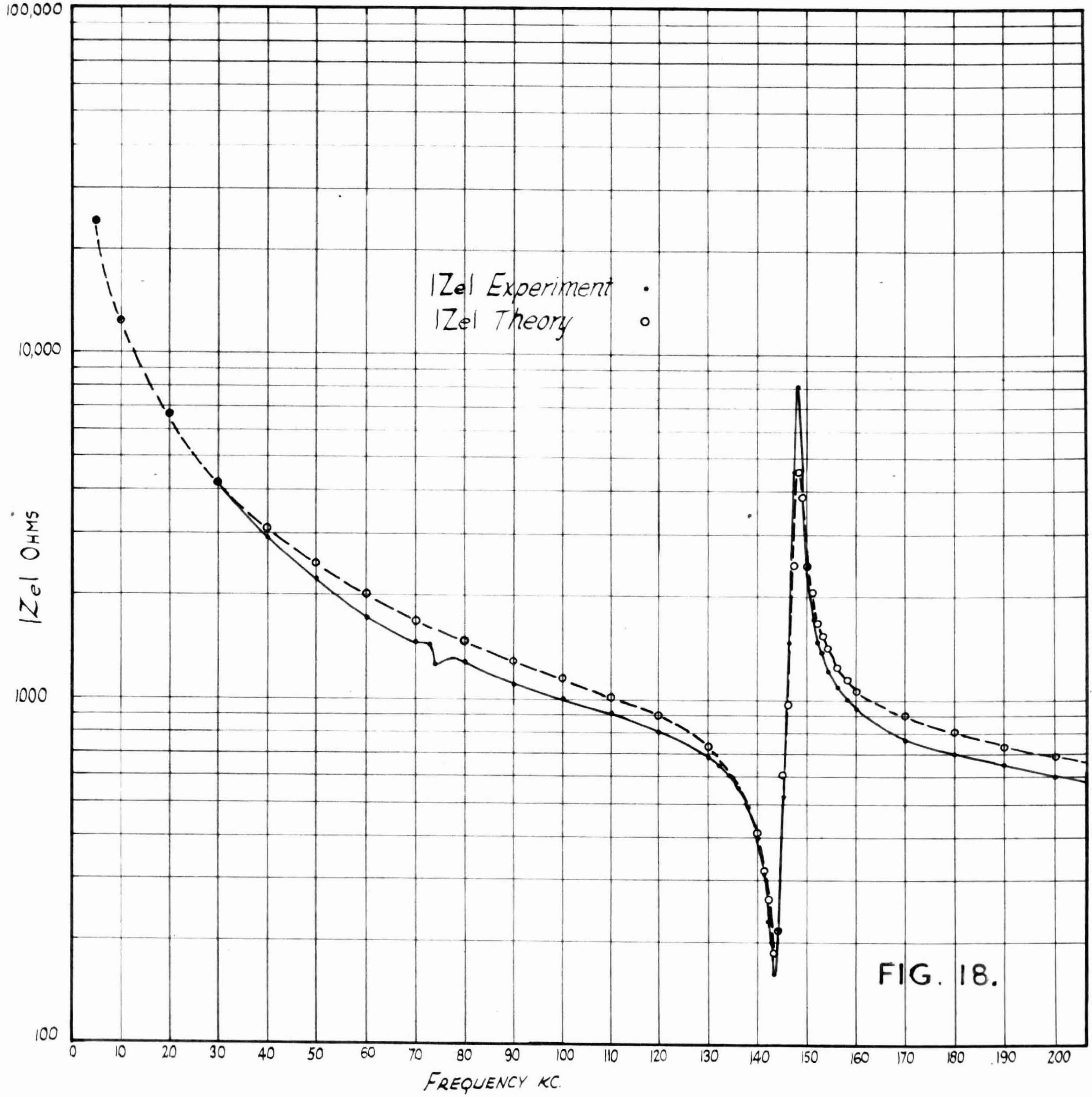
|Ze| Experiment •
|Ze| Theory o
100,000
10,000
1000
100
|Ze| OHMS
0
10
20
30
40
50
60
70
80
90
100
110
120
130
140
150
160
170
180
190
200
FREQUENCY KC.

FIG. 18.

ing and proved satisfactory by the tests of the source pulse described previously, the $|Z_e|$ was measured and the curve is shown plotted in Fig. 19 for water measurements. The loading of the detector face by water had the result of displacing the curve to position of higher $|Z_e|$; this is shown in (Fig. 20) the curve for detector No. 21. This experiment was conducted in the tank, and to avoid reflection off the bottom, a deflector plate was mounted in the water immediately below the detector, at an angle of 45° to its axis. No evidence of resonance was found for both detectors in the readings of V_2. However, there was evidence on V_1 for detector No. 35 which was found to be independant of the value of C_1 used. A curve of V_1 for this detector is given in Fig. 21 and shows that the frequency separation has increased from 3.5 kc.p.s. to 23 kc.p.s.

To achieve the desirable accuracy in the impedance expression, extra terms involving the Q value were included; as explained in the section on low Q in the Appendix, the resulting expression, (equation 24, Appendix) was

$$Z_e = \frac{1}{j\omega C_0} \Bigg/ \left[1 + \frac{k^2}{1-k^2} \frac{(1+\sigma)\left[\left\{(Qj-1)^2 - \frac{1}{8}\left(\frac{\omega a}{V}\right)^2 + (2-Qj)\right\} J_1\left(\frac{\omega a}{V}\right) - \frac{2-Qj}{2}\left(\frac{\omega a}{V}\right) J_0\left(\frac{\omega a}{V}\right)\right]}{\frac{\omega a}{V}\left[(Qj-1)^2 - \frac{1}{8}\left(\frac{\omega a}{V}\right)^2 + \frac{(1-\sigma)(2-Qj)}{2}\right] J_0\left(\frac{\omega a}{V}\right) + \left(\frac{3-2Qj}{4}\right)\left(\frac{\omega a}{V}\right)^2 J_1\left(\frac{\omega a}{V}\right) - (1-\sigma)\left[(Qj-1)^2 - \frac{1}{8}\left(\frac{\omega a}{V}\right)^2 + (2-Qj)\right] J_1\left(\frac{\omega a}{V}\right)} \right]$$

and on substituting the resonant condition, the equation for the Q value was

$$Z_{e_{R_1}} = \frac{1}{j\omega_{R_1} C_0} \Bigg/ \left[1 + \frac{A_1 - R_1}{R_1} \frac{\left(2 + \sigma - \frac{1}{8}R_1^2 - Q^2\right) - Qj\left(\frac{5}{2} + \frac{\sigma}{2}\right)}{\left(1 - \frac{R_1^2}{4\left(R_1^2 + \sigma^2 - 1\right)} - \frac{Qj}{2}\right)} \right] \quad \text{(25) Appendix}$$

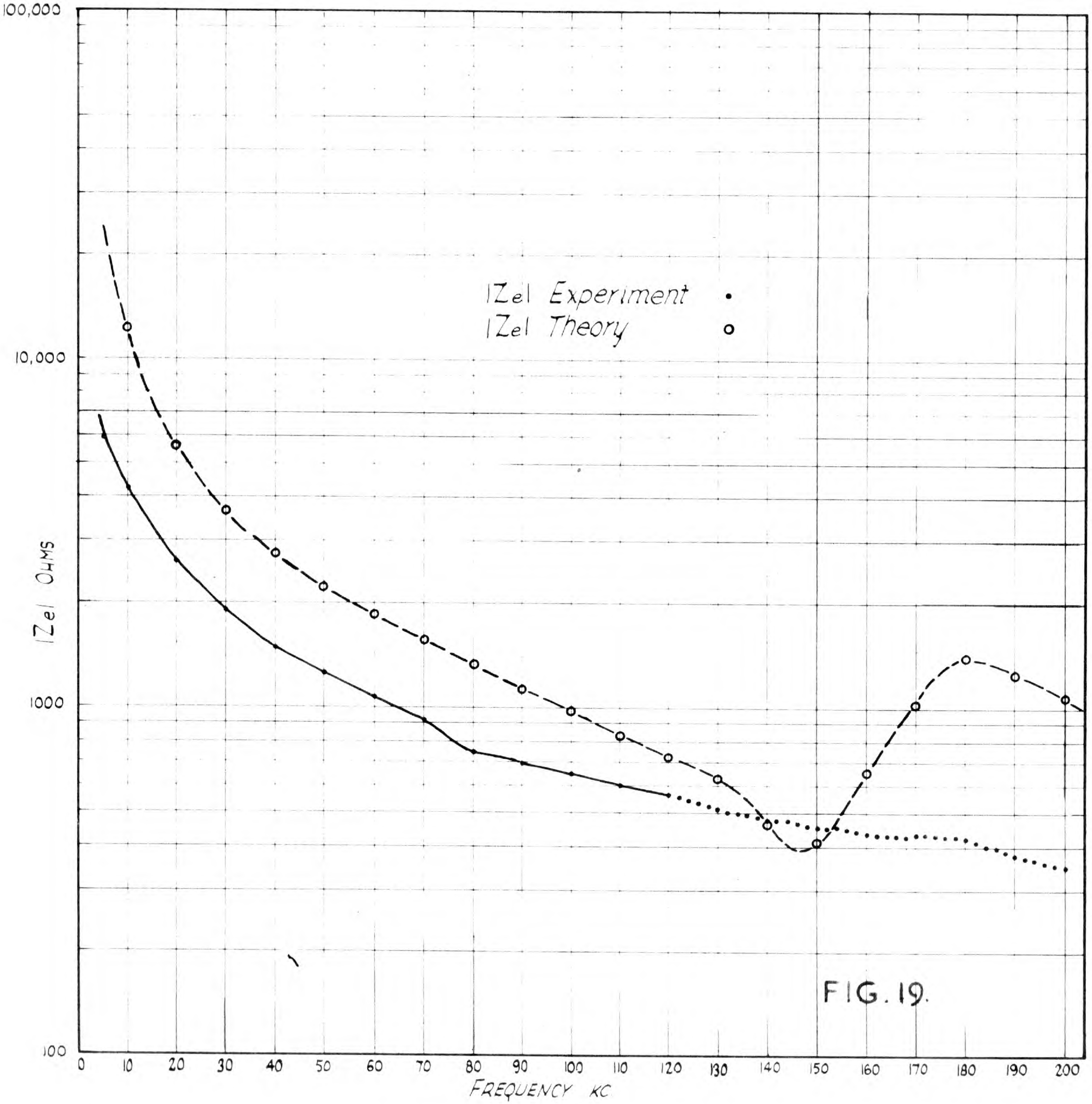

100,000
10,000
1000
100
|Ze| Experiment •
|Ze| Theory o
|Ze| OHMS
0
10
20
30
40
50
60
70
80
90
100
110
120
130
140
150
160
170
180
190
200
FREQUENCY KC

FIG. 19.

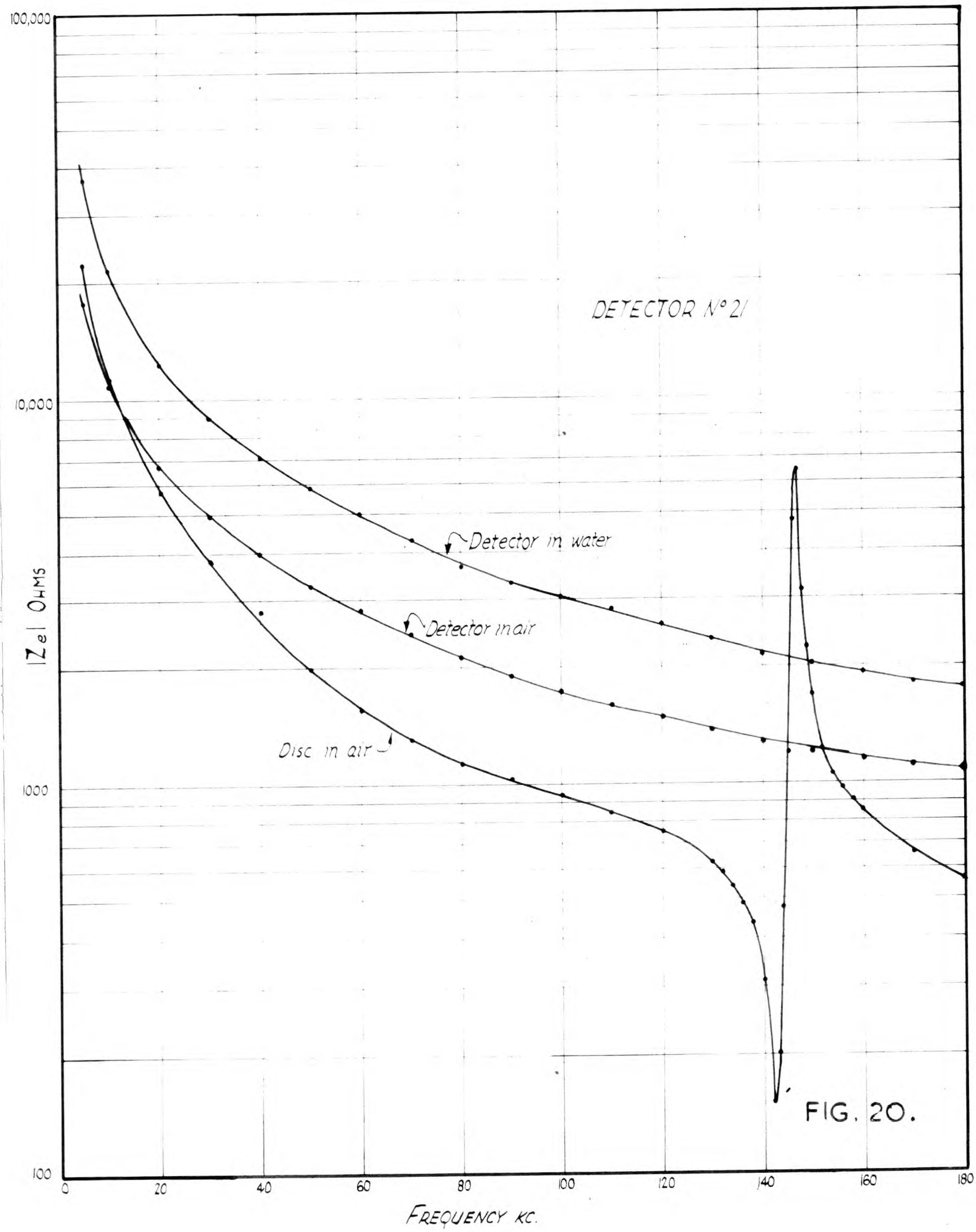

100,000
10,000
1000
100
0
20
40
60
80
100
120
140
160
180
|Ze| OHMS
FREQUENCY KC.
DETECTOR N° 21
Detector in water
Detector in air
Disc in air

FIG. 20.

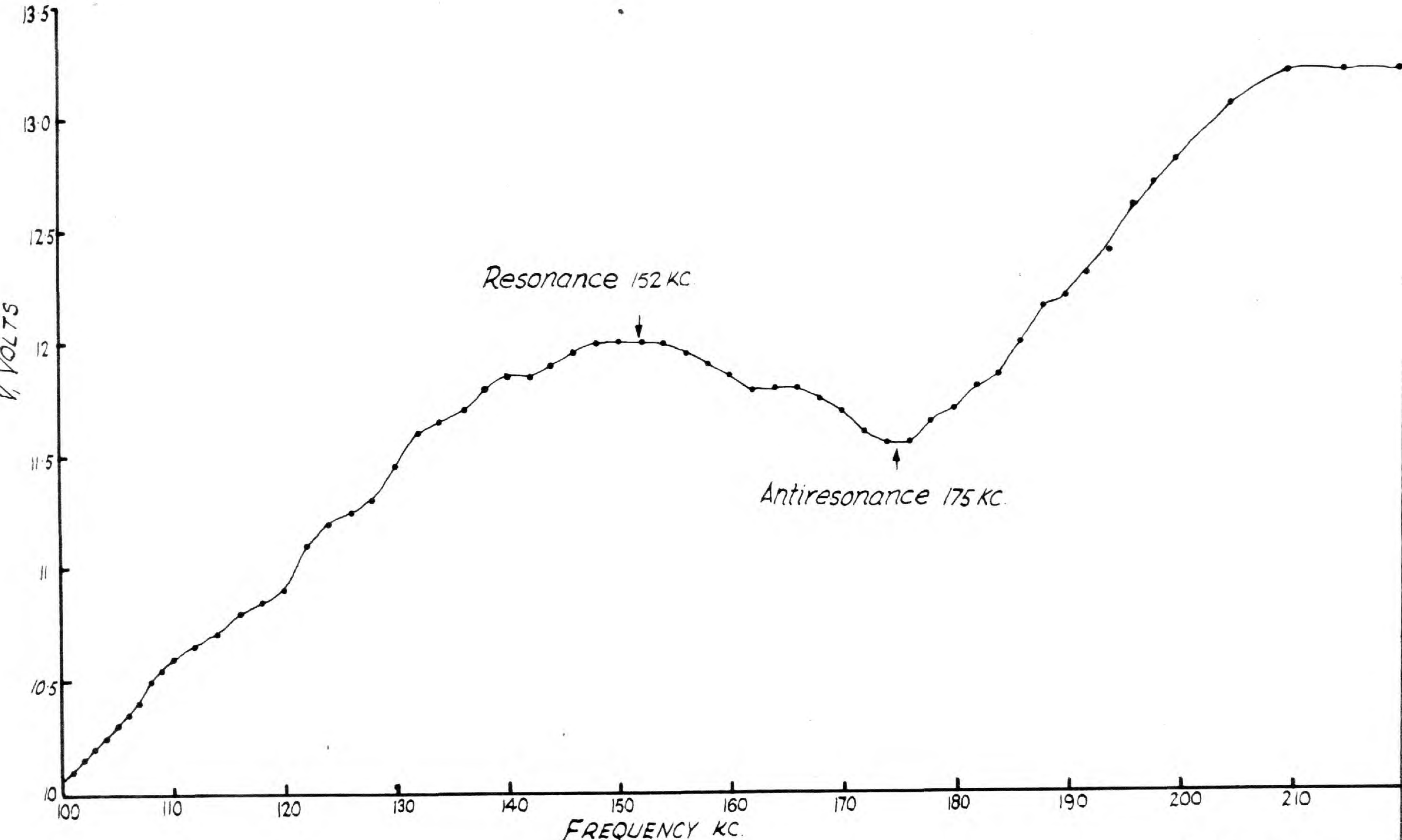

Resonance 152 KC
Antiresonance 175 KC
V_1 VOLTS
FREQUENCY KC
13·5
13·0
12·5
12
11·5
11
10·5
10
100
110
120
130
140
150
160
170
180
190
200
210

FIG. 21.

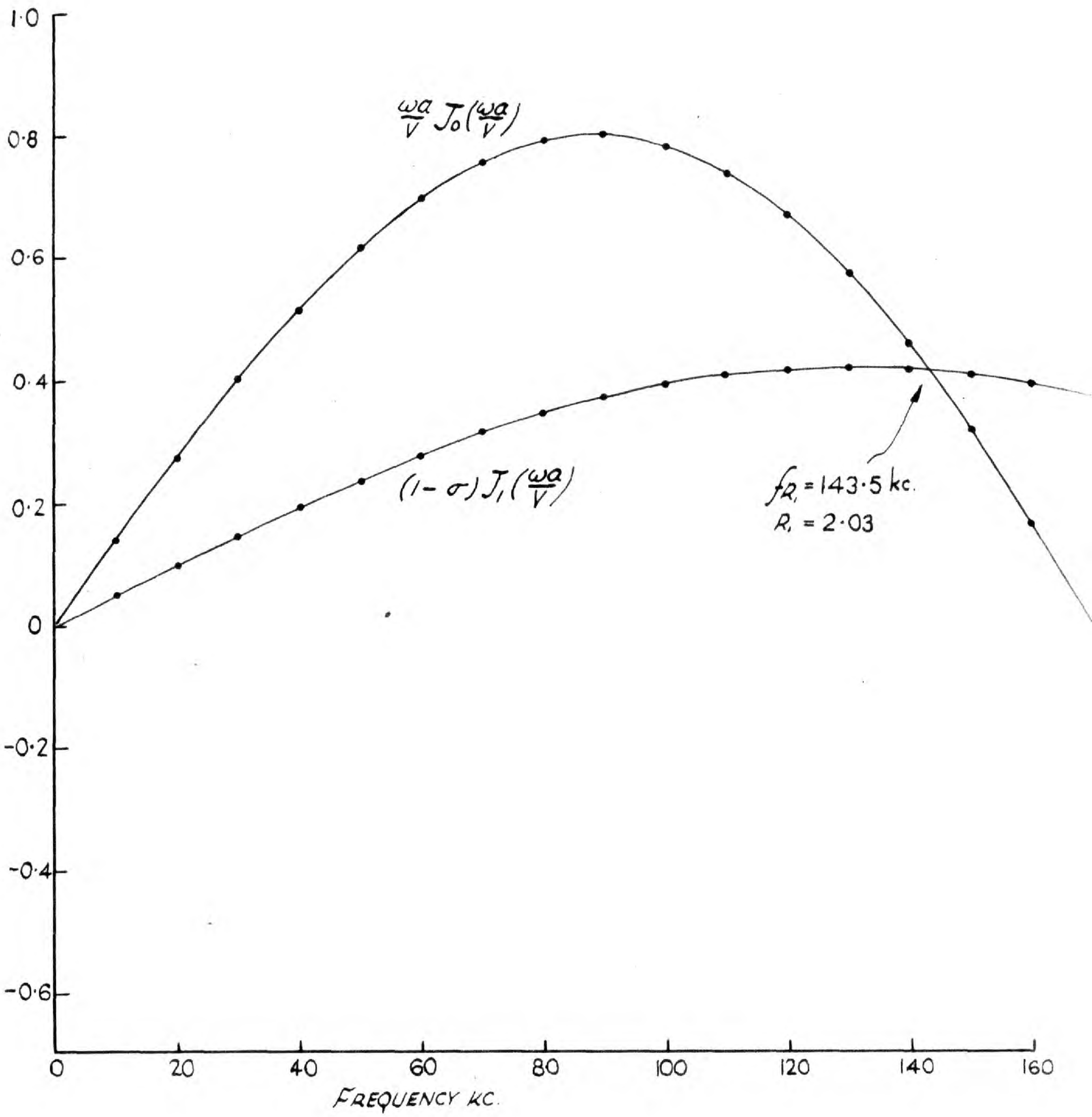
1·0
0·8
0·6
0·4
0·2
0
-0·2
-0·4
-0·6
$\frac{\omega a}{V} J_0(\frac{\omega a}{V})$
$(1-\sigma) J_1(\frac{\omega a}{V})$
f_{R_1} = 143·5 kc.
R_1 = 2·03
0
20
40
60
80
100
120
140
160
FREQUENCY KC.

FIG. 22.

There was no satisfactory agreement between theory and experiment in this case, and the probable cause was the subsequent discovery that No. 35 on which the computation was performed had developed a low insulation resistance, falling from a value $>$ 20 meg ohms to 40,000 ohms. The theoretical curve shown in Fig. 19 suggests however, that the Q value is less than the value computed. For detector No. 21 there was no evidence in the V_1 readings of resonance, and consequently, the computation was not performed.

TABLE I.

(high Q)

	Disc No. 35
Radius (a)	0.9604 cm.
Thickness: before grinding (l_t)	0.2166 cm.
Resonant frequency (f_R)	143.5 kc.
Antiresonant frequency (f_A)	147.7 kc.
Capacity (low frequency) (C)	1310 $\mu\mu F$
Radially clamped capacity (C_0)	1213.6 $\mu\mu F$
Equivalent electrical compliance ($\varphi^2 C_m$)	96.4 $\mu\mu F$
Poisson's ratio (σ)	0.27
Electromechanical coupling factor (k^2)	0.0736
Q value	126
Velocity (v)	4.3×10^5 cm.p.s.
Density (ρ)	5.5
Electrical impedance at resonance (Z_{e_R})	122 Ω
" " antiresonance (Z_{e_A})	8668 Ω

TABLE I (continued)

(low Q)

	Disc No. 35.
Radius (a)	0.9604 cm.
Thickness: after grinding (l_t)	0.2083 cm.
Resonant frequency (f_R)	152 kc.
Antiresonant frequency (f_A)	175 kc.
Capacity low frequency (C)	1400 $\mu\mu F$
Radially clamped capacity (C_0)	867.2 $\mu\mu F$
Equivalent electrical compliance ($\varphi^2 C_m$)	532.8 $\mu\mu F$
Poisson's ratio (σ)	0.27
Electromechanical coupling factor, k^2	0.28
Q value	7
Velocity (v)	4.52×10^5 cm.p.s.
Density (ρ)	5.5
Electrical impedance at resonance (Z_{eR})	452 Ω
" " antiresonance (Z_{eA})	430 Ω

CHAPTER III.

THE MODEL SEISMIC EXPERIMENT.

Procedure.

In making a time-distance traverse across the tank the spark was kept in a fixed position and the detector moved at regular intervals along its supporting rail. For each experiment the depth of the water, the height of the spark above the water and each detector position were measured with an accurately graduated inch steel scale. Since a residual charge remained on the spark electrodes after a "shot" the position of the spark relative to the side of the tank was determined before beginning a traverse and thus it was only necessary to measure the detector position from the same point on the wall. The height of the spark above the water surface was not a true indication of the source point since the discharge arced forward from the electrodes. It was found that for heights less than 2 cms. the explosive force of the discharge splashed water over the electrodes, thus producing a short circuit. The tank was mounted with its floor lying in a horizontal plane and the detector rail was positioned parallel to it.

In preparing for an experiment the amplifier, oscilloscope, control oscillator and high voltage power supply were switched on and allowed to warm up for 5 minutes, but a half-hour was required for the timing oscillator.

Records.

The timing trace is only shown on the records for the nearest and furthest detector positions in the records illustrated, but all time measurements were made on the time trace recorded with each position. This eliminated any error due to shrinkage of the paper and variation of the time base speed. An erratic behaviour of the triggering was experienced necessitating considerable care in the selection of the origin of the shot. This erratic behaviour was due to a variable time delay between the two sparks ranging from 0 to as much as 40 μ secs. However, the presence of pick-up at the beginning of the trace provided a good indication of the zero point. Pick-up was not entirely eliminated and as the records show (Fig. 26), it could also, on occasion, affect the time base in addition to distorting the trace.

Detector No. 35 was used at the outset as less pick-up was encountered. The records with No. 35 did not possess the clarity of those with No. 21 which was used with a different oscilloscope with improved focusing. All records obtained with No. 21 are presented, and it was intended to repeat the same process with No. 35, but lack of time prevented this. Despite its low insulation resistance, No. 35 produced an excellently damped record but its output was much less than that of No. 21. The model selected for study was a slab of purple slate 48 cms. x 63.5 cms. x 3.8 cms., which showed practically no cleavage as when chipped at the edge, it did not break along cleavage planes. A greater thickness would have been preferable, but consideration had to be given to the mass the floor of the tank could bear. In each experiment, the slab was placed in the tank with its longest axis in the vertical plane of the spark-detector line. Its position relative to the tank walls is indicated in the insert on the time-distance curve corresponding to each experiment.

Any air bubbles present on the face of the detector, when immersed in the water, were removed before each experiment as it was found that their presence produced distortion of the wave-form and an apparent loss of gain in the amplifier.

The Results.

The tank was traversed both vertically and horizontally before experimenting with the slate slab in position. The vertical records are shown in Fig. 23 for a spark-detector separation of 30 cms. and a total change in depth of 7.3 cms. The increase in depth of the detector was obtained by adding water to the tank, and as the water level increased, the spark was raised to clear the surface,

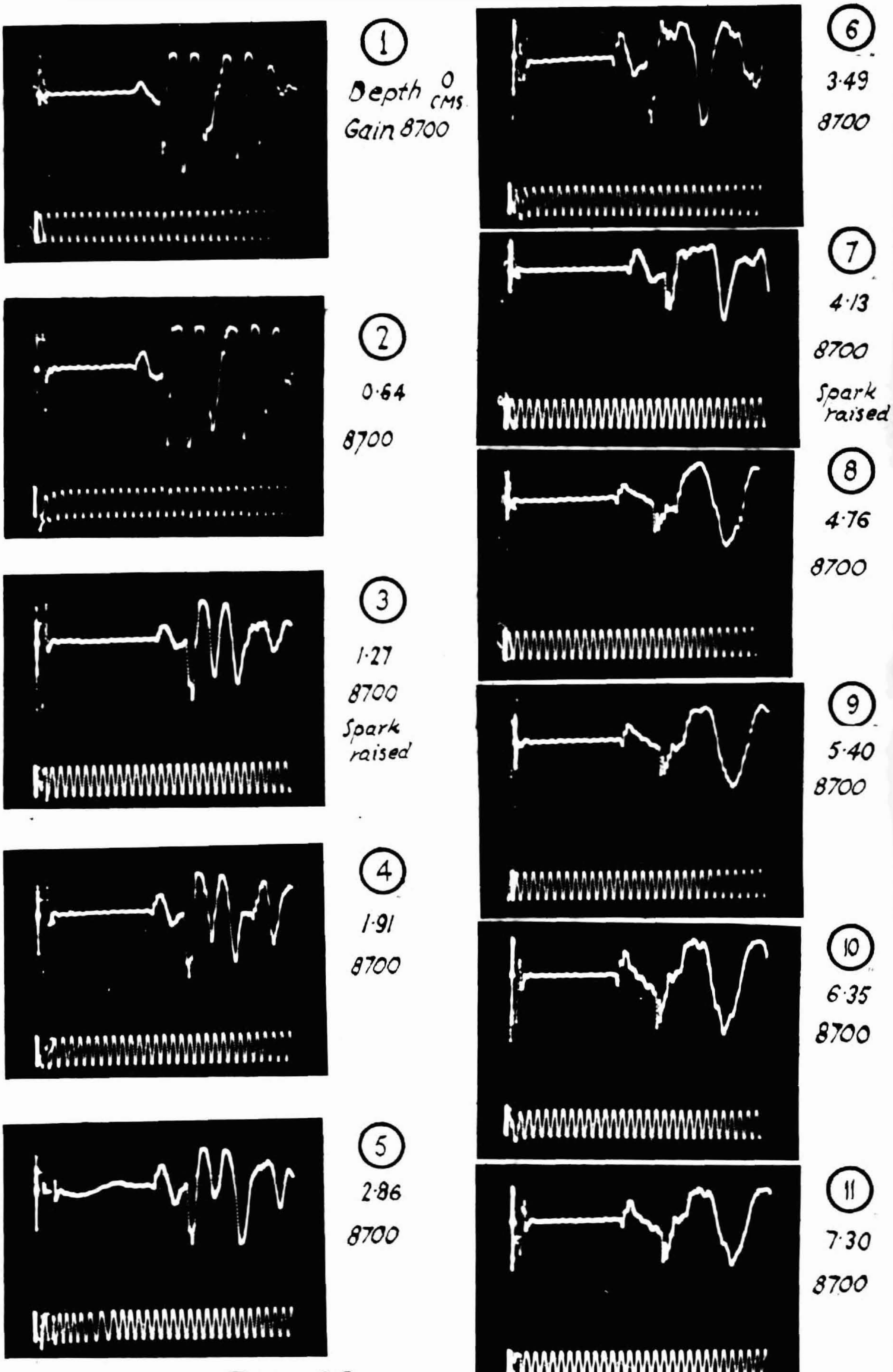
1
Depth 0 CMS
Gain 8700
2
0·64
8700
3
1·27
8700
Spark raised
4
1·91
8700
5
2·86
8700
6
3·49
8700
7
4·13
8700
Spark raised
8
4·76
8700
9
5·40
8700
10
6·35
8700
11
7·30
8700

FIG. 23.

and in no instance did the clearance exceed 3.8 cms. The depth of the detector below the water surface is indicated against each record and the timing wave on each is 50 kc.p.s.

In record No. 1 the first arrival is the direct longitudinal (P) wave followed by a reflection (PP_1) from the floor of the tank. Succeeding this at an interval of 116 μ secs. is a multiple reflection (PP_1^*) between the water surface and tank floor. Both these latter arrivals are characterised by a very high frequency motion, of the order of 150 kc.p.s., superimposed upon the envelope of the direct wave. This characteristic of the reflected wave served as a means of identification of the arrival in the time-distance traverses across the tank.

In records 8 - 11, the first reflection is followed, after a time of 22 μ secs., by a sudden onset. The thickness of the wooden base was 3.5 cms. and the velocity, from measurements on the time-distance curve of T.D. IX (Fig. 25) was 4150 $\pm$ 100 metres p.s. The minimum reflected path within the base therefore corresponds to a time of 16 μ secs. so that in all likelihood this onset arises from reflection within the tank base.

A marked change in waveform occurs as the depth of the detector below the surface increases, the period changing from 54 μ secs. at the surface to 132 μ secs. in record No. 11. This is apparently brought about by the rapid amplitude attenuation of the second rarefaction which is completely absent in record No. 8. The effect seems to be entirely related to the depth of the detector below the water surface, for small changes in the distance of the spark from the water have no noticeable result. A study of the horizontal traverse T.D. IX, Fig. 24, indicates that changes in the path length of the reflected components produce little alteration of the wave form. For each detector position, two records were made and there was no indication of change in the intensity of the spark. In all cases the records were identical. From TD IX, the velocity in water is 1530±20 metres p.s., so that the period of record No. 1 corresponds to a wavelength in water of 8 cms. Since the second rarefaction is entirely eliminated in record No. 7 at a depth of 4.1 cms., there is a possibility of interference occurring between the first reflection and the direct wave. It was unfortunate that further experiments on this phenomenon were prevented by the eventual breakdown of the insulation at the spark electrodes. However, the evidence of TD XI, Fig. 28, a traverse across the tank with the detector immersed in the water to a depth of 8.6 cms., suggests that at greater depths, or as the detector approaches the base of the tank, the period decreases. In all the records of this traverse, the period of the waveform is of the order of 40 μ secs., similar to that of record No. 1 of the vertical traverse.

T.D. IX.

The records of this horizontal traverse are shown in Fig. 24 and the time-distance curve in Fig. 25, the data for which are given in Table II. This experiment was performed with no model present and a depth of 12.7 cms. of water in the tank. Against each record is indicated the total amplifier gain and the shot-detector distance. The lines on the records denote the arrivals plotted on the time-distance curve. The (P) arrival does not pass through the origin since a finite time is required for the passage of the spark pulse through air.

It was virtually impossible to discern any surface wave, which would be expected in the initial records, due to the large phase A at 420 metres p.s. which is possibly the sound wave in air. The first arrival at 1530 ± 20 metres p.s. is the direct longitudinal (P) wave which gives way to the refracted wave (PP_2) from the base of the tank in record No. 12. The base of the tank was made of teak, the refracted wave being propagated along the grain. The velocity, measured on the time-distance curve, Fig. 25, is 4150±100 metres p.s., which, although no published velocity for teak is available, lies within the range 3320-4670 metres p.s.,[21] for wood where the direction of propagation is along the grain.

The second arrival, the reflected PP_1, is

T. D. IX

FIG. 24.

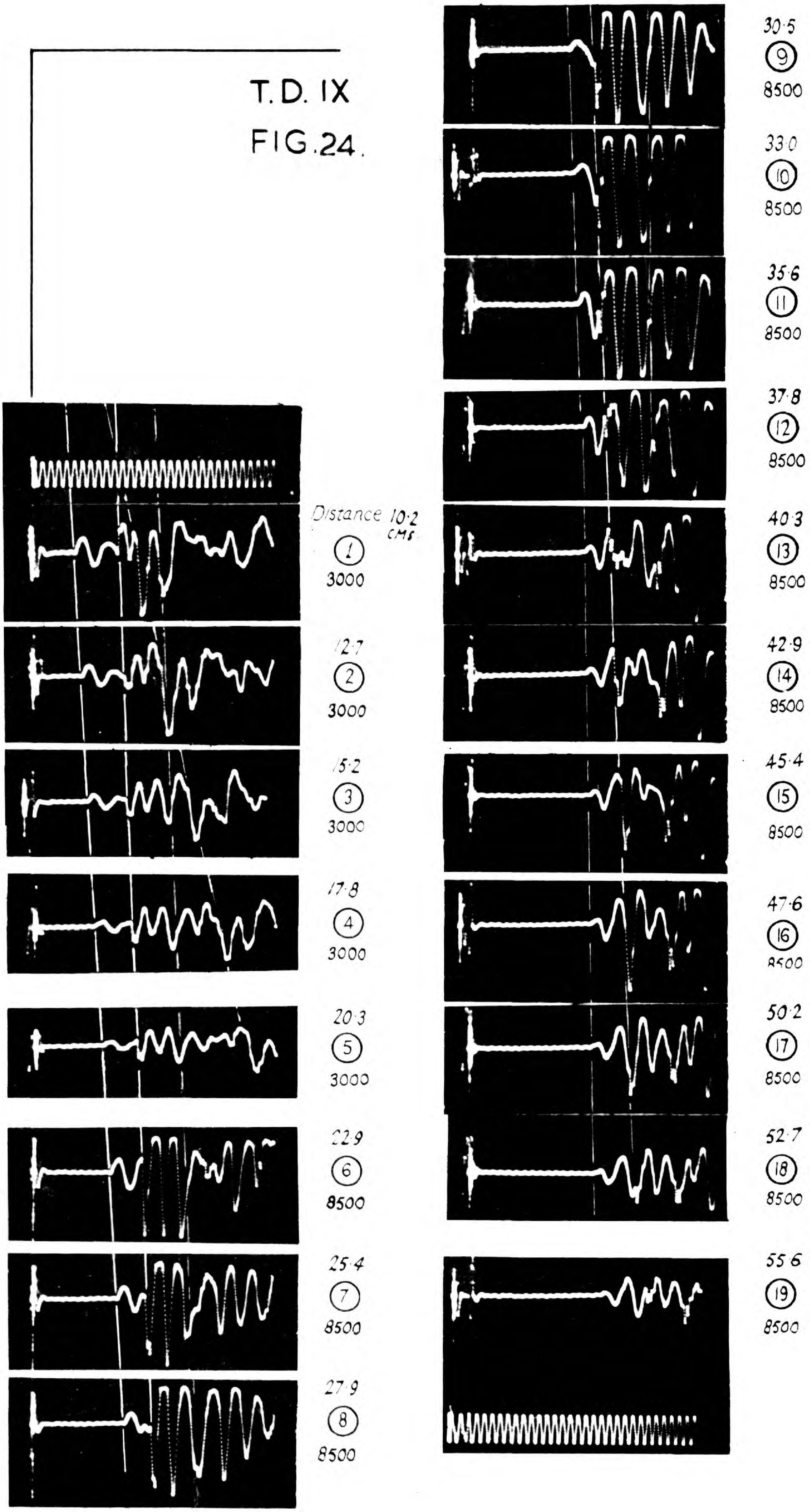
Distance 10·2 CMS
1
3000
12·7
2
3000
15·2
3
3000
17·8
4
3000
20·3
5
3000
22·9
6
8500
25·4
7
8500
27·9
8
8500
30·5
9
8500
33·0
10
8500
35·6
11
8500
37·8
12
8500
40·3
13
8500
42·9
14
8500
45·4
15
8500
47·6
16
8500
50·2
17
8500
52·7
18
8500
55·6
19
8500

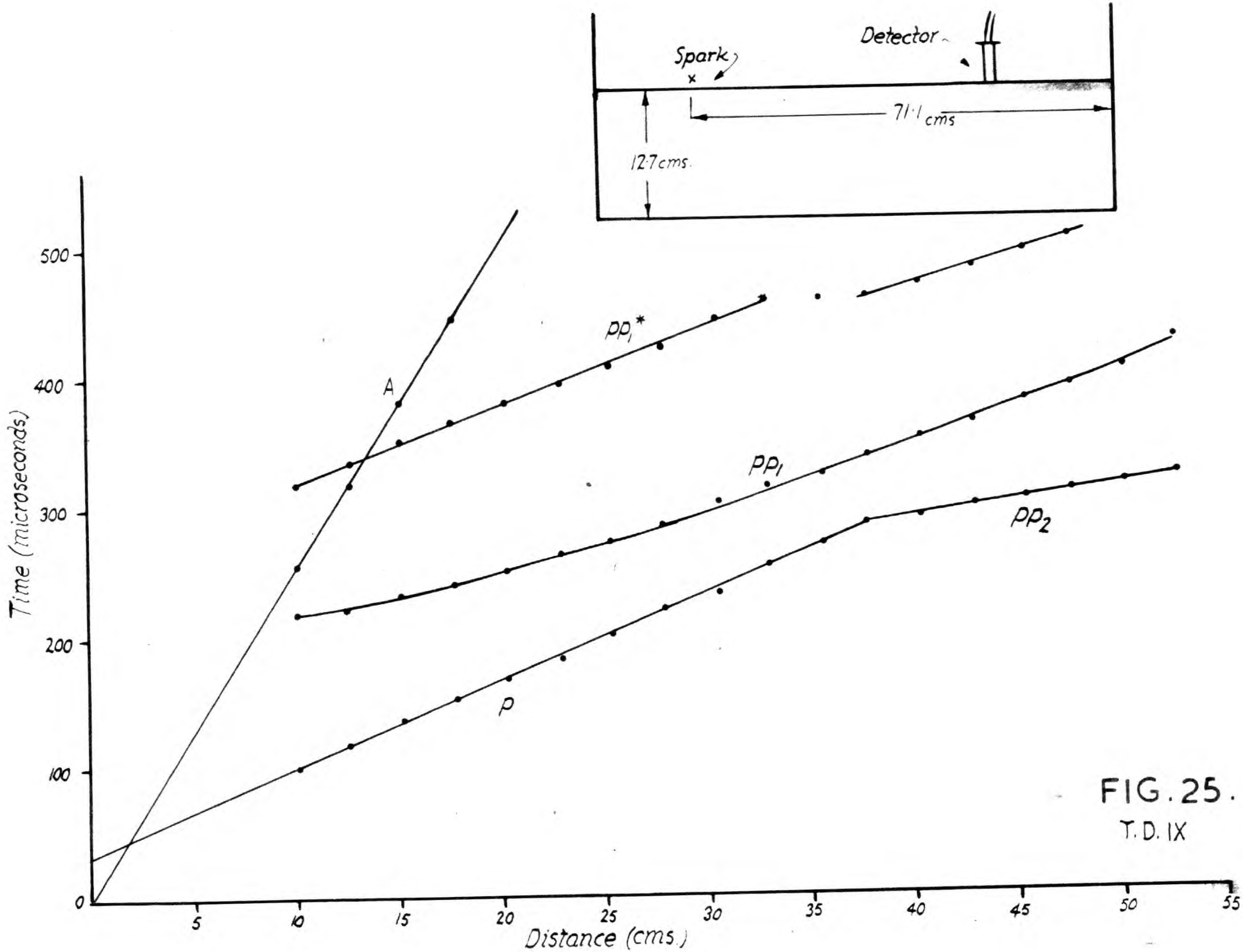
Spark
Detector
71·1 cms
12·7 cms.
Time (microseconds)
500
400
300
200
100
0
A
pp_1^*
pp_1
pp_2
p
5
10
15
20
25
30
35
40
45
50
55
Distance (cms.)

FIG. 25.
T. D. IX

TABLE II.

Time-distance data for T.D. IX.

Record No.	Distance (cms.)	Time (μ secs.)				
		P	PP_1	PP_2	PP_1^*	A
1	10.2	110	220		320	256
2	12.7	124	222		336	318
3	15.2	140	232		352	380
4	17.8	152	241		364	445
5	20.3	176	250		380	
6	22.9	192	263		394	
7	25.4	208	272		408	
8	27.9	227	285		420	
9	30.5	242	302		444	
10	33.0	256	314		458	
11	35.6	274	322		458	
12	37.8	284	336	286	460	
13	40.3		352	290	470	
14	42.9		362	298	482	
15	45.4		380	304	494	
16	47.6		392	310	504	
17	50.2		406	316		
18	52.7		426	320		
19	55.6					

characterized by an onset antiphase to that of P, in addition to the high frequency component which is most evident in record No. 8.

T.D. X.

A similar traverse, Fig. 26, was made with the slate slab resting on the floor of the tank in 17.8 cms. of water. The time-distance data, Table III, are plotted in Fig. 27. The records show the same arrivals as in T.D. IX but of a slightly different character, the number of rarefactions in the waveform being fewer than those appearing in the corresponding records of T.D. IX. In record No. 12, the first arrival (P) at 1530±10 metres p.s. is replaced by a refracted wave from the slab at 4490±170 metres p.s. This arrival is barely perceptible on the records and no great accuracy is attached to the velocity. The onset of the second arrival in records Nos. 1 - 6 is clearly in the same direction as the P wave and is possibly the refraction from the slab, although this event could not be traced through to the first arrival in record No. 12. Using for identification the characteristics noted in T.D. IX for the first reflection, this arrival is clearly evident from record No. 8 onwards. Again there is evidence of a multiple reflection (PP_1^*)

T.D. XI.

In this traverse, the same experimental arrangement

T.D. X.

FIG. 26.

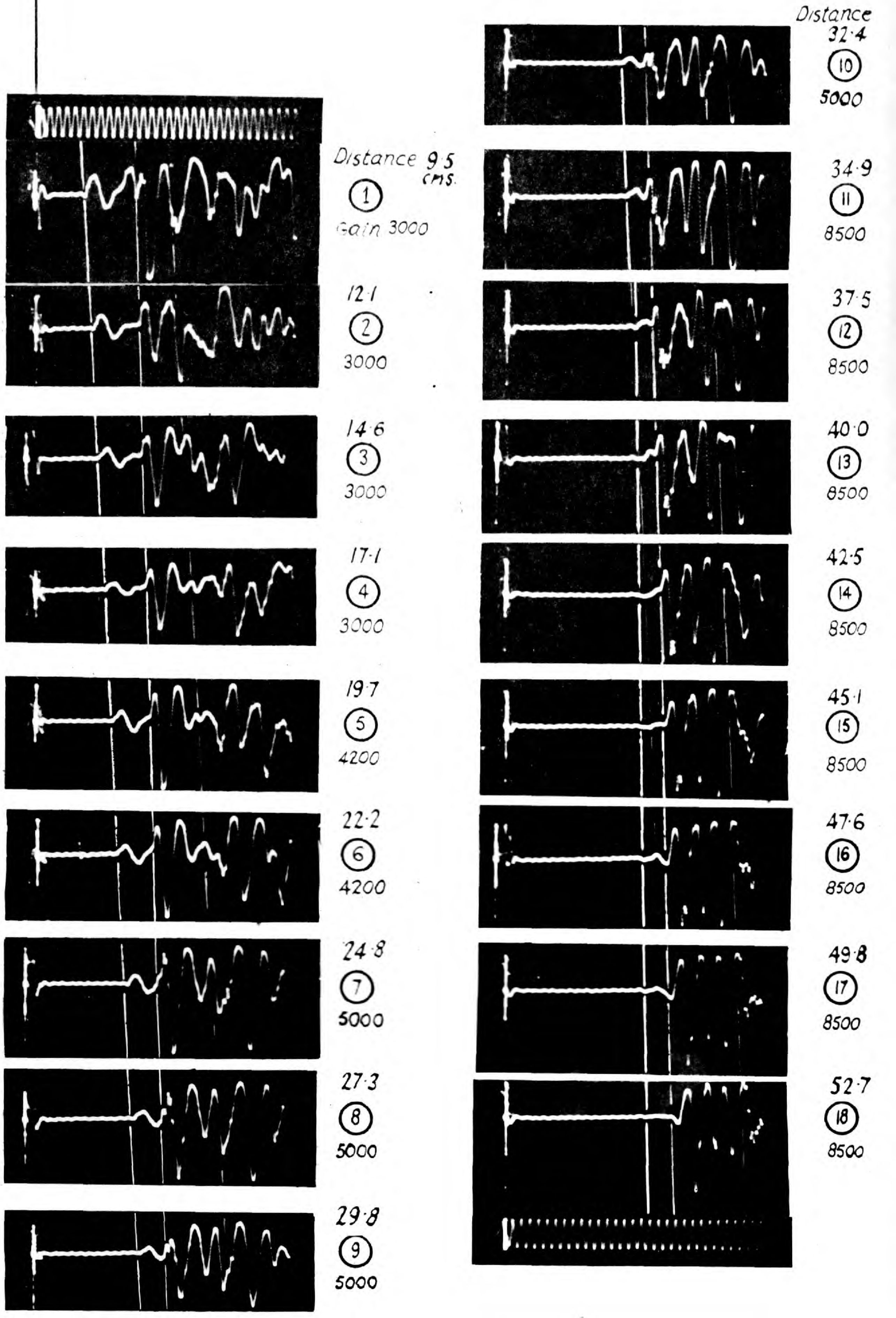
Distance 9.5 cms.
1
Gain 3000
12.1
2
3000
14.6
3
3000
17.1
4
3000
19.7
5
4200
22.2
6
4200
24.8
7
5000
27.3
8
5000
29.8
9
5000
Distance 32.4
10
5000
34.9
11
8500
37.5
12
8500
40.0
13
8500
42.5
14
8500
45.1
15
8500
47.6
16
8500
49.8
17
8500
52.7
18
8500

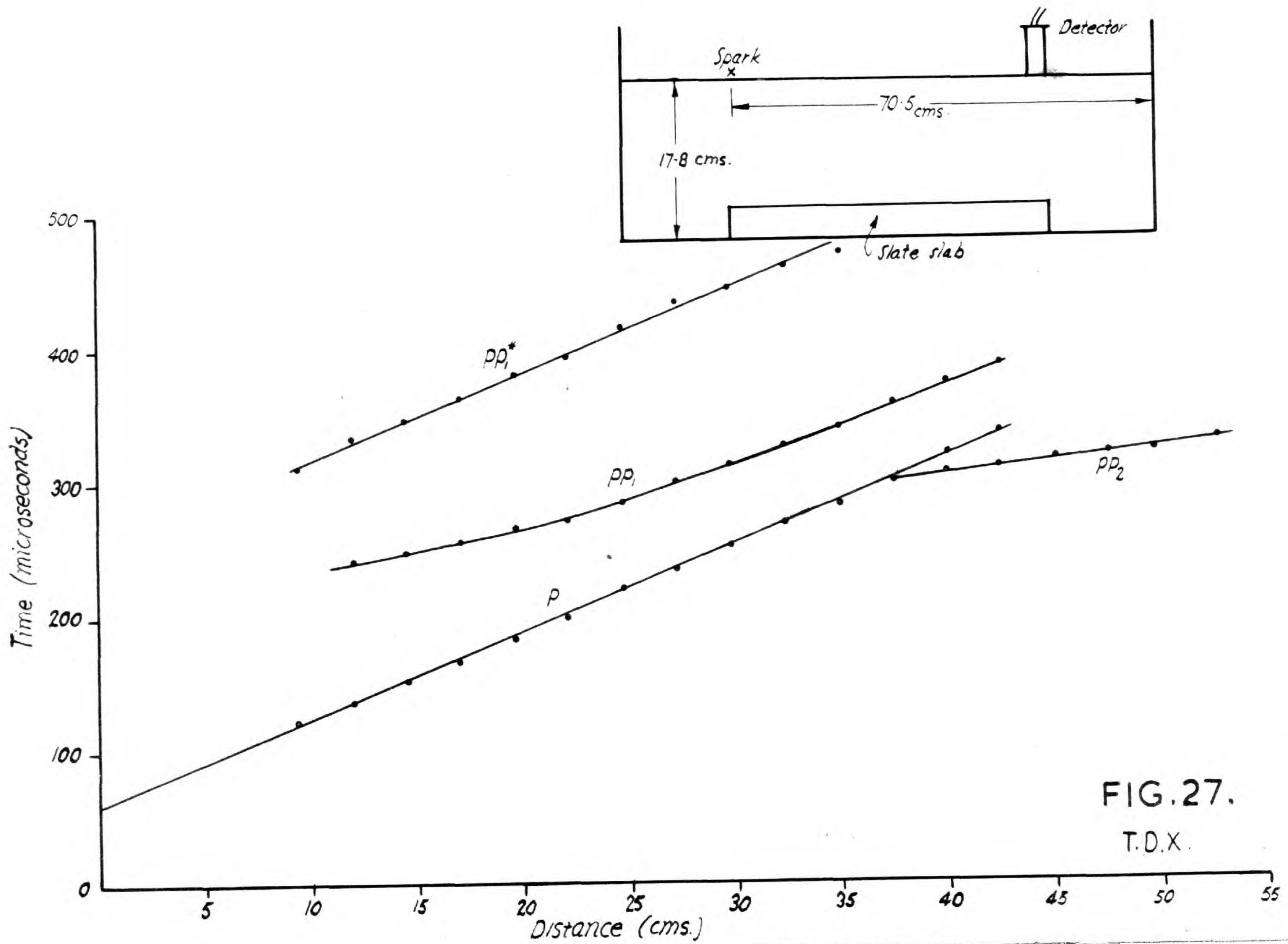
Detector
Spark
70·5 cms.
17·8 cms.
Slate slab
500
400
300
200
100
0
Time (microseconds)
pp$_1^*$
pp$_1$
p
pp$_2$
5
10
15
20
25
30
35
40
45
50
55
Distance (cms.)

FIG.27.

T.D.X.

TABLE III.

Time-distance data for T.D. X.

Record No.	Distance (cms.)	Time (μ secs.)				
		P	PP_1	PP_2	PP_1^*	A
1	9.5	120	235		312	206
2	12.1	136	242		333	242
3	14.6	152	248		346	
4	17.1	166	254		362	
5	19.7	184	262		380	
6	22.2	198	268		394	
7	24.8	220	282		414	
8	27.3	234	294		434	
9	29.8	252	304		444	
10	32.4	268	316		460	
11	34.9	282	324		470	
12	37.5	300	337	296		
13	40.0	320	352	302		
14	42.5	336	360	304		
15	45.1		376	310		
16	47.6			316		
17	49.8			322		
18	52.7			330		

T.D. XI

FIG. 28.

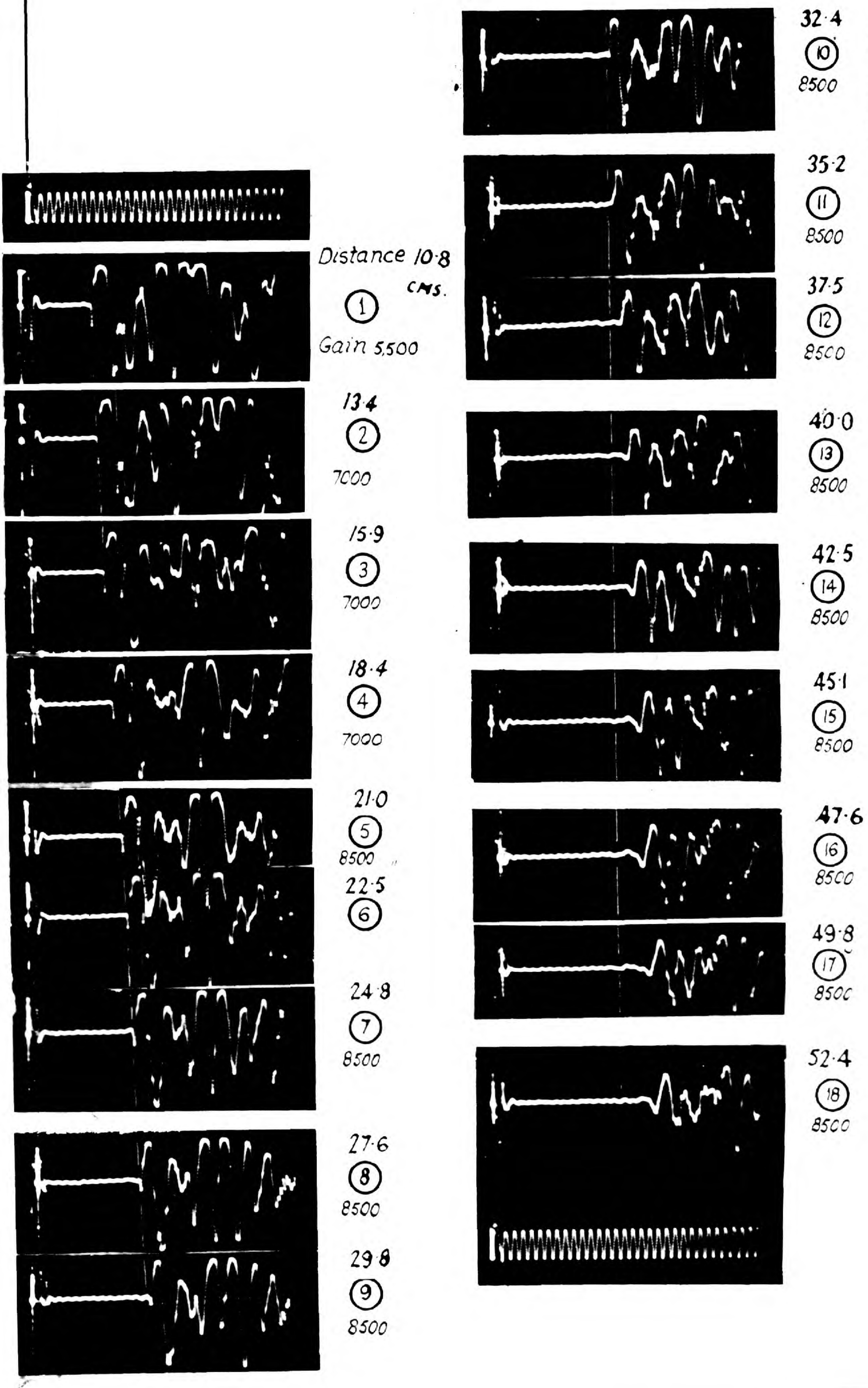
Distance 10·8 CMS.
1
Gain 5,500
13·4
2
7000
15·9
3
7000
18·4
4
7000
21·0
5
8500
22·5
6
24·8
7
8500
27·6
8
8500
29·8
9
8500
32·4
10
8500
35·2
11
8500
37·5
12
8500
40·0
13
8500
42·5
14
8500
45·1
15
8500
47·6
16
8500
49·8
17
8500
52·4
18
8500

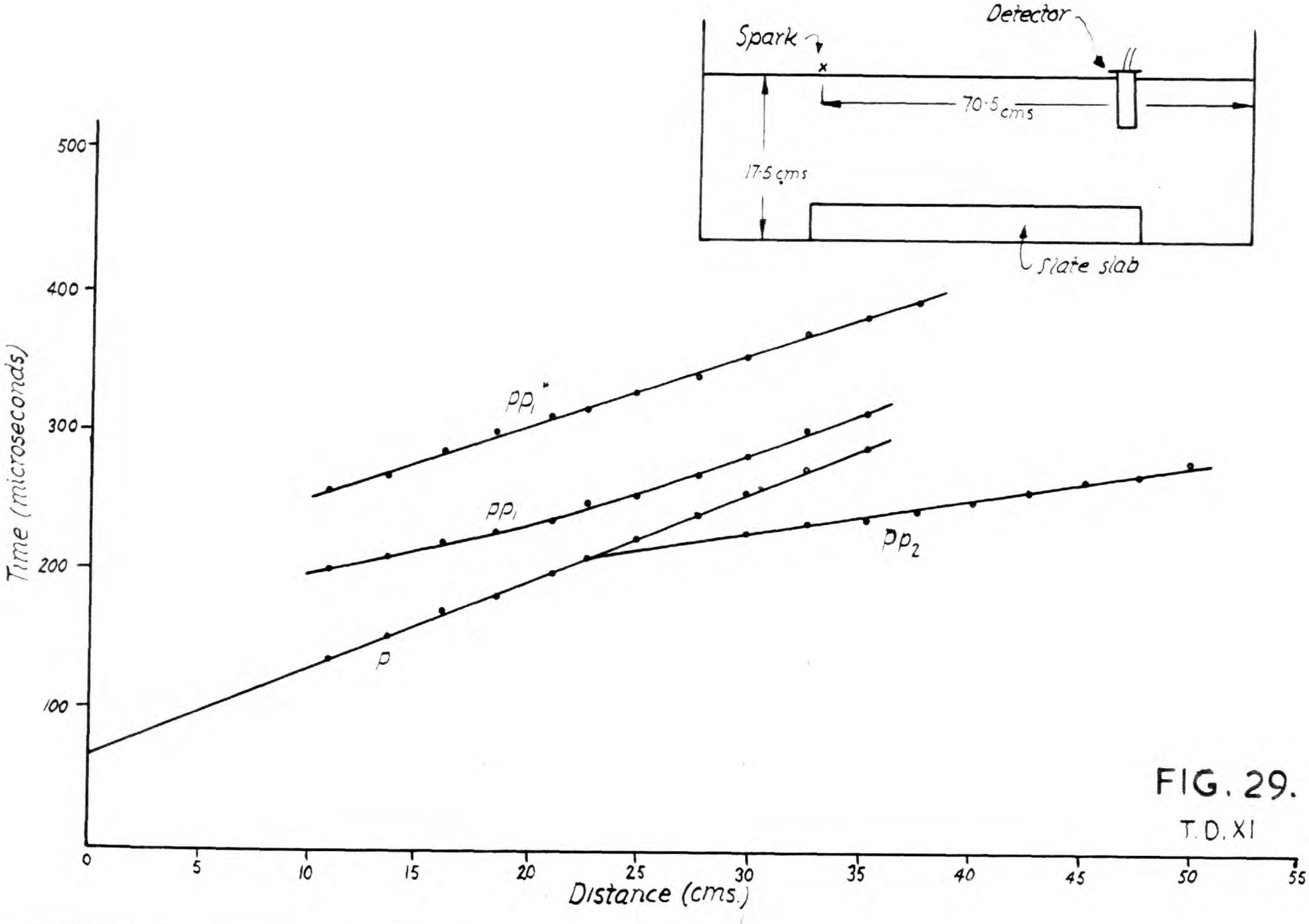
Detector
Spark
70·5 cms
17·5 cms
Slate slab
500
400
300
200
100
Time (microseconds)
pp_1^*
pp_1
pp_2
p
0
5
10
15
20
25
30
35
40
45
50
55
Distance (cms.)

FIG. 29.

T.D. XI

T.D. XII

FIG. 30.

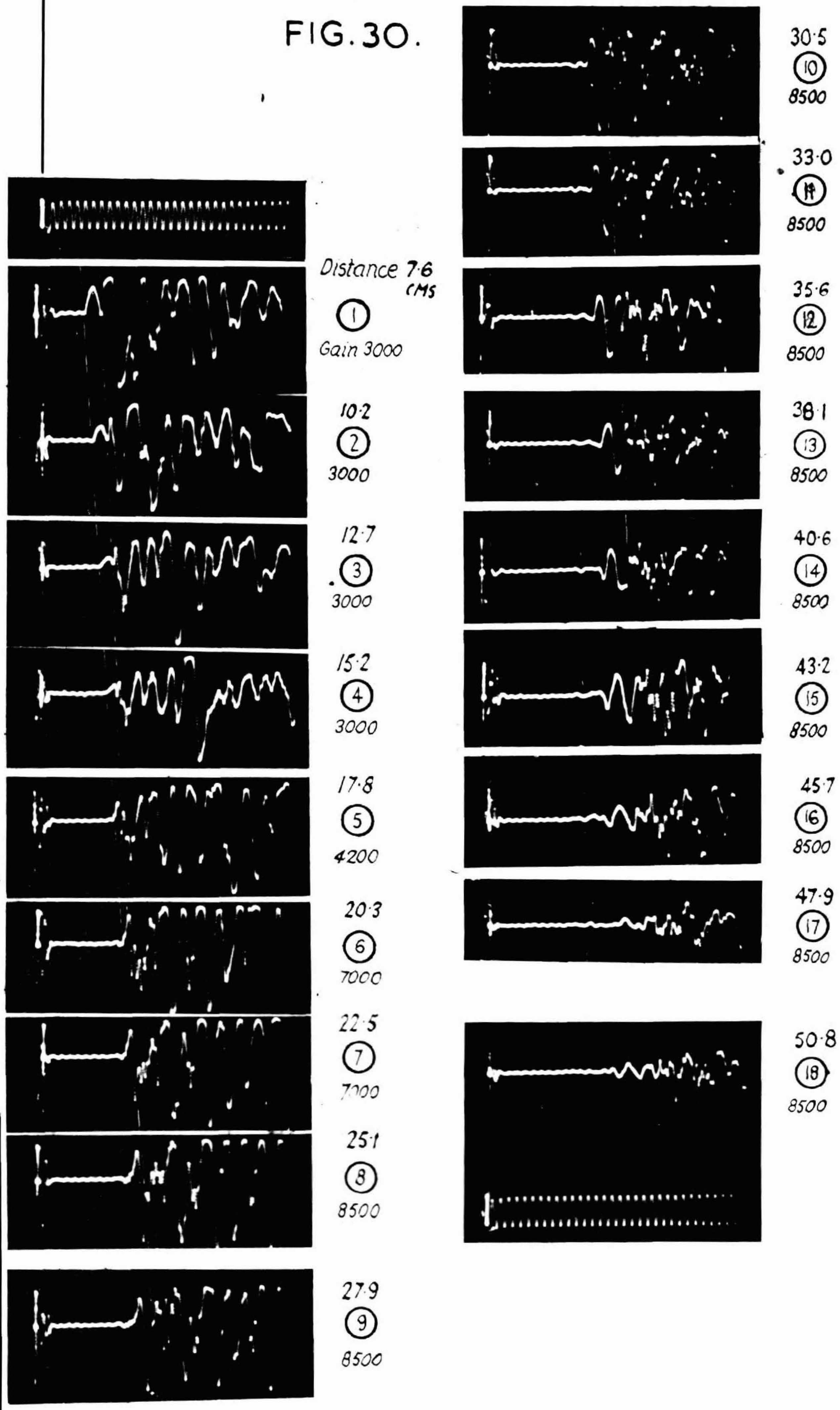

Distance 7·6 CMS
1
Gain 3000
10·2
2
3000
12·7
3
3000
15·2
4
3000
17·8
5
4200
20·3
6
7000
22·5
7
7000
25·1
8
8500
27·9
9
8500
30·5
10
8500
33·0
11
8500
35·6
12
8500
38·1
13
8500
40·6
14
8500
43·2
15
8500
45·7
16
8500
47·9
17
8500
50·8
18
8500

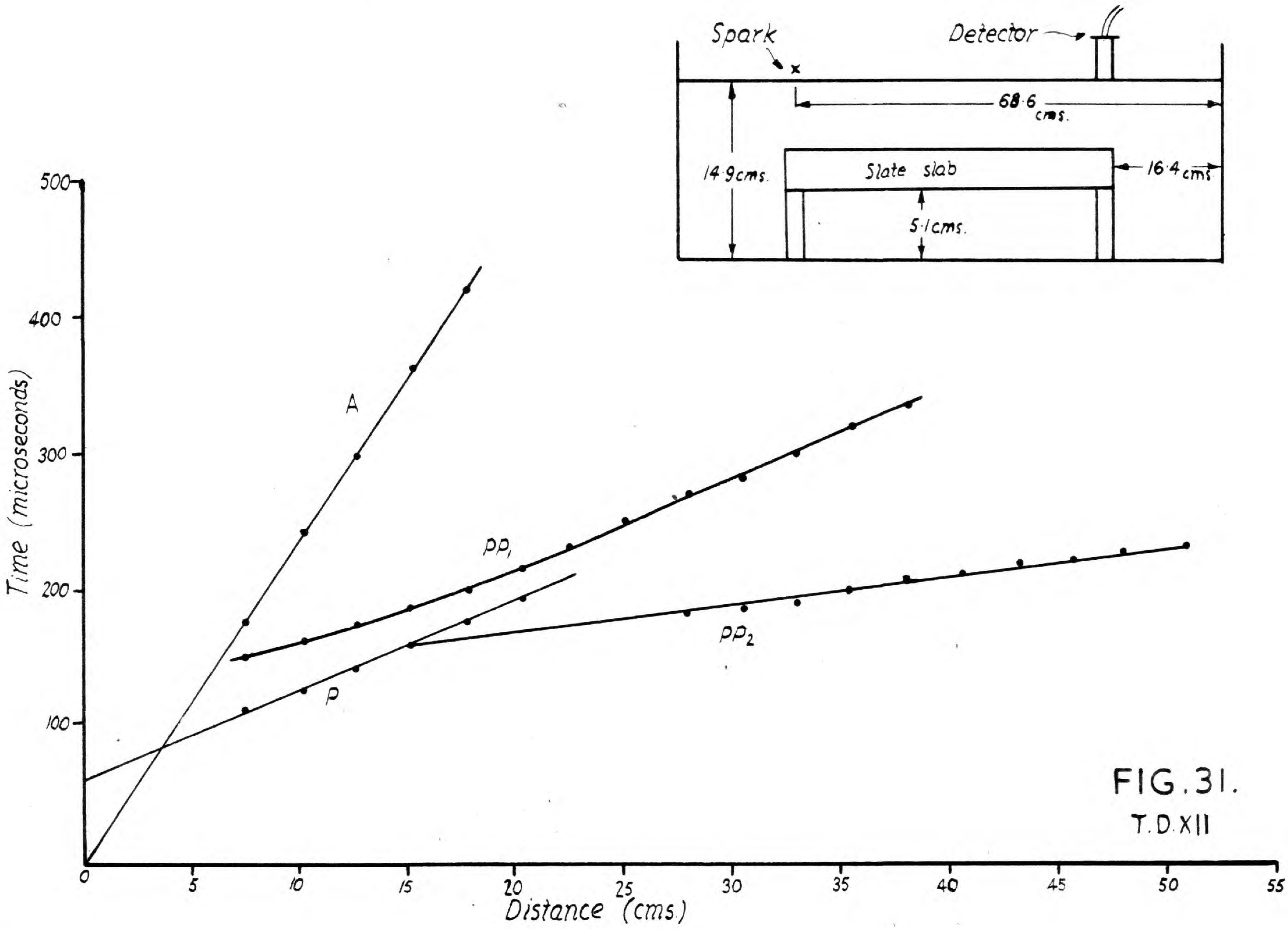

Spark
Detector
68·6 cms.
14·9cms.
Slate slab
16·4 cms
5·1cms.
A
pp1
pp2
p
Time (microseconds)
Distance (cms.)
500
400
300
200
100
0
5
10
15
20
25
30
35
40
45
50
55

FIG.31.

T.D.XII

was used as in T.D. X, but with the detector at a depth of 8.6 cms. below the surface of the water. Time-distance data are given in Table IV and the time-distance curve in Fig. 29. Records Nos. 1 - 9, Fig. 28, show the onset of P at 1570±20 metres p.s. to be opposite in phase to the corresponding shots of T.D. X, but the amplitude of this onset shows a steady decrease for increasing shot-detector distances until in record No. 11 the refracted wave (PP_2) from the slab is the first arrival with a velocity of 4090±70 metres p.s.

Later arrivals include the refelcted P (PP_1) and, as before, the multiple reflected PP_1^{*}. It is remarkable that the first arrival in records Nos. 1 - 9, as represented by the first rarefaction should have such a short period followed by a large compression whose period decreaseswith greater shot detector distances.

T.D. XII.

In this experiment the slate slab was mounted 5.1 cms. above the floor of the tank by means of four 2.5 cm. diameter metal pillars situated at each corner. The detector was traversed across the surface and the records are reproduced in Fig. 30. Figure 31 shows the time distance curve obtained from measurements on the photographic prints. Table V gives the arrival times of those components

TABLE IV.

Time Distance Data for T.D. XI.

Record No.	Distance (cms.)	Time (μ secs.)			
		P	PP_1	PP_2	PP_1^*
1	10.8	136	198		258
2	13.4	152	207		268
3	15.9	170	214		286
4	18.4	182	224		300
5	21.0	200	245		312
6	22.5	210	250		318
7	24.8	224	262		330
8	27.6	242	270		340
9	29.8	258	284	230	356
10	32.4	275	304	236	372
11	35.2	290	316	240	384
12	37.5		336	246	396
13	40.0		346	252	
14	42.5		362	260	
15	45.1			266	
16	47.6			272	
17	49.8			278	
18	52.4				

TABLE V.

Time Distance Data for T.D. XII.

Record No.	Distance (cms.)	Time (μ secs.)				
		P	PP_1	PP_2	PP_1^*	A
1	7.6	110	152			178
2	10.2	126	163			242
3	12.7	143	176			298
4	15.2	160	188			362
5	17.8	176	200			420
6	20.3	194	217			
7	22.5		232			
8	25.1		252			
9	27.9		270	182		
10	30.5		282	186		
11	33.0		300	192		
12	35.6		320	200		
13	38.1		336	208		
14	40.6			212		
15	43.2			220		
16	45.7			222		
17	47.9			228		
18	50.8			234		

plotted on the time-distance curve. The depth of water in the tank was 15 cms., i.e., 6.0 cms. above the upper surface of the slate slab.

For the shorter shot-detector distances (shots 1 - 4), the earliest arrival is P which is shortly supplanted by the refraction from the slate. The onset of this refraction was difficult to fix due to its small amplitude, buts its point of first arrival can be detected in shot 5 by the phase change. At this point also, there appears on the onset a very high frequency component which eventually disappears in shot No. 12 and succeeding ones. The PP_1 from the slab is prominent and there is evidence for PP_1^*. The air wave A is shown on the time distance curve but there is again no evidence of a surface wave.

<u>T.D. XIII</u>.

Finally the tank was traversed (T.D. XIII, Fig. 32) with the slab in the same position as in T.D. XII, but with the detector resting upon it. The first arrival at 4540±60 metres p.s. is the direct compressional wave (P) of the slab which, similarly to T.D. XII, exhibits a high frequency component over a portion of its path (shots 4 - 13). The onset of this phase is very small and therefore no great accuracy is attached to the plot on the time distance curve (Fig. 33). In records 14 - 21 there is slight evidence of a change of period in the first arrival, possibly a transverse wave. The following

T.D. XIII

FIG. 32

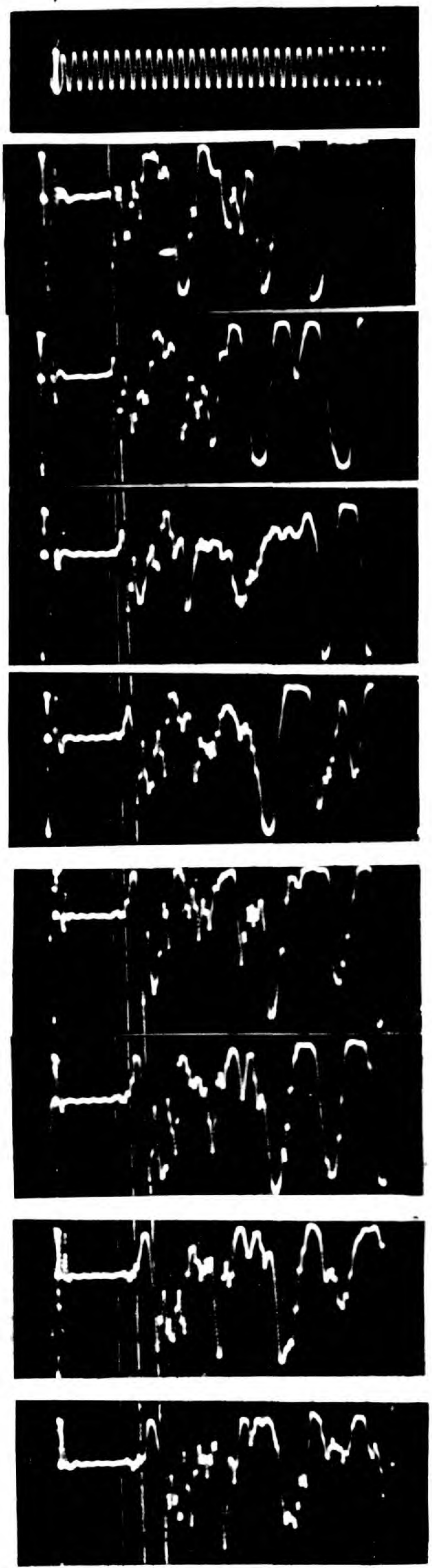

Distance 9·5 cms.
1
Gain 5000

11·4
2
5000

13·3
3
5000

15·2
4
5000

17·1
5
8500

19·1
6
8500

21·0
7
8500

22·9
8
8500

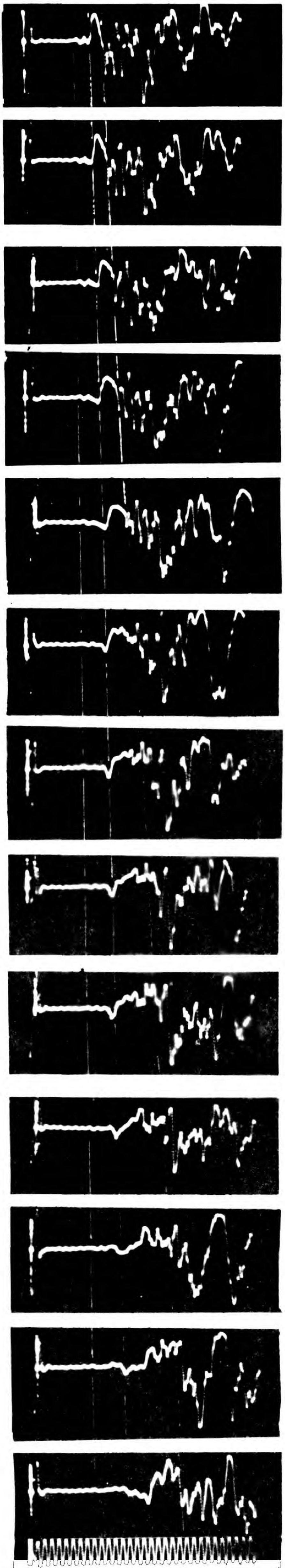

24·8
9
8500

26·7
10
8500

28·6
11
8500

30·5
12
8500

32·4
13
8500

34·3
14
8500

36·2
15
8500

38·1
16
8500

40·0
17

41·9
18
8500

43·8
19
8500

45·7
20
8500

47·6
21
8500

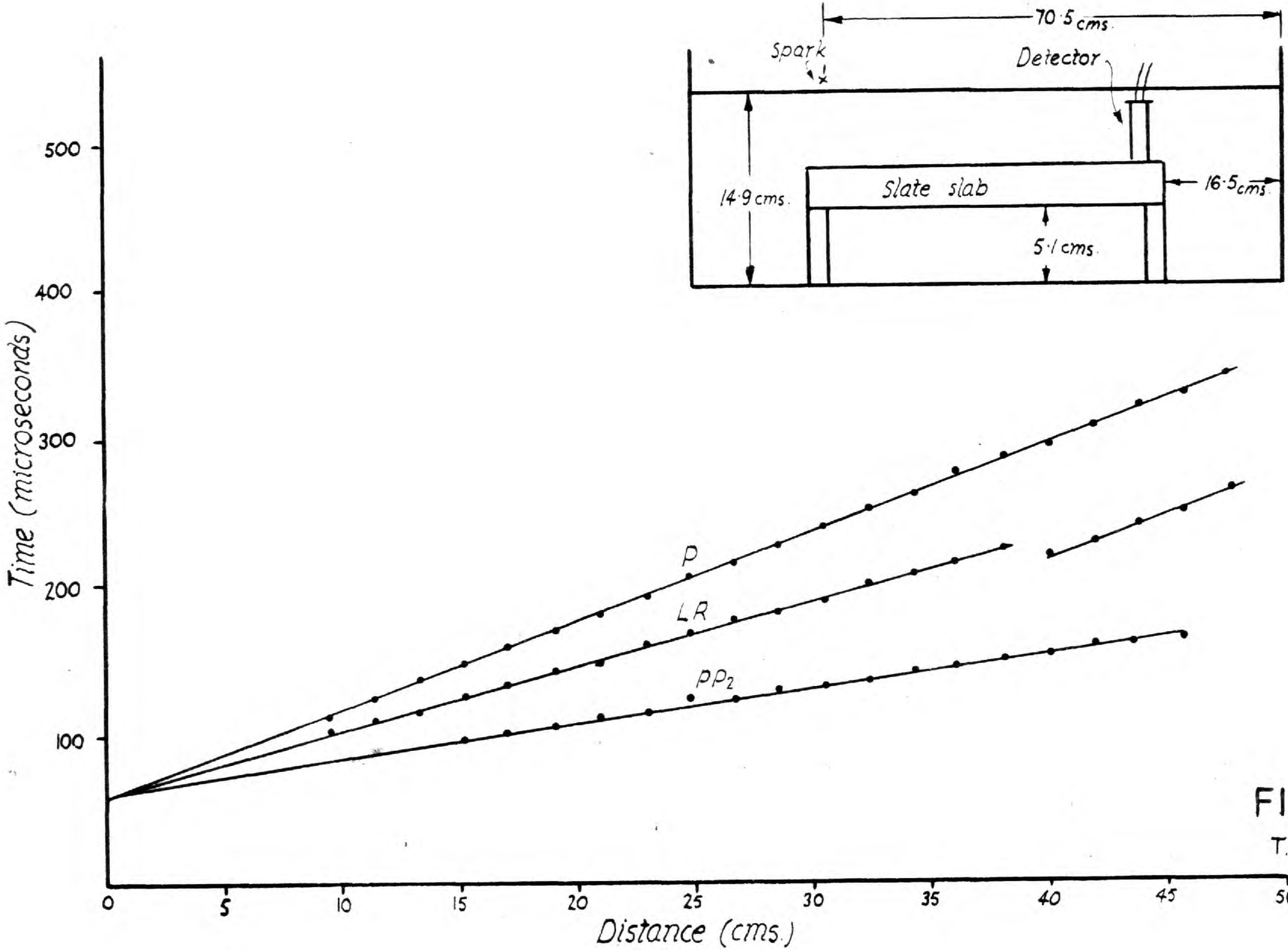

FIG. 33.

T. D. XIII

disturbance of longer period and larger amplitude may be identified as the Rayleigh wave for the slab at 2340±10 metres p.s. An abrupt onset following the surface wave and of higher frequency indicates the arrival of the water wave at 1620±10 metres p.s. The time-distance data for this traverse are given in Table VI.

Velocities.

The velocities of the arrivals plotted on the time-distance curves for all horizontal traverses are given in Table VII. These results have been least squared with the exception of the A arrivals as these did not supply sufficient data to warrant their computation. For the reflected waves (PP_1), the path-length required for least squaring was determined from the geometrical configuration of reflector, detector and source in each case. The centre of the detector face was taken as the point of arrival of the disturbance, which was approximately true for reflections and refractions, but less so for the direct (P) arrivals which would encounter the detector edge nearest to the source first. This difficulty was unavoidable due to the finite size of the detector and since the actual Barium Titanate disc was surrounded by a metal jacket at its edge and sealed in paraffin wax, it was considered best to take the centre of the detector

TABLE VI.

Time Distance Data for T.D. XIII.

Record No.	Distance (cms.)	Time (μ secs.) P	PP_2	LR
1	9.5	112		104
2	11.4	124		110
3	13.3	138		116
4	15.2	150	98	126
5	17.1	160	102	134
6	19.1	170	106	144
7	21.0	180	112	148
8	22.9	194	116	160
9	24.8	206	122	168
10	26.7	216	124	176
11	28.6	226	130	182
12	30.5	240	132	190
13	32.4	252	136	200
14	34.3	262	142	208
15	36.2	276	144	216
16	38.1	286	150	224
17	40.0	294	154	220
18	41.9	307	160	230
19	43.8	320	160	240
20	45.7	328	164	250
21	47.6	342		264

face as the point of arrival. The error in determining the time of arrival on the records was due to several factors, principal among which was the fixing of the shot instant at the beginning of each trace from record to record. Similarly, care was required in choosing the point of onset of a particular arrival from record to record.

Discussion.

The difference in acoustic impedance between air and water

$$\text{air}_{\rho v} = 43 = R_1$$
$$\text{water}_{\rho v} = 1.43 \times 10^5 = R_2$$

is so large that it is to be expected that very little energy would be transmitted when a sound wave is incident upon an air-water interface. The power transmission ratio[16] which indicates the fraction of the incident wave energy transmitted is given by

$$\left(\frac{2R_1}{R_1 + R_2}\right)^2 = 36 \times 10^{-8}$$

on substituting the above values. The square of the amplitude ratio of the pulse received in air and water (Fig. 13) with the detector immediately in front of the spark is 1, which has no correspondence with theabove figure. This discrepancy is so great that it is obvious

TABLE VII.

Velocities (metres p.s.)

	T.D.IX	T.D.X	T.D.XI	T.D.XII	T.D.XIII
P	1530±20	1530±10	1570±20	1510±10	1620±10
PP_1	1570±20	1570±10	1520±20	1450±20	
PP_1^*	1660±10	1570±20			
PP_2	4150±100	4490±170	4090±70	4240±90	4540±60
LR					2340±10

that there is no parallel between the case of a plane wave incident upon a surface separating two media, upon which the above theory is based, and the case of the explosive nature of the spark. The explanation cannot be based solely upon the high velocity of sound in the immediate neighbourhood of an explosive source. A. B. Wood[17] quotes a figure three times the normal value which would not account for the difference. It is most probable that, among other causes, the high air pressure set up in the vicinity of the spark would account for this. Evidence for this was suggested by the fact that on discharge of the spark, the water surface was considerably disturbed so that surface waves were set up.

Within the water medium, the high velocity contrast of 3/1 between slate and water causes severe attenuation of the transmitted wave with the result that refractions are difficult to discern on the records. The smaller contrast of 2/1 between water and the tank floor however, enables refraction from this source to be determined with greater ease. Therefore, in model seismic work further study of refractions would warrant the choice of a medium and model with a small velocity contrast.

Concerning the general features of the records, the direct longitudinal (P) wave in water, for traverses with the detector at the surface, is always characterized by a low frequency onset contrary to that experienced by seismic work at sea.[18] However, in most cases this work is performed with the shot and detector either on the bottom or at depths well below the surface. For long ranges, in shallow work, the first arrival, the refracted wave traversing the bottom, is called the ground wave. Following it and with a much higher frequency, is the second arrival, the water wave. The low frequency onset noted in the surface traverses is, however, no longer evident in T.D. XI, and the depth profile (Fig. 28) with the detector at depth as here, the first arrival, the direct P wave, is a rarefaction of very short period. It is doubtful whether thehigh frequency motion observed following the first arrivals in T.D. XII and T.D. XIII would represent the same phenomenon, since it is obvious from their time of occurrence in the records that they are components of a much higher velocity. It is more probable, since in both cases they follow the refracted PP_2 wave that they represent a coda. Further evidence to suggest that the high frequency expected of the water wave is only to be found at depth is given in the vertical traverse (Fig. 23), for with increase in depth of the detector, the first onset displays greater evidence of a high frequency component "riding" on the principal disturbance. Seismic work at sea does not exhibit this modulation effect, the water wave commencing at a very high frequency which diminishes as the wave proceeds.

The vertical traverse (Fig. 23) is an excellent illustration of the method of images for spherical waves propagated from a point source. Pekeris[3] in deriving the complete normal mode solution for spherical waves incident upon plane boundaries, points out that for a shallow water problem, the source and its image (in the water in this case) constitute a dipole source and this dipole can be represented by a system of images at a spacing of 2H, where H is the depth of water, strung along the vertical through the source. For angles of incidence greater than the angle of total reflection, the strength of all the images becomes unity and the system behaves as a self-luminous diffraction grating. Hence there are certain discrete directions in which constructive interference occurs. In the same manner the dipole images above the surface give rise, in certain directions, to a constructively interfering set of down going waves. The combination of the upgoing waves from dipole images below the surface and the downgoing waves give rise to the normal modes.

In the present case, the critical angle, from the velocities determined in T.D. IX, is 20.3° and the angles of incidence of the wave reflected at the bottom of the tank range between 37.3° and 50.2° for the various levels of water used in this experiment. Hence the angle of incidence throughout the experiment was always greater than that for total reflection. Also, although the source and its image beneath the surface constitute a dipole, the remaining images due to reflection at the tank floor are single images.

This phenomenon demonstrates the advantage, for seismic work at sea, in selecting an optimum depth for the geophone as the high frequencies associated with the records taken at surface positions are attenuated at depth, resulting in a clearer onset for both water and ground waves.

SUMMARY AND CONCLUSIONS.

In the electronic aspect of this model seismic experiment, care has been exercised in design to produce as faithful a record of the medium's motion as possible. For this end the amplifier was designed with a wide bandwidth and the accelerometer natural frequency of 160 kc.p.s. chosen well beyond the region of working frequencies expected. As described in Chapter I, the bandwidth of the pre-amplifier, 100 kc.p.s., determines a rise time of 3 μsecs. and the short time constants give a 1% drop in 5 μ secs. for a step function input.

These values proved quite adequate for the length of time involved, e.g., the 150 and 500 μ sec. timebases.

The design of the detector proved most satisfactory as far as the low Q value secured is concerned, but paradoxically, rendered the theoretical treatment valueless, at least in the case of detector No. 21. Here the choice of backing and the careful fit to the Barium Titanate disc produced a detector in which no resonance could be detected, and therefore none of the quantities necessary to determine Q could be obtained. It is clearly demonstrated in the text that some form of edge damping is essential in this design that the output of the disc will not include the results of the excitation of higher modes and overtones.

The reduction of the rarefaction in the source pulse was an important factor in securing a shortened impulse of 10 μ secs. duration from the spark. This result was achieved by packing the space behind the electrodes with sponge rubber which behaved as an absorbent, at the same time reducing reflections from the electrode mounting, e.g., the Tufnol disc.

Water was used as a medium for experiments in the tank, and although it does not transmit transverse waves, had the virtue that the detector could be immersed in it to any desired depth. A depth profile revealed a striking alteration of the waveform with depth, the change being apparently due to interference between the reflected wave from the floor of the tank and the direct P wave, the period increasing from 54 μ secs. at the surface to 132 μ secs. at a depth of 7.3 cms. below the surface. This traverse together with T.D. XI indicated that the high frequency water wave, of common experience in seismic work at sea, is a feature confined only to recordings at depth; for in these records the onset of the P wave is of a very short period. In addition, compression following the onset of P in T.D. XI is of a longer period, decreasing with increasing shot-detector distance.

The traverses made across the tank filled with water are listed:

T.D. IX-A traverse with no model present in 12.7 cms. water.

T.D. X -A traverse with the slate slab on the floor of the tank in 17.8 cms. of water.

T.D.XI-A traverse with the slab on the floor of the tank in 17.5 cms. of water with the detector 8.6 cms. below the surface.

T.D.XII-A traverse with the slab raised 5.1 cms. above the floor of the tank with 6 cms. of water above the slab and the detector at the surface.

T.D.XIII-A traverse under the same conditions as T.D.XII but with the detector on the slate slab.

These traverses demonstrated that with slight modification of the experimental arrangement, the waveform of the disturbance recorded showed a distinct change of character. The arrivals identified were the direct longitudinal (P) wave, the reflected wave (PP_1), the refracted wave (PP_2), the Rayleigh wave (LR) of the slate slab and a multiple reflection PP_1^*. There was evidence of a coda in the P wave of the slate slab in T.D.XII and T.D.XIII.

In conclusion, it is emphasized that much further work is required on the phenomena encountered in this work and indeed what has been done demonstrates that the possibilities of model seismic investigation are virtually endless. Certain improvements are desirable in the technique, particularly in the electronics.

A shorter time-base, or at the other extreme, a larger tank and model, would help in the identification of the arrivals. Some form of automatic-volume-control would enable the amplifier to be used at larger gain settings without overloading on the higher energy components of the received disturbance. In addition, to help determine onsets, a rectifying unit, as used in sea seismic work, could be incorporated so that rectified and unrectified outputs could be recorded.

APPENDIX.

DETECTOR THEORY.

Equation of Motion.

Consider a thin disc referred to cylindrical co-ordinates R, θ, Z, and polarised in the Z direction. If the disc is sufficiently thin the displacement in the thickness direction can be neglected, and there is no angular displacement.

$$U_\theta = U_Z = 0, \qquad U_r \neq 0.$$

The stress and electrostrictive equations which specify the mechanical and electrical stresses set up in the disc by a radial displacement U_r are

$$T_r = \frac{Y}{1-\sigma^2}\left(S_r + \sigma S_\theta\right) - \frac{2Q_{12}\,\delta_{z0}\,E_z\,Y}{(4\pi\beta^T + O_1\delta_{z0})(1-\sigma)} \qquad \text{Ref. 12.}$$

$$T_\theta = \frac{Y}{1-\sigma^2}\left(S_\theta + \sigma S_r\right) - \frac{2Q_{12}\,\delta_{z0}\,E_z\,Y}{(4\pi\beta^T + O_1\delta_{z0})(1-\sigma)} \qquad (1)$$

$$\delta_z = \frac{E_z}{(4\pi\beta^T + O_1\delta_{z0})} + \frac{2Q_{12}\,\delta_{z0}}{(4\pi\beta^T + O_1\delta_{z0})}\left(T_r + T_\theta\right)$$

where Y = Young's modulus

σ = Poisson's ratio

Q_{12} = electrostrictive constant for the radial mode

β^T = dielectric impermeability

δ_{z0} = remanent polarisation after the removal of the D.C. biassing field

$E_z = \frac{E}{l_t}$ = voltage appearing at the electrodes, where l_t is the thickness of the disc.

The stresses T_r and T_θ are normal stresses, the former acting perpendicular to the cylindrical boundary and the latter acting perpendicular to radial planes containing the axis. (Fig. 34)

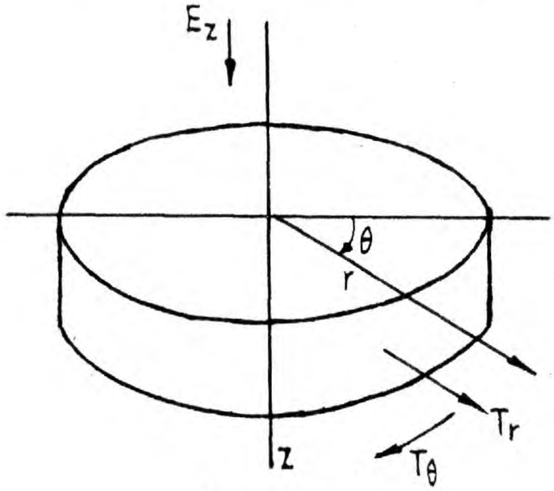

Fig. 34.

The circumferential strain is given by $S_\theta = \frac{U_r}{r}$ and the radial strain by $S_r = \frac{\partial U_r}{\partial r}$. In the electrostrictive theory two dielectric constants are specified, the one $\epsilon_T = 4\pi\beta^T + O_1\delta_{z0}$ appearing in the denominator of the second terms of equations (1) is for constant stress and is related to the other $\epsilon_{RC} = 4\pi\beta^{RC} + O_1\delta_{z0}$ a radially clamped dielectric constant, by the expression

$$\epsilon_{RC} = \epsilon_T\left(1-k^2\right) \qquad (2)$$

The term $O_1\delta_{z0}$ is an additional term to account for the change in dielectric constant on polarising. k is the electromechanical coupling factor.

Substituting $$d_{r\theta} = \frac{2Q_{12}\,\delta_{z0}}{4\pi\beta^T + O_1\delta_{z0}}$$

where $d_{r\theta}$ is known as the equivalent piezoelectric constant, equations (1) reduce to

$$T_r = \frac{Y}{1-\sigma^2}\left(\frac{\partial U_r}{\partial r} + \sigma\frac{U_r}{r}\right) - d_{r\theta}\frac{E}{l_t}\left(\frac{Y}{1-\sigma}\right) \qquad (3a)$$

$$T_\theta = \frac{Y}{1-\sigma^2}\left(\sigma\frac{\partial U_r}{\partial r} + \frac{U_r}{r}\right) - d_{r\theta}\frac{E}{l_t}\left(\frac{Y}{1-\sigma}\right) \qquad (3b)$$

$$\delta z = \frac{E}{\epsilon_T l_t} + d_{r\theta}\left(T_r + T_\theta\right) \qquad (3c)$$

Consider an element of the disc of volume $r\delta r\,\delta\theta\,\delta z$ density ρ subject to normal stresses T_r and T_θ on the faces as shown in Fig. 35.

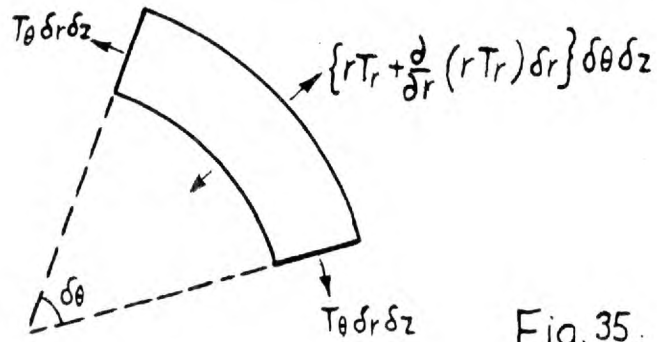

Fig. 35

The equation of equilibrium when the element undergoes vibration in the radial direction is

$$\frac{\partial}{\partial r}(rT_r)\,\delta r\,\delta\theta\,\delta z - T_\theta\,\delta r\,\delta\theta\,\delta z = \frac{\partial^2 U_r}{\partial t^2}\rho\, r\,\delta r\,\delta\theta\,\delta z$$

which on substituting equation (3) becomes for S.H.M.

$$\frac{Y}{1-\sigma^2}\left\{\frac{\partial^2 U_r}{\partial r^2} + \frac{1}{r}\frac{\partial U_r}{\partial r} - \frac{U_r}{r^2}\right\} = -\omega^2 \rho\, U_r$$

This is Bessel's equation of the first order, a solution of which is

$$U_r = A\,J_1\left(\frac{\omega r}{v}\right) \qquad (5)$$

where the velocity v is given by

$$v = \left\{\frac{Y}{\rho(1-\sigma^2)}\right\}^{\frac{1}{2}} \qquad (6)$$

eliminating the constant A, when $r = a$, the radius of the disc, $U_r = U_a$

$$U_r = U_a \frac{J_1 \frac{\omega r}{v}}{J_1 \frac{\omega a}{v}}$$

and

$$\frac{\partial U_r}{\partial r} = U_a\left\{\frac{\frac{\omega}{v} J_0\left(\frac{\omega r}{v}\right) - \frac{1}{r} J_1\left(\frac{\omega r}{v}\right)}{J_1\left(\frac{\omega a}{v}\right)}\right\} \qquad (7)$$

This solution is confined to the disc with $U_r = U_a$ at $r = a$ and $U_r = 0$ at $r = 0$, a more general solution should include values of $r > a$, where the disc is vibrating in an isotropic solid medium of infinite extent, and is given by[19]

$$U_r = U_a \frac{H_1\left(\frac{\omega r}{v}\right)}{H_1\left(\frac{\omega a}{v}\right)}$$

where

$$H_1\left(\frac{\omega r}{v}\right) = J_1\left(\frac{\omega r}{v}\right) + j\, N_1\left(\frac{\omega r}{v}\right)$$

$N_1\left(\frac{\omega r}{v}\right)$ is the Neumann function $\frac{1}{\sin\pi}\left\{J_1\left(\frac{\omega r}{v}\right)\cos\pi - J_{-1}\left(\frac{\omega r}{v}\right)\right\}$

Within the disc, $r \leqslant a$, $H_1\left(\frac{\omega r}{v}\right)$ is inadmissable as it has a singularity at the origin (tends to infinity as $r \to 0$), hence the complete solution is

$$U_r = U_a \frac{J_1\left(\frac{\omega r}{v}\right)}{J_1\left(\frac{\omega a}{v}\right)} \qquad r \leqslant a$$

$$U_r = U_a \frac{H_1\left(\frac{\omega r}{v}\right)}{H_1\frac{\omega a}{v}} \qquad r > a \tag{8}$$

<u>The Force Equation.</u>

To obtain the electrical impedance and equivalent circuit, the stress equations are expressed in terms of the boundary conditions of the disc. Substituting for U_r in (3a) and (3b)

$$T_r = \frac{Y}{1-\sigma^2}\left\{\frac{\omega U_a}{v}\frac{J_0\left(\frac{\omega r}{v}\right)}{J_1\left(\frac{\omega a}{v}\right)} - \frac{U_a}{r}\frac{J_1\left(\frac{\omega r}{v}\right)}{J_1\left(\frac{\omega a}{v}\right)}(1-\sigma)\right\} - d_{r\theta}\frac{E}{l_t}\left(\frac{Y}{1-\sigma}\right)$$

$$T_\theta = \frac{Y}{1-\sigma^2}\left\{\frac{\sigma\omega U_a}{v}\frac{J_0\left(\frac{\omega r}{v}\right)}{J_1\left(\frac{\omega a}{v}\right)} + \frac{U_a}{r}\frac{J_1\left(\frac{\omega r}{v}\right)}{J_1\left(\frac{\omega a}{v}\right)}(1-\sigma)\right\} - d_{r\theta}\frac{E}{l_t}\left(\frac{Y}{1-\sigma}\right)$$

at $r = a$

$$T_{r(r=a)} = \frac{Y}{1-\sigma^2}\left\{\frac{\omega U_a}{v}\frac{J_0\left(\frac{\omega a}{v}\right)}{J_1\left(\frac{\omega a}{v}\right)} - \frac{U_a}{a}(1-\sigma)\right\} - d_{r\theta}\frac{E}{l_t}\left(\frac{Y}{1-\sigma}\right)$$

$$T_{\theta(r=a)} = \frac{Y}{1-\sigma^2}\left\{\frac{\sigma\omega U_a}{v}\frac{J_0\frac{\omega a}{v}}{J_1\frac{\omega a}{v}} + \frac{U_a}{a}(1-\sigma)\right\} - d_{r\theta}\frac{E}{l_t}\left(\frac{Y}{1-\sigma}\right)$$

Since T_r and T_θ are normal stresses, the boundary conditions require that a force F_a at the cylindrical surface is only related to the radial stress

$$F_a = T_{r(r=a)}\, 2\pi a l_t$$

The radial stress then yields the force equation

$$F_a = \frac{2\pi a l_t Y}{1-\sigma^2}\left\{\frac{\omega u_a}{V}\frac{J_0\left(\frac{\omega a}{V}\right)}{J_1\left(\frac{\omega a}{V}\right)} - \frac{u_a}{a}(1-\sigma)\right\} - d_{r\theta}\frac{E}{l_t}\left(\frac{2\pi a l_t Y}{1-\sigma}\right)$$

$$= \omega u_a Z_0 \frac{J_0\left(\frac{\omega a}{V}\right)}{J_1\left(\frac{\omega a}{V}\right)} - Z_0 \frac{V(1-\sigma)}{a} u_a - \varphi E$$

$$= -jZ_0 \frac{J_0\left(\frac{\omega a}{V}\right)}{J_1\left(\frac{\omega a}{V}\right)} \dot{u}_a + jZ_0 \frac{V}{\omega a}(1-\sigma)\dot{u}_a - \varphi E \qquad (9)$$

where the characteristic impedance of the disc $Z_0 = \dfrac{2\pi a l_t Y}{(1-\sigma^2)V}$

and the transformation factor $\varphi = \dfrac{d_{r\theta} Y}{1-\sigma} 2\pi a$ (10)

<u>The Current Equation.</u>

To complete the equations for the equivalent circuit the charge Q appearing on the surface of the disc under the action of an applied stress is evaluated by integrating δ_z over the surface

$$Q = \int_0^{2\pi} d\theta \int_0^a \delta_z\, r\, dr$$

on substituting

$$= \frac{E\pi a^2}{l_t \epsilon_T} + d_{r\theta}\int_0^{2\pi} d\theta \int_0^a r\,(T_r + T_\theta)\,dr$$

$$= \frac{E\pi a^2}{l_t \epsilon_T} + d_{r\theta}\int_0^{2\pi} d\theta \int_0^a r\left\{\frac{Y}{1-\sigma^2}\,\frac{\omega u_a}{V}(1+\sigma)\,\frac{J_0\left(\frac{\omega r}{V}\right)}{J_1\left(\frac{\omega a}{V}\right)} - 2d_{r\theta}\frac{E}{l_t}\left(\frac{Y}{1-\sigma}\right)\right\}dr$$

$$= \frac{E\pi a^2}{l_t \epsilon_T} + d_{r\theta}\frac{2\pi a Y}{1-\sigma}u_a - \frac{2\pi a^2 Y}{l_t(1-\sigma)}d_{r\theta}^2 E$$

The first term includes the radially clamped capacity $C_0 = \dfrac{\pi a^2}{l_t \epsilon_{RC}}$ and the second reduces to φu_a

The third term

$$\frac{2\pi a^2 Y}{l_t(1-\sigma)} d_{r\theta} E = \frac{2\pi a^2 Y}{l_t(1-\sigma)} \cdot \frac{4Q_{12}^2 \delta_{z0}^2}{\epsilon_T^{\,2}} E$$

$$= \frac{\pi a^2 k^2 E}{l_t \epsilon_{RC}(1-k^2)}$$

$$= \frac{k^2}{1-k^2} C_0 E$$

where $k^2 = \dfrac{8Q_{12}^2 \delta_{z0}^2 Y}{\epsilon_T(1-\sigma)}$ is defined as the electromechanical coupling factor. Then the equation of charge and hence the current equation is

$$Q = C_0 E + \varphi u_a$$

or

$$i = j\omega C_0 E + \varphi \dot{u}_a \qquad (11)$$

Equations (9) and (11) together give the equivalent circuit, Fig. 36, for all frequencies

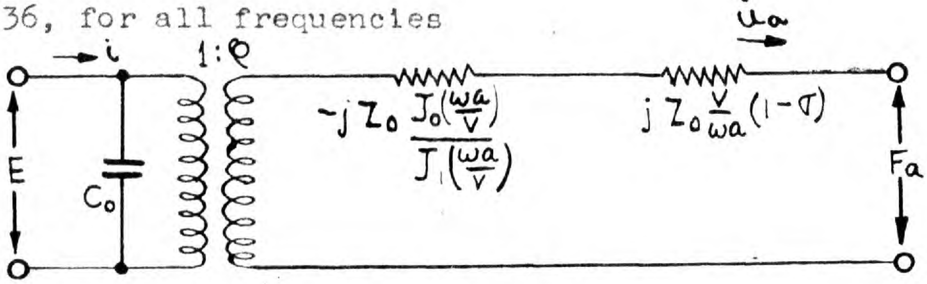

Fig. 36

The transformation factor φ is represented as a transformer converting the mechanical quantities to electrical by division by φ^2 for the impedances and division by φ for the force and velocity.

The Electrical Impedance.

Piezoelectric crystals vibrating in longitudinal or thickness modes have stress components appearing at two faces, the face opposite the working medium being loaded with a suitable backing material to reduce unwanted radiation. For a disc excited to radial vibration there is one free face and since the boundary conditions require $U_r = 0$ when $r = 0$ it behaves as a crystal backed by an infinite mechanical impedance.

Terminating the disc at the free face by a mechanical impedance Z_a where

$$F_a = Z_a \dot{u}_a$$

from (9) $$U_a = \frac{-\mathcal{Q} E}{Z_a + j Z_0 \left\{ \frac{J_0(\frac{\omega a}{v})}{J_1(\frac{\omega a}{v})} - \frac{v}{\omega a}(1-\sigma) \right\}}$$

substituting in (11)

$$Z = \frac{E}{i} = 1 \Big/ \left[j\omega C_0 - \frac{\mathcal{Q}^2}{Z_a + j Z_0 \left\{ J_0(\frac{\omega a}{v}) / J_1(\frac{\omega a}{v}) - \frac{v}{\omega a}(1-\sigma) \right\}} \right] \quad (12)$$

If the disc vibrates in air, the characteristic impedance across the face is sufficiently low that the termination is virtually a short circuit, the electrical impedance then becomes $$Z_e = 1 \Big/ \left[j\omega C_0 - \frac{\mathcal{Q}^2}{j Z_0 \left\{ \frac{J_0(\frac{\omega a}{v})}{J_1(\frac{\omega a}{v})} - \frac{v}{\omega a}(1-\sigma) \right\}} \right]$$

and on rearranging $$= \frac{1}{j\omega C_0} \Big/ \left[1 + \frac{k^2}{1-k^2} \frac{(1+\sigma) J_1(\frac{\omega a}{v})}{\frac{\omega a}{v} J_0(\frac{\omega a}{v}) - (1-\sigma) J_1(\frac{\omega a}{v})} \right] \quad (13)$$

which is identical with the electrical impedance derived by W. P. Mason.[12] The motional electrical impedance of the short-circuited disc

$$Z_m = \frac{j Z_0}{\mathcal{Q}^2} \left\{ \frac{v}{\omega a}(1-\sigma) - \frac{J_0(\frac{\omega a}{v})}{J_1(\frac{\omega a}{v})} \right\}$$

is similar to the result obtained by H. Pursey[19] except that Bessel functions of the first kind are replaced by functions of the third. Since these functions have a markedly different behaviour for small values of ω, the curves of H. Pursey do not represent the motional impedance of the disc but rather the motional impedance of the isotropic medium in radial vibration at its surface. His results show that for values of $0.4 < \sigma < 0.5$ the motional impedance is largely resistive, but for $\sigma < 0.4$ the impedance becomes a capacitive reactance at low frequencies. Hence the mechanical impedance presented to the disc by a medium undergoing radial vibration is composed of reactive and resistive components. Furthermore, the disturbance within the medium arising from the spark impulse is of a more diverse character leading to a mechanical impedance term of greater complexity. In addition, the backing material, the mounting and sealing of the detector must be considered. By measuring the Q of the complete detector immersed in water all these effects are taken into account. In the following section the short-circuited electrical impedance is corrected for mechanical loss, the Q value of the disc alone was replaced by the above Q in the theoretical impedance which was then compared with the measured.

Resonance occurs when the electrical impedance is zero

$$\frac{\omega a}{V} J_0\left(\frac{\omega a}{V}\right) - (1-\sigma) J_1\left(\frac{\omega a}{V}\right) = 0 \qquad (14)$$

and antiresonance for zero admittance is given by

$$\frac{\omega a}{V} J_0\left(\frac{\omega a}{V}\right) - \left(1 - \frac{\sigma + k^2}{1-k^2}\right) J_1\left(\frac{\omega a}{V}\right) = 0 \qquad (15)$$

The frequency of antiresonance is always greater than for resonance. As the frequency increases, the roots $\frac{\omega a}{V} = R_1, R_2, \cdots$ approach the zeros of $J_0\left(\frac{\omega a}{V}\right)$. Similarly for antiresonance, the zeros $\frac{\omega a}{V} = A_1, A_2, \cdots$ also approach the zeros of $J_0\left(\frac{\omega a}{V}\right)$.

The first root of the resonance equation yields the value of Young's modulus for the disc

$$f_{R_1} = \frac{R_1}{2\pi a} \sqrt{\frac{Y}{\rho(1-\sigma^2)}} \qquad (16)$$

where $\rho = 5.5$, $\sigma = 0.27$

and the frequency separation Δf between resonance and antiresonance gives the electromechanical coupling factor

$$k^2 = \frac{\Delta f}{f_R}\left[\frac{R_1^2 - (1-\sigma^2)}{1+\sigma} + \cdots\right] \qquad (17)$$

With a knowledge of these two constants, low frequency considerations give the capacity, compliance and equivalent piezoelectric constant of the disc. The admittance is

$$\frac{1}{Z_e} = j\omega C_0\left[1 + \frac{k^2}{1-k^2}\,\frac{(1+\sigma)J_1\left(\frac{\omega a}{V}\right)}{\frac{\omega a}{V}J_0\left(\frac{\omega a}{V}\right) - (1-\sigma)J_1\left(\frac{\omega a}{V}\right)}\right]$$

substituting the general expansion of the Bessel function

$$J_0\left(\frac{\omega a}{V}\right) = \sum_0^{\infty}(-1)^m \frac{(\omega a/2V)^{2m}}{m!\,\Gamma(m+1)} \quad , \quad J_1\left(\frac{\omega a}{V}\right) = \sum_0^{\infty}(-1)^m \frac{(\omega a/2V)^{2m+1}}{m!\,\Gamma(m+2)}$$

Then the second term within the square brackets

$$\frac{k^2}{1-k^2}\,\frac{(1+\sigma)J_1\left(\frac{\omega a}{V}\right)}{\frac{\omega a}{V}J_0\left(\frac{\omega a}{V}\right) - (1-\sigma)J_1\left(\frac{\omega a}{V}\right)} = \frac{k^2}{1-k^2}\,\frac{(1+\sigma)\left\{\frac{\omega a/2V}{\Gamma(2)} - \frac{(\omega a/2V)^3}{\Gamma(3)} + \cdots\right\}}{\frac{\omega a}{V}\left\{1 - \frac{(\omega a/2V)^2}{\Gamma(2)} + \cdots\right\} - (1-\sigma)\left\{\frac{\omega a/2V}{\Gamma(2)} - \frac{(\omega a/2V)^3}{\Gamma(3)} + \cdots\right\}}$$

$$= \frac{k^2}{1-k^2}\,\frac{(1+\sigma)\left\{\frac{1}{\Gamma(2)} - \frac{(\omega a/2V)^2}{\Gamma(3)} + \cdots\right\}}{2\left\{1 - \frac{(\omega a/2V)^2}{\Gamma(2)} + \cdots\right\} - (1-\sigma)\left\{\frac{1}{\Gamma(2)} - \frac{(\omega a/2V)^2}{\Gamma(3)} + \cdots\right\}}$$

taking this to the limit when $\frac{\omega a}{V} \to 0$

$$\mathcal{L}t_{\frac{\omega a}{V}\to 0}\;\frac{k^2}{1-k^2}\,\frac{(1+\sigma)\left\{\frac{1}{\Gamma(2)} - (\omega a/2V)^2/\Gamma(3) + \cdots\right\}}{2\left\{1 - \frac{(\omega a/2V)^2}{\Gamma(2)} + \cdots\right\} - (1-\sigma)\left\{\frac{1}{\Gamma(2)} - \frac{(\omega a/2V)^2}{\Gamma(3)} + \cdots\right\}} = \frac{k^2}{1-k^2}$$

$$\therefore \mathcal{L}t_{\frac{\omega a}{V}\to 0}\;\frac{1}{Z_e} = \frac{j\omega C_0}{1-k^2} = j\frac{\omega\pi a^2\epsilon_T}{l_t} = j\frac{\omega\pi a^2}{l_t}\epsilon_{RC}\left(1 + \frac{k^2}{1-k^2}\right) \qquad (18)$$

$$= j\frac{\omega\pi a^2}{l_t}\epsilon_{RC} + j\frac{\omega\pi a^2}{l_t}\,\frac{2d_{r\theta}^2 Y}{1-\sigma} = j\omega(C_0 + C_1) \qquad (19)$$

Hence, as the frequency becomes small the impedance of the disc approaches the above expression which is the sum of two capacities, the radially clamped capacity $C_0 = \frac{\pi a^2}{l_t}\epsilon_{RC}$ (20)

and the electrical equivalent of the compliance

$$C_1 = \frac{\pi a^2}{l_t}\,\frac{2d_{r\theta}^2 Y}{1-\sigma} = \varphi^2 C_m \qquad (21)$$

$$\varphi = \frac{2\pi a d_{r\theta} Y}{1-\sigma} \quad , \quad C_m = \frac{1-\sigma}{2\pi l_t Y}$$

φ is the transformation factor between electrical and mechanical quantities and C_m the mechanical compliance. It follows that a measurement of the capacitance at low frequencies yields the free dielectric constant in equation (18) and with the electromechanical coupling factor (20) and (21) are known.

The equivalent piezoelectric constant is determined from

$$d_{r\theta} = k\sqrt{\frac{\epsilon_T(1-\sigma)}{2Y}}$$

Electrical Impedance and Mechanical Loss.

The electrical impedance, equation (13), consists solely of reactive elements and to account for the inherent internal damping of the disc a mechanical hysteresis term is introduced based upon the conception of attenuation losses in solids. These losses are directly proportional to frequency[12] and cannot be attributed to thermal or relaxation effects which are proportional to the square of the frequency. Thermal losses do, however, become predominant at very high frequencies (100 megacycles). Rewriting the stress as

$$T = (Y + jH)S$$

the imaginary component has the dimensions of elasticity.

Because the frequency separation between resonance and antiresonance is small it is not possible to determine the Q by the half-maximum method. Instead, an approximate result has been obtained which depends upon the value of the electrical impedance at resonance and antiresonance as well as the respective frequencies.

On replacing Y by $Y + jH$, the propagation constant $\frac{\omega}{v}$ becomes

$$\omega\sqrt{\frac{\rho(1-\sigma^2)}{Y+jH}} \doteq \frac{\omega}{v}\left(1 - j\frac{H}{2Y}\right) = \frac{\omega}{v}\left(1 - \frac{j}{2Q}\right)$$

and the Q of the disc is defined by W. P. Mason as

$$Q = \frac{\omega/v}{\omega/v\ \frac{H}{Y}} = \frac{Y}{H}$$

The question arises as to how this Q is related to the Q value determined by the half-maximum method. Since the losses are proportional to frequency, the disc behaves as a Voight solid and it is shown by Kolsky[20] that for small damping, the ratio $\frac{\pi H}{Y}$ is equal to the logarithmic decrement Δ' and since, by the half-maximum method Q is defined as

$$Q = \frac{\pi}{\Delta'} = \frac{Y}{H}$$

then the relation is approximately true when the Q value is high.

High Q: Considering first the internal damping of the disc alone, the electrical impedance, equation (13), on substituting $\frac{\omega a}{V}\left(1-\frac{j}{2Q}\right)$ for $\frac{\omega a}{V}$ becomes

$$Z_e = \frac{1}{j\omega C_0} \Big/ \left[1 + \frac{k^2}{1-k^2}\,\frac{(1+\sigma)\, J_1\left\{\left(\frac{\omega a}{V}\right)\left(1-\frac{j}{2Q}\right)\right\}}{\frac{\omega a}{V}\left(1-\frac{j}{2Q}\right) J_0\left\{\frac{\omega a}{V}\left(1-\frac{j}{2Q}\right)\right\} - (1-\sigma)\, J_1\left\{\frac{\omega a}{V}\left(1-\frac{j}{2Q}\right)\right\}}\right]$$

An approximation to this expression is obtained by means of the multiplication theorem for Bessel functions.[21]

$$J_0\left\{\left(\frac{\omega a}{V}\right)\left(1-\frac{j}{2Q}\right)\right\} = \sum_{m=0}^{\infty} \frac{(-1)^m \left(-\frac{j}{Q}\right)^m \left(\frac{\omega a}{2V}\right)^m J_m\left(\frac{\omega a}{V}\right)}{m!}$$

$$\doteq J_0\left(\frac{\omega a}{V}\right) + \frac{j}{2Q}\left(\frac{\omega a}{V}\right) J_1\left(\frac{\omega a}{V}\right)$$

$$J_1\left\{\left(\frac{\omega a}{V}\right)\left(1-\frac{j}{2Q}\right)\right\} = \left(1-\frac{j}{2Q}\right) \sum_{m=0}^{\infty} \frac{(-1)^m \left(-\frac{j}{Q}\right)^m \left(\frac{\omega a}{2V}\right)^m J_{m+1}\left(\frac{\omega a}{V}\right)}{m!}$$

$$\doteq \left(1-\frac{j}{2Q}\right)\left\{J_1\left(\frac{\omega a}{V}\right) + \frac{j}{2Q}\left(\frac{\omega a}{V}\right) J_2\left(\frac{\omega a}{V}\right)\right\}$$

where powers higher than the first of $\frac{\omega a}{V}$ are neglected. With this approximation the electrical impedance is written

$$Z_e = \frac{1}{j\omega C_0} \Big/ \left[1 + \frac{k^2}{1-k^2}\,\frac{(1+\sigma)\left\{J_1\left(\frac{\omega a}{V}\right) + \frac{j}{2Q}\left(\frac{\omega a}{V}\right) J_2\left(\frac{\omega a}{V}\right)\right\}}{\frac{\omega a}{V} J_0\left(\frac{\omega a}{V}\right) + \left(\frac{\omega a}{V}\right)^2 \frac{j}{2Q} J_1\left(\frac{\omega a}{V}\right) - (1-\sigma) J_1\left(\frac{\omega a}{V}\right) - (1-\sigma)\frac{j}{2Q}\frac{\omega a}{V} J_2\left(\frac{\omega a}{V}\right)}\right] \quad (22)$$

The modulus of this result is employed in the theoretical calculation and to obtain the Q the resonant condition, equation (14), is substituted, giving

$$Ze_{R_1} = \frac{1}{j\omega_{R_1}C_0} \Big/ \left[1 + \frac{k^2}{1-k^2}\,\frac{(1+\sigma)\{J_1(R_1) + \frac{j}{2Q}R_1 J_2(R_1)\}}{R_1^2 \frac{j}{2Q} J_1(R_1) - (1-\sigma)\frac{j}{2Q} R_1 J_2(R_1)}\right]$$

the recurrence formula

$$J_2(R_1) = \frac{2}{R_1} J_1(R_1) - J_0(R_1)$$

together with the resonant condition gives $J_2(R_1)$ in terms of $J_1(R_1)$

$$J_2(R_1) = \frac{1+\sigma}{R_1} J_1(R_1)$$

$$\therefore \quad Ze_{R_1} = \frac{1}{j\omega_{R_1}C_0} \Big/ \left[1 + \frac{k^2}{1-k^2}\,\frac{(1+\sigma)\{1 + \frac{j}{2Q}(1+\sigma)\}}{\frac{j}{2Q}\{R_1^2 + \sigma^2 - 1\}}\right]$$

It has been shown[12] that when the impedance, equation (13), is expanded as a Taylor's series about the resonant frequency

$$\frac{\Delta f}{f_R} = \frac{A_1 - R_1}{R_1} = \frac{\frac{k^2}{1-k^2}(1+\sigma)}{R_1^2 + \sigma^2 - 1}$$

then

$$Ze_{R_1} = \frac{1}{j\omega_{R_1}C_0} \Big/ \left[1 + \frac{2Q}{j}\left(\frac{A_1 - R_1}{R_1}\right) + (1+\sigma)\left(\frac{A_1 - R_1}{R_1}\right)\right]$$

whence

$$\left|\frac{1}{Ze_{R_1}}\right| = \omega_{R_1} C_0 \left[4Q^2 \frac{(A_1 - R_1)^2}{R_1^2} + \left\{1 + (1+\sigma)\left(\frac{A_1 - R_1}{R_1}\right)\right\}^2\right]^{\frac{1}{2}}$$

giving

$$Q^2 = \frac{R_1^2}{4(A_1 - R_1)^2}\left[\left(\frac{1}{\omega_{R_1} C_0 |Ze_{R_1}|}\right)^2 - \left\{1 + (1+\sigma)\frac{A_1 - R_1}{R_1}\right\}^2\right] \quad (23)$$

from which the Q value can be determined.

Low Q: The total error introduced by neglecting powers of $\frac{\omega a}{V}$ higher than the first is considerable here since the effect for both numerator and denominator is accumulative. In more precise terms the propagation constant is restated as

$$\omega a \sqrt{\frac{\rho(1-\sigma^2)}{Y + jH}} = \frac{\omega a}{V}\sqrt{\frac{1}{1 + j/Q}} = \frac{\omega a}{V}\sqrt{1 + \frac{1}{Qj - 1}}$$

and from the multiplication theorem

$$J_0\left\{\frac{\omega a}{V}\sqrt{1 + \frac{1}{Qj-1}}\right\} = m\sum_0^\infty \frac{(-1)^m \left\{\frac{1}{2(Qj-1)}\frac{\omega a}{V}\right\}^m J_m\left(\frac{\omega a}{V}\right)}{m!}$$

$$\doteqdot J_0\left(\frac{\omega a}{V}\right) - \frac{1}{2}\,\frac{1}{Qj-1}\,\frac{\omega a}{V} J_1\left(\frac{\omega a}{V}\right) + \frac{1}{8}\left(\frac{1}{Qj-1}\right)^2\left(\frac{\omega a}{V}\right)^2 J_2\left(\frac{\omega a}{V}\right)$$

$$J_1\left\{\left(\frac{\omega a}{V}\right)\sqrt{1+\frac{1}{Qj-1}}\right\} = \sqrt{1+\frac{1}{Qj-1}}\sum_{m=0}^{\infty}(-1)^m \frac{\left\{\frac{1}{2}\frac{1}{Qj-1}\frac{\omega a}{V}\right\}^m J_{m+1}\left(\frac{\omega a}{V}\right)}{m!}$$

$$\doteq \sqrt{1+\frac{1}{Qj-1}}\left\{J_1\left(\frac{\omega a}{V}\right) - \frac{1}{2}\frac{1}{Qj-1}\frac{\omega a}{V}J_2\left(\frac{\omega a}{V}\right) + \frac{1}{8}\left(\frac{1}{Qj-1}\right)^2\left(\frac{\omega a}{V}\right)^2 J_3\left(\frac{\omega a}{V}\right)\right\}$$

where powers of $\frac{\omega a}{V}$ higher than the second are neglected. Introducing these expansions into the impedance expression

$$Ze = \frac{1}{j\omega C_0}\Big/\left[1 + \frac{k^2}{1-k^2}\frac{(1+\sigma)J_1\left\{\frac{\omega a}{V}\sqrt{1+1/(Qj-1)}\right\}}{\frac{\omega a}{V}\sqrt{1+\frac{1}{Qj-1}}\,J_0\left\{\frac{\omega a}{V}\sqrt{1+\frac{1}{Qj-1}}\right\} - (1-\sigma)J_1\left\{\left(\frac{\omega a}{V}\right)\sqrt{1+\frac{1}{Qj-1}}\right\}}\right]$$

$$= \frac{1}{j\omega C_0}\Big/\left[1 + \frac{k^2}{1-k^2}\frac{(1+\sigma)\sqrt{1+\frac{1}{Qj-1}}\left\{J_1\left(\frac{\omega a}{V}\right) - \frac{1}{2}\frac{1}{Qj-1}\frac{\omega a}{V}J_2\left(\frac{\omega a}{V}\right) + \frac{1}{8(Qj-1)^2}\left(\frac{\omega a}{V}\right)^2 J_3\left(\frac{\omega a}{V}\right)\right\}}{\begin{array}{l}\frac{\omega a}{V}\sqrt{1+\frac{1}{Qj-1}}\left\{J_0\left(\frac{\omega a}{V}\right) - \frac{1}{2}\frac{1}{Qj-1}\frac{\omega a}{V}J_1\left(\frac{\omega a}{V}\right) + \frac{1}{8}\left(\frac{1}{Qj-1}\right)^2\left(\frac{\omega a}{V}\right)^2 J_2\left(\frac{\omega a}{V}\right)\right\} \\ -(1-\sigma)\sqrt{1+\frac{1}{Qj-1}}\left\{J_1\left(\frac{\omega a}{V}\right) - \frac{1}{2}\frac{1}{Qj-1}\frac{\omega a}{V}J_2\left(\frac{\omega a}{V}\right) + \frac{1}{8(Qj-1)^2}\left(\frac{\omega a}{V}\right)^2 J_3\left(\frac{\omega a}{V}\right)\right\}\end{array}}\right]$$

$$= \frac{1}{j\omega C_0}\Big/\left[1 + \frac{k^2}{1-k^2}\frac{(1+\sigma)\left[\left\{1 - \frac{1}{8}\frac{1}{(Qj-1)^2}\left(\frac{\omega a}{V}\right)^2\right\}J_1\left(\frac{\omega a}{V}\right) + \frac{2-Qj}{(Qj-1)^2}\frac{1}{2}\frac{\omega a}{V}J_2\left(\frac{\omega a}{V}\right)\right]}{\begin{array}{l}\frac{\omega a}{V}\left\{J_0\left(\frac{\omega a}{V}\right) - \frac{1}{2}\frac{1}{Qj-1}\frac{\omega a}{V}J_1\left(\frac{\omega a}{V}\right) + \frac{1}{8}\frac{1}{(Qj-1)^2}\left(\frac{\omega a}{V}\right)^2 J_2\left(\frac{\omega a}{V}\right)\right\} \\ -(1-\sigma)\left[\left\{1 - \frac{1}{8}\frac{1}{(Qj-1)^2}\left(\frac{\omega a}{V}\right)^2\right\}J_1\left(\frac{\omega a}{V}\right) + \frac{2-Qj}{2(Qj-1)^2}\frac{\omega a}{V}J_2\left(\frac{\omega a}{V}\right)\right]\end{array}}\right]$$

$$= \frac{1}{j\omega C_0}\Big/\left[1 + \frac{k^2}{1-k^2}\frac{(1+\sigma)\left[\left\{(Qj-1)^2 - \frac{1}{8}\left(\frac{\omega a}{V}\right)^2 + (2-Qj)\right\}J_1\left(\frac{\omega a}{V}\right) - \left(\frac{2-Qj}{2}\right)\frac{\omega a}{V}J_0\left(\frac{\omega a}{V}\right)\right]}{\begin{array}{l}\frac{\omega a}{V}\left[(Qj-1)^2 - \frac{1}{8}\left(\frac{\omega a}{V}\right)^2 + (1-\sigma)\frac{(2-Qj)}{2}\right]J_0\left(\frac{\omega a}{V}\right) + \left(\frac{3-2Qj}{4}\right)\left(\frac{\omega a}{V}\right)^2 J_1\left(\frac{\omega a}{V}\right) \\ -(1-\sigma)\left[(Qj-1)^2 - \frac{1}{8}\left(\frac{\omega a}{V}\right)^2 + (2-Qj)\right]J_1\left(\frac{\omega a}{V}\right)\end{array}}\right] \quad (24)$$

The modulus of this result is also employed in the calculation of the theoretical impedance for low Q. To ascertain the Q value, the electrical impedance at resonance is

$$Ze_{R_1} = \frac{1}{j\omega_{R_1}C_0}\Big/\left[1 + \frac{k^2}{1-k^2}\frac{(1+\sigma)\left[(Qj-1)^2 - \frac{1}{8}R_1^2 + 2 - Qj - \left(\frac{2-Qj}{2}\right)(1-\sigma)\right]}{\begin{array}{l}(1-\sigma)\left[(Qj-1)^2 - \frac{1}{8}R_1^2 + \frac{(1-\sigma)(2-Qj)}{2}\right] + \left(\frac{3-2Qj}{4}\right)R_1^2 \\ -(1-\sigma)\left[(Qj-1)^2 - \frac{1}{8}R_1^2 + 2 - Qj\right]\end{array}}\right]$$

$$= \frac{1}{j\omega_{R_1}C_0}\Big/\left[1 + \frac{k^2}{1-k^2}\frac{(1+\sigma)\left[\left(2 + \sigma - \frac{1}{8}R_1^2 - Q^2\right) - Qj\left(\frac{5}{2} + \frac{\sigma}{2}\right)\right]}{\left\{1 - \frac{R_1^2}{4(R_1^2+\sigma^2-1)} - \frac{Qj}{2}\right\}(R_1^2+\sigma^2-1)}\right]$$

$$= \frac{1}{j\omega_{R_1}C_0} \Bigg/ \left[1 + \frac{A_1 - R_1}{R_1} \, \frac{\left(2 + \sigma - \frac{1}{8}R_1^2 - Q^2\right) - Qj\left(\frac{5}{2} + \frac{\sigma}{2}\right)}{\left(1 - \frac{R_1^2}{4(R_1^2 + \sigma^2 - 1)} - \frac{Qj}{2}\right)} \right] \qquad (25)$$

Where the separation between the resonant and anti-resonant roots has been substituted for $\frac{k^2}{1-k^2}$ as before. On taking the modulus of the right-hand side of this equation and equating it to the value of $|Z_e|$ obtained from the experimental curve, a cubic in Q^2 is obtained and hence the Q can be evaluated.

ACKNOWLEDGEMENTS.

The author wishes to express his thanks to Dr. J. McG. Bruckshaw for his guidance and encouragement throughout this work. Appreciation is also expressed for the donation of three Barium Titanate discs by Mr. Kelly of Cosmocord Radio Limited. Special thanks are due to the Anglo-Iranian Oil Company and the Anglo-Saxon Oil Company for providing the finance for this research.

BIBLIOGRAPHY.

1. H. Jeffreys, The Earth, 3rd. Ed., 99, (1952)
2. M. Newlands, J. Acoust. Soc. Amer., 26, 434, (1954)
3. M. Ewing, J.L. Worzel, C.L. Pekeris, Propagation of Sound in the Ocean, Geol. Soc. Amer., Memoir 27, (1948)
4. S. Kaufman, W.L. Roever, Proc. Third World Petroleum Congress, The Hague, (1951)
5. T.D. Northward, D.V. Anderson, Bull. Seismol. Soc. Amer., 43, 239, (1953)
6. E.T. Howes, L.H. Tejada-Flores, L. Randolph, J. Acoust. Soc. Amer., 25, 915, (1953)
7. J.F. Evans, C.F. Hadley, J.D. Eisler, D. Silverman, Geophysics, 19, 220, (1954)
8. F.K. Levin, H. Hibbard, (Abstract of paper read at U.C.L.A. Conference, Nov. 4-5, 1953), Geophysics, 19, 358, (1954)
9. J. Oliver, F. Press, M. Ewing, Geophysics, 19, 202, (1954)
10. W.C. Elmore, M.L. Sands, Electronics, Experimental Techniques, National Nuclear Energy Series, McGraw-Hill(1949)
11. H.J.H. Starks, Dept. of Scientific and Industrial Research, Road Research Laboratory, Note No. JD/39/HJHS, July, 1946 (unpublished)
12. W.P. Mason, Piezoelectric Crystals and their Application to Ultrasonics, D. van Nostrand, (1950)
13. H. Schmidt, Akustische Beihefte, 2, 83, (1952)
14. R.R. Aggarwal, J. Acoust. Soc. Amer., 24, Part I 463, Part II 663, (1952)
15. M. Harrison, A. Sykes, P. Marcotti, J. Acoust. Soc. Amer., 24, 384, (1952)
16. C.A. Heiland, Geophysical Exploration, Prentice-Hall, (1946)
17. A.B. Wood, A Textbook of Sound, p. 297, G. Bell & Sons, (1946)

18. M. M. Hill, W.B.R. King, Quart. J. Geol. Soc. London, 109, 1, (1953)

19. H. Pursey, Brit. J. Appl. Phys., 4, 12, (1953)

20. H. Kolsky, Stress Waves in Solids, p. 159, Oxford, (1953)

21. F.E. Fowle, Smithsonian Physical Tables, 8th ed., p. 190, (1934)